The Pennsylvania State University

The Graduate School

Department of Mechanical and Nuclear Engineering

YAW-CONTROL ENHANCEMENT FOR BUSES

BY ACTIVE FRONT-WHEEL STEERING

A Thesis in

Mechanical Engineering

by

Nan Yu

Submitted in Partial Fulfillment
of the Requirements
for the Degree of
Doctor of Philosophy

May 2007

The thesis of Nan Yu was reviewed and approved* by the following:

Sean N. Brennan
Assistant Professor of Mechanical Engineering
Thesis Advisor
Chair of Committee

Mark Levi
Professor of Mathematics

John M. Mason Jr.
Professor of Civil Engineering

Christopher D. Rahn
Professor of Mechanical Engineering

Karen A. Thole
Professor of Mechanical Engineering
Head of the Department of Mechanical and Nuclear Engineering

*Signatures are on file in the Graduate School

ABSTRACT

The number of bus accidents is rather small in comparison with that of cars or trucks. However, bus accidents always attract high public attention due to the severity of each accident. According to a bus-accident survey conducted at PTI (The Pennsylvania Transportation Institute), loss of yaw stability is one of the major causes leading to bus accidents. Maintaining yaw stability is difficult and sometimes impossible for a human driver under critical driving situations. In this case, it is very natural to consider the use of automatic driver-assistance systems to avoid accidents. In order to improve the safety level of buses as well as that of the overall transportation system, a yaw-stability enhancement system needs to be developed for buses. However, very few studies have been conducted on handling characteristics and yaw-stability improvement for buses.

This thesis focused on studying bus handling characteristics and developing a yaw-stability enhancement system for heavy-duty transit buses.

In the thesis work, an active front-wheel steering (AFS) system was developed for a typical 40-foot transit bus. A crucial part in the design of an AFS system is dealing with the nonlinear characteristics of the tire forces. Tires are the parts in vehicle dynamics afflicted with the highest degree of nonlinearity due to vehicle motions, tire-road friction, vertical load, and many other factors. It is obvious that an AFS system has to be robust with respect to the huge uncertainty caused by the nonlinearity in the tire forces. Following the approach recommended by Ono *et al.*, the nonlinear tire force was characterized by uncertain cornering stiffness. Ono suggested that if a controller is able to regulate the motions for a linear vehicle model with uncertain cornering stiffnesses, the

same controller can be applied to the vehicle model with nonlinear tire forces. Based on this approach, a proportional-integral (PI) controller was designed using the constrained optimization method proposed by Åström *et al.*. The designed AFS controller was evaluated on a three degree-of-freedom nonlinear bus model using a series of test scenarios. The computer-simulation results demonstrated the effectiveness of the AFS system in yaw-stability enhancement for buses. In addition, a comparison between the PI controller and a H_∞ loop-shaping controller revealed that, for the specified test cases, the robustness about road friction variation the simple PI controller achieved was similar to that of the advanced H_∞ loop-shaping controller.

This thesis also investigated the handling characteristics of a typical 40-foot transit bus both experimentally and numerically. The experimental data showed that heavy-duty buses exhibit unique handling characteristics, which are different from those of cars or trucks. Compared to a car, a bus has a narrower linear operating range and a much slower yaw response. Compared to a truck, a bus has a much higher rollover-threshold. The results from the computer simulation suggested that vehicle weight has only a minor effect on bus handling during normal operation.

TABLE OF CONTENTS

LIST OF FIGURES

LIST OF TABLES

ACKNOWLEDGEMENTS

To

Bohdan Tadeusz Kulakowski

and

Danning

Chapter 1

Introduction

1.1 Motivation - From Bus Rollover Accidents to Yaw-Control Enhancement

This thesis work originated from a bus-rollover study conducted at The Pennsylvania Transportation Institute (PTI). It was discovered during a statistical analysis on bus-rollover accidents that the safety of buses in rollover crashes is even worse than the notorious SUVs in terms of fatality probability (Kulakowski et al. 2003). As shown in Figure **1-1**, approximately 8% of bus rollover accidents have involved fatalities in 2001, 2002, and 2004, which is considerably higher than the percentage of all other types of vehicles (NHTSA 2002; NHTSA 2003; NHTSA 2005). And, this percentage climbed up to a record high of 20% in 2003 (NHTSA 2004). In addition, according to the statistical data, *almost all bus rollover accidents have involved fatalities and/or injuries without an exception in the past 6 years*.
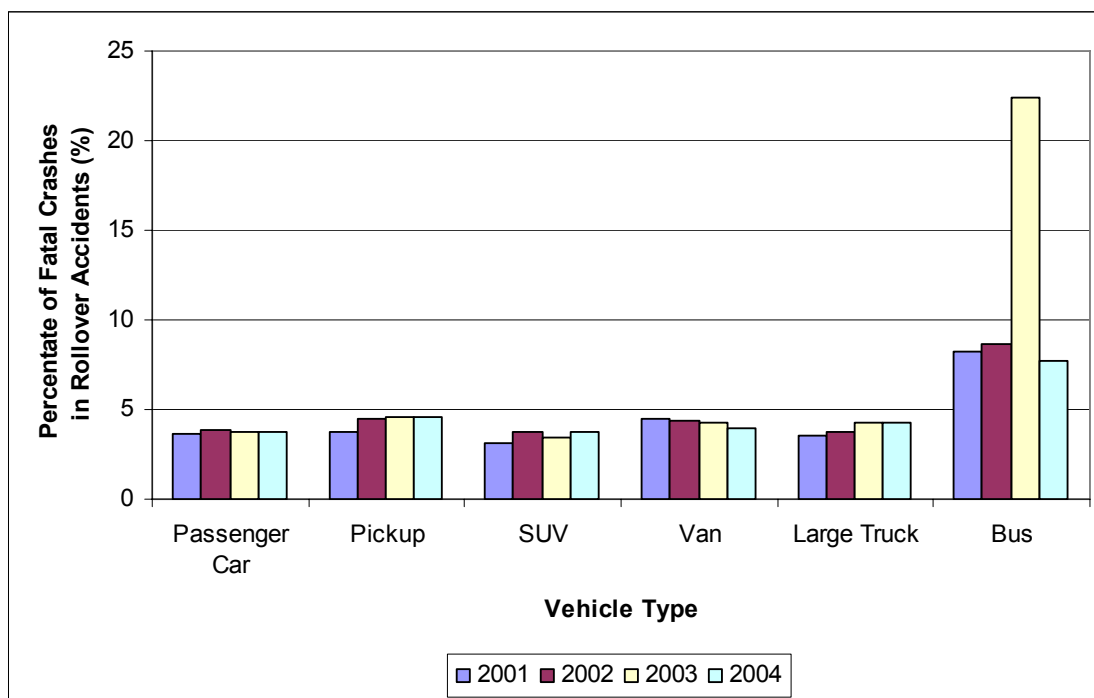
Figure **1-1**: Percentage of fatal crashes in rollover accidents.

Generally speaking, vehicle rollovers can be categorized into three types: the on-road rollover, the tripped rollover, and the run-off-road rollover. An on-road rollover is usually induced by a severe maneuver input, such as a fish-hook turning. Tripped rollover refers to a rollover accident caused by the vehicle's sideward collision with the road curb, or being tripped in soft soil while side skidding. In a run-off-road rollover accident, the vehicle is tilted to an unstable effective roll angle as a result of departing the paved roadway and running on the side slope.

On-road rollovers are highly unlikely to happen on heavy-duty buses. One of the necessary conditions for an on-road rollover to happen is that the lateral tire forces must be able to produce a lateral acceleration level that is higher than the vehicle's rollover

threshold[1]. Buses usually feature relatively low centers of gravity, wide track widths, and can maintain roll stability at moderate levels of lateral acceleration. The expected rollover threshold of buses is well over 0.6 g, while the peak lateral acceleration typical truck/bus tires can achieve is only around 0.5~0.6 g (Diaz et al. 2004; Fancher and Mathew 1987; Kulakowski et al. 2003). Therefore, when a bus is exposed to a high lateral acceleration caused by an improper maneuver, the vehicle is more likely to skid on the road than ending up with an on-road rollover. A review of National Transportation Safety Board (NTSB) accident reports (NTSB 1998-2005) from 1985 to 2004 reveals that most of the bus rollover accidents belong to either the tripped rollover or the run-off-road rollover, and the major cause leading to bus rollovers is loss of yaw stability under critical maneuvers or panic situations. This finding agrees with the conclusions in previous studies (Marine et al. 1999; NHTSA 2000; Parenteau et al. 2001). An accident analysis on a serious bus rollover that occurred in 1999 near Canon City, Colorado is provided below as an example.

The 59-passenger motor coach was traveling eastbound on State Highway 50 at 63mph along a 7-mile-long downgrade west of Canon City, Colorado, when it began to fishtail while negotiating a curve. The motor coach gained speed as it descended the mountain. Approximately 36 seconds later, the driver lost control of the vehicle on a curve. The motor coach drifted off the right side of the road, struck a mile post and a delineator, returned to the road, rotated clockwise 180 degrees toward the centerline, and

---

[1] According to ISO 16333:2004, rollover threshold is defined as the limit of lateral acceleration (usually in g unit) that a vehicle can sustain without rolling over.

departed the north side of the roadway backward. The vehicle then rolled at least 1.5 times down a 40-foot-deep embankment and came to rest on its roof. The driver and 2 passengers were killed; 33 passengers sustained serious injuries and 24 sustained minor injuries. The National Transportation Safety Board has determined that the probable cause of this accident was the motor coach driver's inability to control his vehicle under the icy conditions of the roadway (NTSB 2002).

As illustrated by the accident, yaw stability and roll stability are coupled, because when yaw instability occurs, roll stability is threatened. Yaw divergence may cause uncontrollably lateral motions for the bus, which ultimately lead the vehicle to strike an obstacle, slide into another vehicle, or leave the road, possibly resulting in a rollover. Moreover, according to the statistical data (Matteson et al. 2004; Matteson et al. 2005; Shrank et al. 2005) from CNTB (Center for National Truck and Bus Statistics), at least 20% of the fatal bus accidents could be related to the yaw-stability problem.

In addition, among all the 227 traffic accident reports published on the NTSB database since 1967 (NTSB), about 30% involve buses. It implies that bus accidents always attract high public attention because of their severity (similar to aircraft accidents), even though the number is rather small in comparison with that of passenger cars. Furthermore, as the number of buses has been steadily increasing with an annual rate of 1-2% in the last ten years (BTS 2005), the probability for the occurrence of bus accidents are also rising. Taking a broader view, accidents on public commuting media, such as buses, would also shake the public faith on the overall transportation system.

According to the above discussion, loss of yaw control constitutes a serious safety problem for buses. Therefore, enhancing yaw control will significantly improve the safety level of buses as well as that of the overall transportation system.

1.2 The Necessity of the Active Steering System

It is difficult and sometimes impossible for a human driver to maintaining yaw control for a vehicle under extreme environmental conditions. Actually, the driver's natural deficiency is one of the primary causes for the traffic accidents (Liebemann et al. 2005; Palkovics 2001). The yaw motion of a vehicle can be disturbed by asymmetric braking, variations of tire-road friction, or side-wind gust. Under such critical situations, the handling behavior of the vehicle is rather different from what the driver expects. When caught in such situations, many drivers, especially inexperienced and/or fatigued drivers, tend to panic and overreact thus destabilizing the vehicle (Sienel 1997). Furthermore, a driver needs at least 0.5 seconds before he/she can react to unexpected yaw motions (Ackermann 1996). During this period the uncontrolled vehicle may produce a dangerous yaw rate and side-slip angle, which even an experienced driver is not able to handle.

To assist the human driver in maintaining yaw control, it is very natural to consider the use of automatic control systems. Recent reports suggest that driver-assistance systems can prevent up to 40% of traffic accidents (Gietelink et al. 2006; Tingvall et al. 2003). Further, such systems may reduce driver fatigue, compensate for

human error (Stanton and Marsden 1996), and bridge over the slow reaction time of the human driver (Ackermann and Bunte 1996).

One example of a driver-assistance system is active steering system, which provides a practical approach to improve driving safety under emergency situations (Ackermann 1996; Reiger et al. 2005; Sienel 1997; Svenson and Hac 2005; van Zanten 2001). Generally speaking, an active steering system assists driver in vehicle handling by automatically producing a compensating moment to suppress yaw instability, such that the vehicle can stay maneuverable to the driver in presence of the disturbances, such as variation in tire-road friction, and side-wind gust.

Due to the large size and weight, the heavy-duty bus has several "flaws" in its handling characteristics, which necessitates the development of an active steering system for buses.

1. Owing to the high center of gravity and large axle load, the load transfer effect on the variation of tire cornering stiffness is very significant on buses, even in low lateral acceleration maneuvers. A large load transfer during cornering considerably lowers the effective cornering capability of a bus, thus making it very difficult for the driver to contain yaw stability of the vehicle when subject to external disturbances.

2. Heavy-duty buses have a highly unbalanced front-rear weight distribution. According to a transit bus axle-weight study (Kulakowski et al. 2002), the rear-axle weight of a 40-foot bus can be over twice that of the front axle, while the effective cornering stiffness of the rear axle is usually less than twice that

of the front axle. This property is likely to cause oversteer for the bus, which is an unfavorable vehicle handling characteristic. Consequently buses are more easily to be caught in spin-out than other types of passenger vehicles under the same operating condition.

3. Being the longest and heaviest single unit vehicle, a heavy-duty bus has a very large yaw-moment of inertia resulting in a soggy yaw response. This characteristic consequently requires a bus driver to react more quickly and accurately to the emerging situations than a car driver, because the bus probably is not swift enough to respond to a second correction should the first one not prevent an accident.

4. The inertial properties of a bus, such as mass, moment of inertia, axle-weight distribution, vary over a wide range during daily operation. These variations may significantly change the yaw dynamics of the bus. To adapt to such changes would definitely increase the work load of bus drivers.

Besides the inherited vehicle-handling characteristics, bus safety is also closely associated with the working environment of the driver. Bus drivers face a monotonous working environment filled with fatigue and stress. Fatigue ultimately can deteriorate the safety of the bus, if the operating errors from a fatigued driver cannot be properly compensated.

Based on the above arguments, bus is a suitable candidate for pioneering the active steering system.

1.3 Literature Survey on Active Steering Control - Differential Braking Control and Active Front-Wheel Steering

The early research on steering control was motivated by the concept of "Electric Highway" in 1950's. "Electronic Highway" is the archetype of today's Automated Highway System (AHS). The first published work on steering control was implemented by General Motors and RCA in the late 1950's (Gardels 1960; Shladover 1995). Currently there are two branches in steering control research, "automatic steering" and "active steering". The automatic steering system is analogous to the autopilot on the airplane. Its primary function is automatic lane following according to the road reference signals without involving human drivers. The concept of active steering is different from creating a fully autonomous vehicle where the vehicle relies purely upon automatic control systems and the driver becomes merely a passenger. The major task of an active steering system, as discussed in the last section, is to prevent the vehicle from exhibiting unintended behaviors when subject to disturbances and to assist the driver in maintaining yaw control in emergency situations. Under the approach of active steering, the human driver still commands the vehicle. An active steering system interprets the driver's intention by monitoring his/her driving activities, and then regulates vehicle motions according to the driver's intention if necessary.

"Automatic steering" and "active steering" are just two practical terms. The essential differences between these two systems are nonetheless ambiguous, and research studies for these two types of steering systems are interrelated. The survey provided in this thesis focuses on the development active steering systems.

The idea of using active steering control was first practiced in Bendix company during late 1960's to "automatically correct for lateral disturbance caused aerodynamics, road, inertial forces, or vehicle-component malfunctions such as brake pull or tire blow-out" (Kasselmann and Keranen 1969). The structure of the control system is shown in Figure **1-2**. During their research, Kasselmann and Keranen also discovered that "yaw rate is the best control variable for automobile directional control".
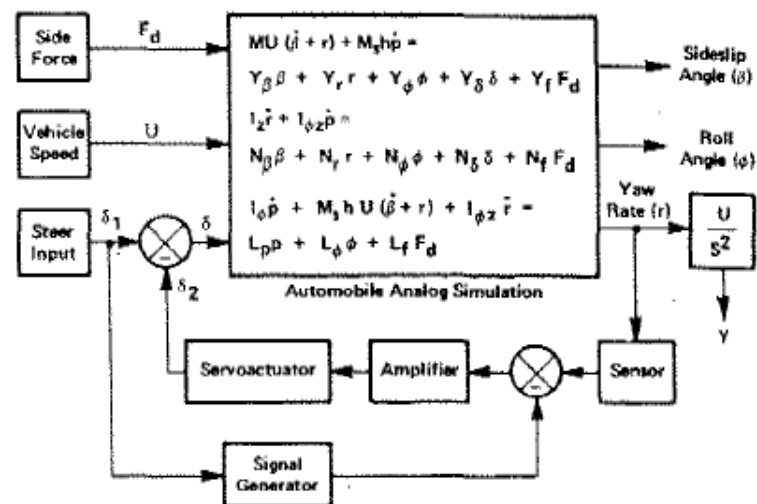
Figure **1-2**: Adaptive steering system (Kasselmann and Keranen 1969)

The research on active steering control was very active in the 1990's due to the large number of systems under development. Extensive reviews on the development of active steering systems can be found in various articles (Furukawa and Abe 1997; Palkovics 2001; Shladover 1995; Tomizuka and Hedrick 1995).

On heavy-duty vehicles, three main techniques were used to implement active steering control. One is to correct the driver's steering by actuating the front road wheels. This technique is referred to as Front-Wheel Steering control (Ackermann et al.

1995; Hingwe et al. 2000). The second technique is to develop a steering moment by introducing difference in braking forces between the right and left sides of the vehicle. This asymmetric braking technique is referred to as Differential Braking Control (DBC) or Direct Yaw-Moment Control (DYC) (Hecker et al. 1997; Winkler et al. 1999). The third one is to generate an additional steering moment at the rear axle by steering the rear wheels according to the steering input at the front wheels, known as Rear-Wheel Steering (RWS) or 4-Wheel Steering (4WS) (de Bruin 2001; LeBlanc and El-Gindy 1992).

Among these three techniques, 4WS provides advantages in high-speed stability and low-speed maneuverability (Furukawa et al. 1989). Unfortunately, the complexity and high implementation cost of 4WS have hampered its wide application on production vehicles (Hebden et al. 2004; Jiang et al. 2000; Selby et al. 2001). For heavy-duty buses, 4WS is particularly unsuitable, because steering the dual-tire rear wheels along with heavy axle load requires an impractically large steering effort. Furthermore, many of the transit buses are RR (rear-engine, rear drive) and low floor, leaving very limited space for installing the actuating system at the rear axle. Computer simulation results even suggested that, 4WS is only as good as front-wheel steering theoretically (Alleyne 1997a; Jiang et al. 2000).

Due to the complexity of 4WS and the then difficulty in designing a fault-tolerant front-wheel steering system, differential brake control (DBC) has become the most widely used active steering system during the last ten years. A DBC system developed by Bosch company, known as the ESP (electronic stability program), has been produced for more than 10 millions sets since 1995 (Liebemann et al. 2005). One of the major

advantages of DBC is its ease of implementation through the existing ABS actuators, since it can use the available functions of braking and traction control components (van Zanten 2001; van Zanten et al. 1995). DBC also has a superior performance in vehicle stabilization under limit driving conditions when the lateral tire force is near saturation or already saturates (Abe et al. 1995). However, the effect of DBC is limited under some commonly seen difficult driving situations, such as split-μ driving/braking, since the maximum braking forces on the two sides of the vehicle are different (Zeyada et al. 1998). In addition, a braking maneuver on split-μ or low-friction surfaces may cause the vehicle to deviate from the driver's intended direction, requiring a prompt steering input to maintain a straight line trajectory. When these situations arise unexpectedly, especially while traveling at high speeds, they can put the vehicle and drive in danger (Hebden et al. 2004). Another obvious shortcoming of DBC is the possible reduction of the total braking force (Zeyada et al. 1998). In an emergency situation the DBC controller would partially release the brakes on one side of the vehicle resulting a longer stopping distance than if maximum brake forces are applied at all wheels (this is probably acceptable if a collision can be avoided by the turning maneuver). Also, most drivers regulate their steering inputs based on the expected deceleration due to the braking, but with DBC in operation, the driver might encounter unexpected changes of vehicle speed that could lead to erratic steering. This behavior has been reported by professional drivers in tests of some DBC systems (Frank 1996).

In recent years, the technology for front-wheel steering control has shown remarkable development (Kojo et al. 2005). There exist two common approaches to

implement the front-wheel steering control. One is called steer-by-wire (SBW), the other is named active front-wheel steering (AFS).

In a steer-by-wire system, the steering wheel commands from the driver are transmitted electronically to the actuators, which will then steer the road wheels. The steering wheel is no longer mechanically connected to the road wheels in a steer-by-wire system. The absence of the mechanical connections in the steering system offers great flexibilities in both handling-characteristic modifications and structure design for a vehicle. However, there are two major concerns about steer-by-wire design, which limit the practical industrial applications of this technology.   Since steer-by-wire system removes the mechanical connections in the steering system, the driver will (1) totally lose steering control when a fault situation occurs to the system; (2) lose haptic interaction between the road wheels and the steering wheel, generally known as road feel, which is transmitted to the driver through the steering column.

The AFS (active front-wheel steering) system realizes front-wheel steering control by superimposing an "active angle" to the steering-wheel input from the driver as shown in Figure **1-3** (Reinelt et al. 2004).   Unlike steer-by-wire, the AFS system is distinguished by a permanent mechanical connection between the steering wheel and road wheels, owing to an innovative design of the planetary gear set. With the retained mechanical connection, AFS mitigates the concerns about maintaining steering control in a fault condition and haptic interactions between the driver and the road. As an advanced driver-assistance system, AFS has already been successfully applied to production vehicles (Krenn and Richter 2004).
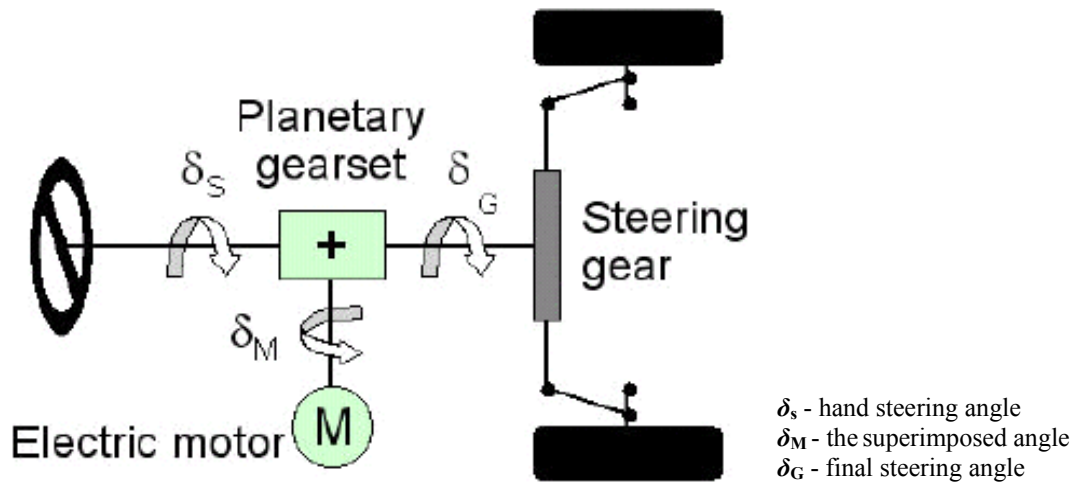
Figure **1-3**: A diagram for AFS

The AFS system has attractive benefits on vehicle handling improvement, and is more efficient with regard to tire usage (Ackermann et al. 1999; Alleyne 1997a; Alleyne 1997b). AFS can be used to effectively reject yaw as well as roll disturbances that rise from split-μ running, asymmetric braking, wind forces, even under decreased road adhesion conditions (Ackermann 1996). Heizl concurred with Ackermann's opinions: "when large braking forces need to be applied at a high lateral acceleration for instance emergency braking while cornering, an interference of the ABS and the demand to stabilize the vehicle motion by unilateral braking may be unavoidable. In this respect, additional steering of front or rear wheels can help to overcome such adverse effects in particular" (Heinzl et al. 2002). Hayama et al. compared the performance of yaw-disturbance attenuation during split-μ braking for DBC and AFS systems on instrumented vehicles (Hayama et al. 2000). The comparison results suggested that AFS is superior to DBC regarding direction control. More recently, Segawa et al. demonstrated that AFS could achieve greater yaw stability for vehicles than DBC in not only split-μ braking, but

also in side-wind disturbance running and lane change on low-friction roads (Nakano et al. 2000; Segawa et al. 2002).

One further advantage of AFS is that it requires less front wheel tire force compared to DBC. As illustrated by Figure 1-4, for a 40-foot bus, the steering moment arm for AFS is usually four times that of DBC. For simplification, it is assumed that the maximum longitudinal force and lateral force from the tire are the same, denoted by F. The available steering torque is $3F{\cdot}a$ from DBC wheel braking, and $8F{\cdot}a$ from AFS. In other words, comparing to DBC, AFS requires only about 40% of the front-wheel tire force to generate the same amount of corrective torque.
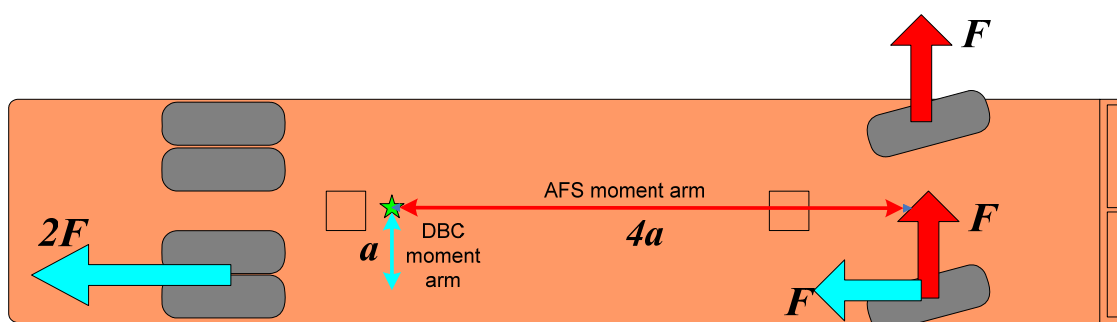
Figure **1-4**: Tire force requirement in yaw disturbance rejection: differential braking vs. front-wheel steering

One of the major weaknesses of AFS is that it is not very effective when the vehicle is experiencing a high lateral acceleration. The steering control depends on tire lateral forces. Under high lateral acceleration situations, the lateral tire forces will saturate due to inherent nonlinear characteristics of pneumatic tire forces. As a result, the steering wheels cannot generate enough correction moment to maintain vehicle stability.

To summarize the previous discussion, AFS and DBC are two types of active steering systems applicable in different operating ranges (Mokhiamar and Abe 2002; Selby et al. 2001; Yamamoto 1991; Zeyada et al. 1998). The AFS is effective in the operating range where the lateral tire forces are not near saturation, and it aims to help the driver to avoid dangerous situations. The task of the AFS is to enhance the maneuverability and stability of the vehicle subject to disturbances, such as side-wind gust, split-μ, and roadway irregularities. The DBC should be applied to improve the stability of the vehicle when AFS becomes less effective in limit lateral condition, i.e. when the lateral tire forces are close to or past saturation.

The maximum lateral acceleration level that vehicles normally experience is determined by the roadway design (geometry and speed limit). In North America, the lateral acceleration a vehicle experiences is usually less than 0.2 g. The highest designed lateral acceleration on European highways can range from 0.3 to 0.4 g (Roland 1983). These lateral acceleration levels are well below the lateral traction a bus tire can provide on the dry road (0.65 g). Therefore, the lateral stability of a bus in normal driving situations is ensured by roadway design. However, yaw instability of buses usually results from abnormal yaw disturbances caused by collisions or collision avoidance, side wind forces, unilateral loss of tire pressure, μ–split braking, or road-friction variations. The unanticipated vehicle motions in these situations are likely to cause improper driver maneuvers, which will ultimately lead accidents. According to the survey, AFS appears more suitable a choice for dealing with these critical situations than DBC. In addition, as illustrated by Figure **1-4**, front-wheel steering should be especially attractive for bus

applications. Since the distance between the front-wheel center and the C.G. (center of gravity) is usually more than twice of the track width for a heavy-duty bus, the correction torque generated by front-wheel steering could be nearly four times that from differential braking. Therefore, in this thesis research AFS is selected as the active steering control device for the buses.

1.4 Scope of the Research

Designing an active steering system is a very broad subject. It is a system engineering involving many technologies, such as vehicle stabilization, system integration, driver-intention detection, system safety, driver-vehicle interaction, and hardware implementation. The work conducted under this thesis research has focused only on developing control algorithms for the functions of vehicle stabilizing and external disturbance attenuation. Some of the neglected aspects are briefly discussed in the chapter 8.

1.5 Objectives

In light of the foregoing discussions on bus accidents and active steering systems, an AFS (active front-wheel steering) system will be developed for buses with the following primary objectives:

1. Explore the handling characteristics of buses. Compared to other types of vehicles such as passenger cars and heavy-duty trucks, studies on buses are

seldom found in literatures regarding handling characteristics. Thus, an investigation in this area is necessary to characterize typical handling characteristics for buses, and study how an active safety system can help the bus driver in vehicle handling.

2. Propose an AFS (active front-wheel steering) control algorithm for specific application to buses. The algorithm will focus on rejecting external disturbances caused by side-wind or split-μ, and will address robustness problems caused by the uncertainties in vehicle parameters and the variations in tire-road friction.

1.6 Contributions of the Thesis

1. Promote bus-accident study and determine yaw instability is one of the major causes for bus accidents.

2. Conduct a comprehensive research on handling characteristics for buses both experimentally and analytically – Historically, little research has been done for buses. According to a thorough survey conducted during the past four years, only about fifty papers or technical reports on bus handling characteristics have been published within the last thirty years. The bus handling study performed under this thesis provides an insight into the handling characteristics of modern buses and shows that the handling characteristics of buses are significantly different from those of both passenger cars and heavy-duty trucks.

3. Obtain vehicle dynamics models, and identify vehicle parameters for a 40-foot transit bus. Although mathematically, the bus model is very similar to the car

model, there still exist notable differences, such as the linear operating range and the effect of roll dynamics. A commonly seen mistake in modeling tire cornering stiffness on low-friction surfaces is also addressed during vehicle dynamics modeling process.

4. Develop a robust AFS (active front-wheel steering) system to enhance yaw stability for buses - "The application of advanced, electronically controlled systems in commercial vehicles somehow has not been as fast as in the passenger cars in the past" (Palkovics 2001). This statement is especially true for buses. While the last two decades have witnessed tremendous commercial growth in and development of active safety system for other types of vehicles, very few studies that focus on the steering control of buses were found in the literature (Ackermann et al. 1995; de Bruin 2001; Hingwe and Tomizuka 1996). In addition, most of the publish works on AFS controller design tend to practice sophisticated design technologies, such as two degree-of-freedom H_∞ design and feedback linearization. In this thesis, an AFS system is developed using a simple controller structure that is more likely to bridge the current practice (e.g. no active safety whatsoever) to the use of a control solution. The system is proved to be very effective in enhancing yaw-stability for buses under difficult driving conditions.

1.7 Thesis Outline

The remaining of this thesis is organized as follows:

Chapter 2 discusses various issues regarding vehicle dynamics modeling. A linear 2-DOF (two degree-of-freedom) model, a linear 3-DOF model, and a nonlinear 3-DOF model are developed and compare to each other. The comparison results will be used to facilitate proper selections of vehicle models for controller design and simulation in the future chapters. In particular, vehicle modeling under low-friction condition is discussed. A modeling error commonly seen in the publications is addressed.

Chapter 3 introduces a fundamental concept on vehicle handling, understeer versus oversteer. The definition of understeer/oversteer is provided, followed by the implications of this steady-state vehicle handling property on transient responses.

Chapter 4 presents the experimental results from the bus-handling study conducted at PTI from 2004 to 2006. The data from a series of field tests demonstrate that bus handling properties are significantly different from those of cars and trucks. The vehicle-parameter identification results are also presented in this chapter.

Chapter 5 discusses the effects of loading conditions on the yaw-rate response of buses. Since a bus would experience significant loading changes during its daily operation, it is of interest to see how these operational changes influence the yaw-rate response. The study concludes that the variation of loading condition has only minor effects on yaw-rate response of a bus during normal operation, and thus can be mostly neglected in linear controller design.

Chapter 6 introduces the design process of a PI (proportional-integral) controller for the AFS system. Computer simulation results from the controller-evaluation tests on a 40-foot transit bus will also be presented in this chapter.

Chapter 7 introduces an advanced AFS controller designed with a modern H_∞ loop-shaping technique. A comparison between the PI controller and the H_∞ loop-shaping is then performed. The results suggest that the two controllers perform similarly in enhancing yaw stability for a 40-foot transit bus. This similarity in results motivates a selection of the PI controller for its simplicity in structure and implementation.

Chapter 8 summarizes the main results of this thesis and provides some suggestions for the future research work.

References

1. Abe, M., Ohkubo, N., and Kano, Y. (1995). "Comparison of 4WS and direct yaw moment control for improvement of vehicle handling performance." *JSAE Review*, 16(2).

2. Ackermann, J. (1996). "Robust control prevents car skidding." *IEEE*.

3. Ackermann, J., and Bunte, T. (1996). "Automatic car steering control bridges over the driver reaction time."

4. Ackermann, J., Bunte, T., and Odenthal, D. (1999). "Advantage of active steering for vehicle dynamics control."

5. Ackermann, J., Sienel, W., and Steinhauser, R. (1995). "Robust automatic steering of a bus." *Proceedings of the Second European Control Conference*.

6. Alleyne, A. (1997a). "A comparison of alternative intervention stratagies for unintended roadway departure control." *Vehicle System Dynamics*, 27.

7. Alleyne, A. (1997b). "A comparison of alternative obstacle avoidance strategies for vehicle control." *Vehicle System Dynamics*, 27.

8. BTS. (2005). "Bus Fuel Consumption and Travel."

9. de Bruin, D. (2001). "Lateral Guidance of All-Wheel Steered Multiple-Articulated Vehicles," Technology University Eindhoven.

10. Diaz, V., Fernandez, M. G., Roman, J. L. S., Ramirez, M., and Garcia, A. (2004). "A new methodology for predicting the rollover limit of buses." *International Journal of Vehicle Design*, 34(4).

11. Fancher, P. S., and Mathew, A. (1987). "A vehicle dynamics handbook for single-unit and articulated heavy trucks." UMTRI.

12. Frank, M. (1996). "Stability enhancement systems: trick or treat?" *Car and Driver*, June.

13. Furukawa, Y., and Abe, M. (1997). "Advanced chassis control system for vehicle handling and active safety." *Vehicle System Dynamics*, 28.

14. Furukawa, Y., Yuhara, N., Sano, S., Takeda, H., and Matsushita, Y. (1989). "A review of four-wheel steering studies from the viewpoint of vehicle dynamics control." *Vehicle System Dynamics*, 18.

15. Gardels, K. (1960). "Automatic car controls for electronic highway." *Report GMR-276*, GMR General Motors Corp., Warren, MI.

16. Gietelink, O., Ploeg, J., de Schutter, B., and Verhaegen, M. (2006). "Development of advanced driver assistance systems with vehicle hardware-in-loop simulations." *Vehicle System Dynamics*, 44(7).

17. Hayama, R., Nishizaki, K., Nakano, S., and Katou, K. (2000). "The vehicle stability control responsibility improvement using steer-by-wire." *Proceedings of the IEEE Intelligent Vehicle Symposium 2000*.

18. Hebden, R. G., Edwards, C., and Spurgeon, S. K. (2004). "Automotive steering control in a split-mu mavoeuvre using an observer-based sliding mode controller." *Vehicle System Dynamics*, 41(3).

19. Hecker, F., Hummel, S., Jundt, O., Leimbach, K. D., Faye, I., and Schramm, H. (1997). "Vehicle dynamics control for commercial vehicles." *SAE 973284*.

20. Heinzl, P., Lugner, P., and Plochl, M. (2002). "Stability control of a passenger car by combined additional steering and unilateral braking." *Vehicle System Dynamics*, suppl 37.

21. Hingwe, P., and Tomizuka, M. (1996). "Experimental study of chatter free sliding model control for lateral control of commuter buses in AHS." *UCB-ITS-PRR-96-31*.

22. Hingwe, P., Wang, J. Y., Tai, M. H., and Tomizuka, M. (2000). "Lateral control of heavy duty vehicles for automated highway system: experimental study on a tractor semi-trailer." *UCB-ITS-PWP-2000-1*.

23. Jiang, L., Wang, Y. Q., and Nagai, M. (2000). "A theoretical study on front steering angle compensation control for commercial vehicles." *The Proceedings of 2000 FISITA World Automotive Congress*.

24. Kasselmann, J., and Keranen, T. (1969). "Adaptive steering." *Bendix Technical Journal*, 2.

25. Kojo, T., Suzumura, M., Tsuchiya, Y., and Hattori, Y. (2005). "Development of active front steering control system." *SAE 2005-01-0404*.

26. Krenn, M., and Richter, T. (2004). "Active Steering - BMW's approach to modern steering technology."

27. Kulakowski, B., El-Gindy, M., Hoskins, A., Yu, N., and Chae, S. K. (2002). "Transit Bus Axle-Weight Study." The Pennsylvania Transportation Institute.

28. Kulakowski, B. T., Muthiah, M., and Yu, N. (2003). "Effects of weight on performance of transit vehicles." *Proceedings Of International Symposium on Heavy Vehicle Weight and Size*.

29. LeBlanc, P. A., and El-Gindy, M. (1992). "Directional stability of a straight truck equipped with a self-steering axle." *International Journal of Vehicle Design*, 12.

30. Liebemann, E. K., Meder, K., Schuh, J., and Nenninger, G. (2005). "Safety and performance enhancement: the Bosch electronic stability control (ESP)."

31. Marine, M., Wirth, J., and Thomas, T. (1999). "Characteristics of on-road rollovers." *SAE 1999-01-0122*.

32. Matteson, A., Blower, D., and Hershberger, D. (2004). "Buses Involved in Fatal Accidents Factbook 2000." Center for National Truck and Bus Statistics, University of Michigan Transportation Research Institute.

33. Matteson, A., Blower, D., Hershberger, D., and Woodrooffe, J. (2005). "Buses Involved in Fatal Accidents Factbook 2001." Center for National Truck and Bus Statistics, University of Michigan Transportation Research Institute.

34. Mokhiamar, O., and Abe, M. (2002). "Active wheel steering and yaw moment control combination to maximize stability as well as vehicle responsiveness during quick lane change for active vehicle handling safety." *IMechE D08101*.

35. Nakano, S., Takamatsu, T., Nishihara, O., and Kumamoto, H. (2000). "Steering control strategies for the steer-by-wire system." *Transactions of JSAE*, 31(2).

36. NHTSA. (2000). "http://www-nrd.nhtsa.dot.gov/vrtc/ca/rollover.htm."

37. NHTSA. (2002). "Traffic Safety Facts 2001." National Highway Traffic Safety Administration.

38. NHTSA. (2003). "Traffic Safety Facts 2002." National Highway Traffic Safety Administration.

39. NHTSA. (2004). "Traffic Safety Facts 2003." National Highway Traffic Safety Administration.

40. NHTSA. (2005). "Traffic Safety Facts 2004." National Highway Traffic Safety Administration.

41. NTSB. "National Transportation Safety Board Highway Accidents Publications."

42. NTSB. (1998-2005). "National Transportation Safety Board Highway Accidents Publications."

43. NTSB. (2002). "Highway Accident Brief - Accident No. HWY-00-FH011." National Transportation Safety Board.

44. Palkovics, L. (2001). "Intelligent electronic systems in commercial vehicles." *Vehicle System Dynamics*, 35(4).

45. Parenteau, C., Thomas, P., and Lenard, J. (2001). "US and UK field rollover characteristic." *SAE 2001-01-0167*.

46. Reiger, G., Scheef, J., Becker, H., Stanzel, M., and Zobel, R. (2005). "Active safety systems change accident environment of vehicle significantly - a challenge for vehicle design."

47. Reinelt, W., Klier, W., Reimann, G., Schuster, W., and Grossheim, R. (2004). "Active front steering (part 2): safety and functionality." *SAE 2004-01-1101*.

48. Roland, M. A. (1983). "Some aspects on suspension design parameters for improve vehicle response at the limit of adhesion." *IMechE C115/83*.

49. Segawa, M., Nishizaki, K., and Nakano, S. "A study of vehicle stability control by steer by wire system." *Proceedings of the International Symposium on Advanced Vehicle Control 2000*, Ann Arbor, MI.

50. Selby, M., Manning, W. J., Brown, M. D., and Crolla, D. A. (2001). "A coordination approach for DYC and active front steering." *SAE 2001-01-1275*.

51. Shladover, S. E. (1995). "Review of the state of development of advanced vehicle control systems (AVCS)." *Vehicle System Dynamics*, 24.

52. Shrank, M., Matteson, A., Hershberger, D., and Woodrooffe, J. (2005). "Buses Involved in Fatal Accidents 2002." Center for National Truck and Bus Statistics, University of Michigan Transportation Research Institute.

53. Sienel, W. (1997). "Estimation of the tire cornering stiffness and its application to active car steering." *Proceedings of the 36th Conference on Decision & Control*.

54. Stanton, N. A., and Marsden, P. (1996). "From fly-by-wire to drive-by-wire: Safety implications by vehicle automation." *Safety Science*, 24(1).

55. Svenson, A. L., and Hac, A. (2005). "Influence of chassis control systems on vehicle handling and rollover stability."

56. Tingvall, C., Krafft, M., Kullgren, A., and Lie, A. (2003). "The effectiveness of ESP in reducing real life accident." *ESV Conference 2003*.

57. Tomizuka, M., and Hedrick, J. K. (1995). "Advanced control methods for automotive applications." *Vehicle System Dynamics*, 24.

58. van Zanten, A. T. (2001). "Bosch ESP systems: 5 years of experience." *SAE 2000-01-1633*.

59. van Zanten, A. T., Erhardt, R., and Pfaff, G. (1995). "VDC The vehicle dynamic control system of Bosch." *SAE 950759*.

60. Winkler, C. B., Fancher, P. S., and Ervin, R. D. (1999). "Intelligent systems for aiding the truck driver in vehicle control." *SAE 1999-01-1301*.

61. Yamamoto, M. (1991). "Active control strategy for improved handling and stability." *SAE 911902*.

62. Zeyada, Y., Karnopp, D., El-Arabi, M., and El-Behiry, E. (1998). "A combined active-steering differential-braking yaw rate control strategy for emergency maneuvers." *SAE 980230*.

Chapter 2

Vehicle Dynamics Modeling

In the process of system analysis or controller design for a physical system, trade-offs are usually necessary between modeling accuracy and mathematical complexity. An extremely accurate model often requires large computational effort that might be too excessive for system analysis and controller-design purposes (Armstrong 1993). Furthermore, many of the most widely used controller-design techniques work best for moderate-order, linear, time-invariant design models (Maciejowski 1989). In practice, a high-order nonlinear model is usually linearized about an operating point to obtain a simplified linear model that conforms to computational limitations or controller-implementation constraints.

The rest of this chapter is organized as follows: First, nonlinear two degree-of-freedom (2-DOF) and 3-DOF vehicle models are introduced. Secondly, linear 3-DOF and 2-DOF vehicle models are derived from the nonlinear vehicle model and compared to each other. The linear 2-DOF model will be selected as the nominal model for controller design. Detailed discussion of the modeling issues under various situations is provided. A commonly seen yet inappropriate modeling practice is also brought up and clarified. Thirdly, the linear 2-DOF model is compared to the 3-DOF nonlinear model. As will be shown, the linear model can approximate the nonlinear model up to a lateral acceleration level around 0.2 g for a heavy-duty bus - this level sets a difference between

buses and passenger cars. Finally, the implications from the modeling perspective on controller design are presented.

2.1 Nonlinear Models

2.1.1 Coordinate System

The vehicle motions are defined with reference to a vehicle-fixed (local) right-hand orthogonal coordinate system, which originates at C.G. (center of gravity) and travels with the vehicle. As shown in Figure **2-1,** the sign convention for the coordinates by SAE (SAE 1976) are:

- X – parallel to the road surface, forward and on the longitudinal plane of symmetry
- Y – parallel to the road surface and lateral out the right side of the vehicle
- Z – vertical to the road surface and downward with respect to the vehicle
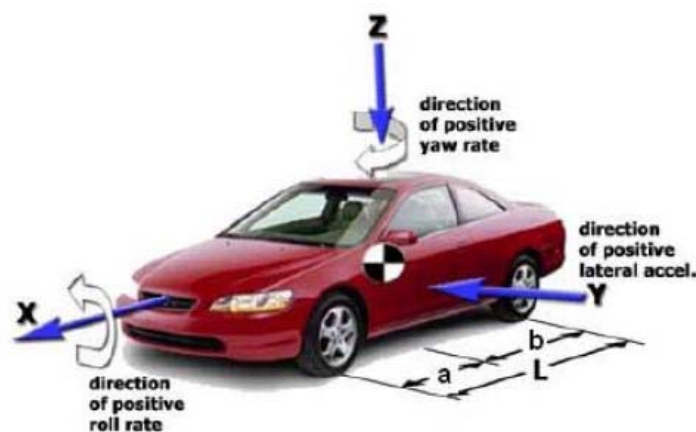
Figure **2-1**: SAE sign convention for vehicle fixed the coordinate system

2.1.2 Two Degree-Of-Freedom Model

As a common practice, the vehicle's handling dynamics can be represented by a two degree-of-freedom single track model, known famously as the 'bicycle model' (Milliken and Milliken 1995) shown in Figure **2-2**. The bicycle model describes the vehicle motions in the yaw plane, which is parallel to the road surface. The state variables of the vehicle model are sideslip angle (β) measured at the center of gravity (C.G.) and yaw rate (r). The following assumptions are made for the 2-DOF bicycle model:

- No lateral load transfer

- No longitudinal load transfer

- No rolling, pitching and bouncing motions of the body

- Constant forward vehicle speed

- No aerodynamic effects

- No chassis or suspension compliance effects
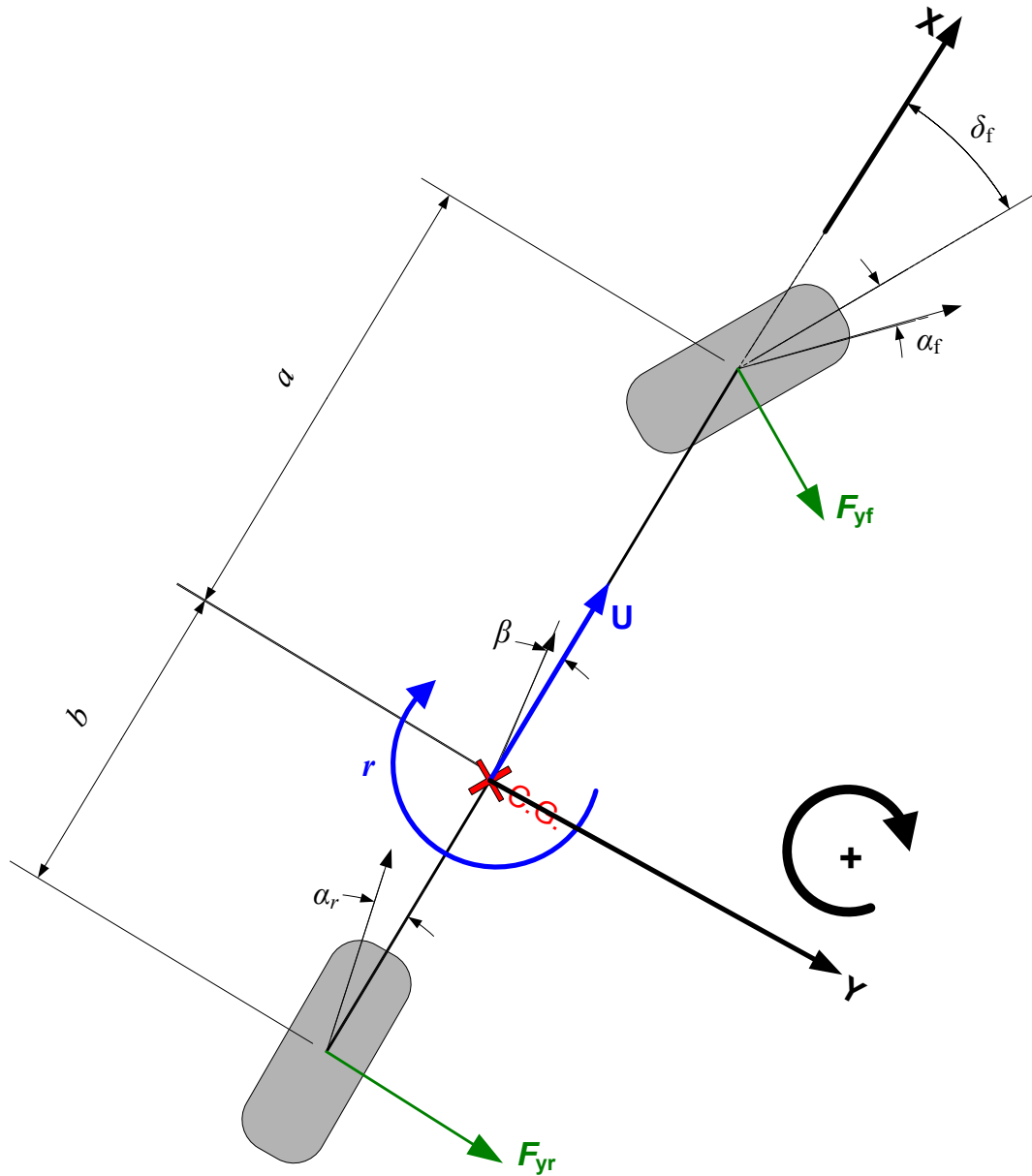
Figure **2-2**: Two degree-of-freedom vehicle dynamics model (Bicycle Model).

a	distance from C.G. to front tire center
b	distance from C.G. to rear tire center
F_{yf}	lateral tire force by the front tire
F_{yr}	lateral tire force by the rear tire

I_{zz} yaw moment of inertia

m mass of the vehicle

U vehicle speed

r yaw rate

α_f front-tire slip angle (**Appendix B**)

α_r rear-tire slip angle

β side-slip angle of the vehicle at C.G.

δ_f steering angle of the front wheel

Derivation of the equations of motion for the bicycle model follows from the force and moment balance as follows:

$$mU \cdot (\frac{d}{dt}\beta + r) = F_{yf} + F_{yr}$$

$$I_{zz} \cdot \frac{d}{dt}r = (aF_{yf} - bF_{yr})$$

or   **(2.1)**

$$\frac{d}{dt}\begin{pmatrix} \beta \\ r \end{pmatrix} = \begin{pmatrix} \dfrac{F_{yf} + F_{yr}}{mU} - r \\ \dfrac{aF_{yf} - bF_{yr}}{I_{zz}} \end{pmatrix}$$

The nonlinear characteristics of the lateral tire forces F_{yf} and F_{yr} are modeled using the Magic Tire Formula (Bakker et al. 1989). The relation between lateral force F_y and slip angle α is presented both analytically and graphically in Eq. **2.2** and Figure **2-3**, respectively.

$$F_{yi} = D_y \sin\{C_y \tan^{-1}[B_y\alpha_i - E_y(B_y\alpha_i - \tan^{-1}(B_y\alpha_i))]\}$$

$$i = f, r$$ **(2.2)**

where B_y, C_y, D_y, E_y are constant coefficients, and the tire-slip angles α_f and α_r are calculated using the following formulae:

$$\alpha_f = \tan^{-1}(\beta + \frac{a}{U} \cdot r) - \delta_f$$

$$\alpha_r = \tan^{-1}(\beta - \frac{b}{U} \cdot r)$$

$$(2.3)$$
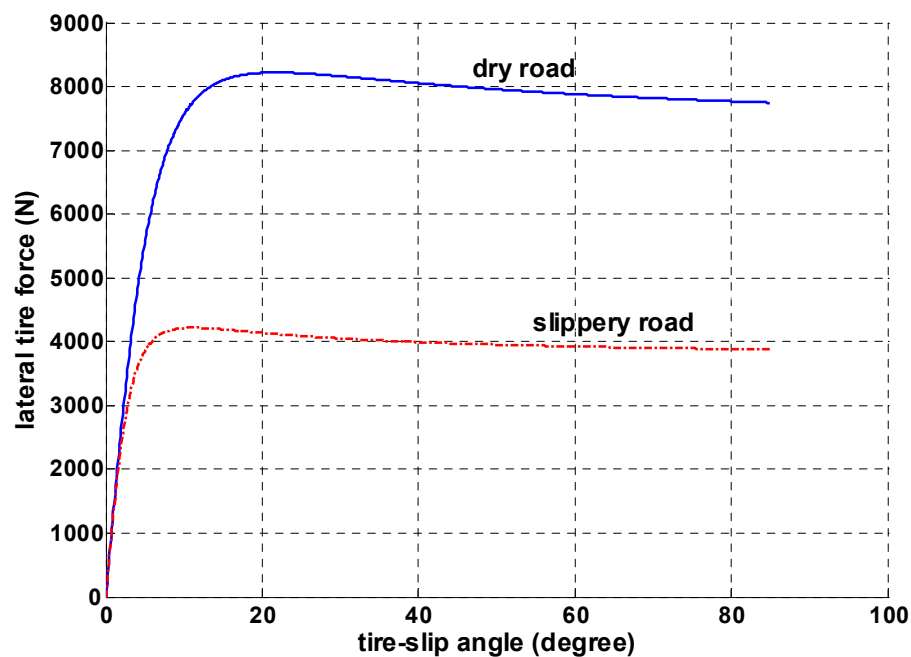
Figure **2-3**: Lateral tire force vs. Tire-slip angle

2.1.3 Three Degree-Of-Freedom Model

As just stated in **2.1.2**, the 2-DOF bicycle model does not include pitching, bouncing, and roll motions of the vehicle in the formulation. While the effects of pitching and bouncing on vehicle-handling behaviors may be neglected, roll motion can

have considerable effects on vehicle handling, especially for heavy-duty vehicles. A heavy-duty vehicle, such as a 40-foot transit bus, is characterized by high C.G. and heavy sprung mass. As a result, even a moderate roll motion would induce a significant lateral load transfer. Such a load transfer will in turn affect the tire cornering stiffness (**Appendix B**). Figure **2-4** depicts how the cornering stiffness of a bus/truck tire varies with lateral load transfer (Fancher et al. 1986). When lateral load transfer takes place during vehicle cornering, the vertical load on the outer side tire is increased and so is its cornering stiffness (C_{out}). At the same time, the vertical load on the inner side tire is reduced and the tire cornering stiffness (C_{in}) is consequently lowered. As the figure shows, due to the nonlinear variation of the cornering stiffness with respect to the vertical load, the effective cornering stiffness ($(C_{out} + C_{in}) < C_0$) of the axle is lowered. Therefore, the roll motion sometimes would have negative effect on handling properties of the vehicle. As will be presented in chapters 4 and 5, it was observed in both numerical simulation and field testing, the lateral tire forces of a heavy-duty bus would start to exhibit nonlinear characteristics due to the load transfer induced by roll motion at the lateral acceleration level of 0.2 g, which is much lower than the corresponding level typically reported for passenger cars (0.4g) (Milliken and Milliken 1995; Segel 1956b).
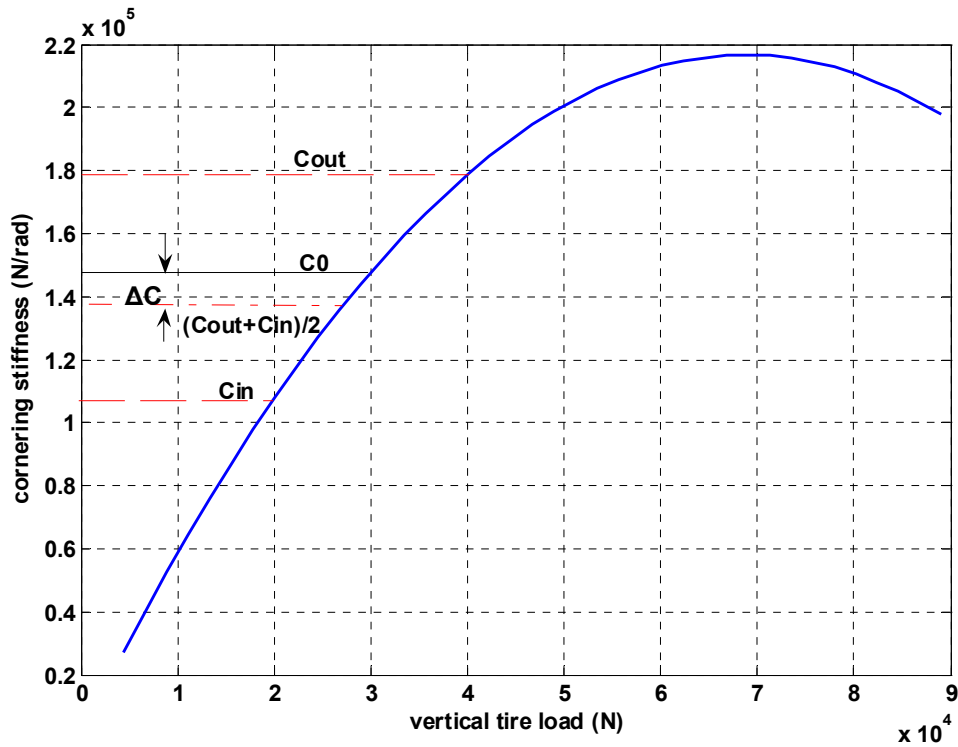
Figure **2-4**: Variation of the cornering stiffness with respect to vertical load

As the above discussion suggested, it would be critical to include roll motion in the modeling in order to accurately predict the handling behavior of the bus, especially when the vehicle is approaching the nonlinear operating range. Incorporating the effect of roll into Eq. **2.1**, the equations of motion for the vehicle become (Segel 1956b):

$$\begin{cases} mv(\dot{\beta} + r) + m_s h\ddot{\phi} = F_{yf} + F_{yr} \\ I_{zz}\dot{r} + I_{xz}\ddot{\phi} = (aF_{yf} - bF_{yr}) \\ I_{xz}\dot{r} + I_{xx}\ddot{\phi} = m_s gh\phi + m_s hU(\dot{\beta} + r) - K_{\phi}\phi - C_{\phi}\dot{\phi} \end{cases}$$

or

$$\frac{d}{dt}\begin{pmatrix} \beta \\ r \\ \phi \\ \dot{\phi} \end{pmatrix} = \begin{pmatrix} \dfrac{F_{yf} + F_{yr}}{mU} - r - m_s h\ddot{\phi} \\ \dfrac{(aF_{yf} - bF_{yr}) - I_{xz}\ddot{\phi}}{I_{zz}} \\ \dot{\phi} \\ \dfrac{m_s gh\phi + m_s hU(\dot{\beta} + r) - K_{\phi}\phi - C_{\phi}\dot{\phi} - I_{xz}\dot{r}}{I_{xx}} \end{pmatrix}$$

(2.4)

a	distance from C.G. to front-tire center
b	distance from C.G. to rear-tire center
F_{yf}	lateral tire force by the front tire
F_{yr}	lateral tire force by the rear tire
I_{xx}	roll moment of inertia
I_{zz}	yaw moment of inertia
h	C.G. height measured from roll center
K_{φ}	suspension roll stiffness
C_{φ}	suspension roll damping
m	mass of the vehicle
m_s	sprung mass
U	vehicle speed
r	yaw rate
α_f	front-tire slip angle
α_r	rear-tire slip angle
β	side-slip angle of the vehicle at C.G.
φ	roll angle of sprung mass

For simplification, constant roll stiffnesses and damping coefficients are assumed for the front and rear axles in Eq. **2.4** (Segel 1956a; Takano et al. 2003; Weir et al. 1968; Willumeit et al. 1992). The lateral tire forces are model by the enhanced Magic Tire Formula (Bakker et al. 1989; TNO 2001) as in Eq. **2.5**, which takes into account the effects of vertical load and road-friction condition on lateral tire force. In this formula, P_{Cy1}, P_{Dy1}, P_{Dy2}, P_{Ey1}, P_{Ey2}, P_{Ky1}, and P_{Ky1} are constants obtained empirically. μ_y represents the tire-road frictional coefficient, which is sensitive to the vertical load F_z. Using the above constants, coefficients B_y, C_y, D_y, E_y, and K_y are derived. Then the lateral tire force can be estimated according to the slip angle α.

$$F_{yi} = D_y \sin\{C_y \tan^{-1}[B_y\alpha_i - E_y(B_y\alpha_i - \tan^{-1}(B_y\alpha_i))]\}$$
$$i = f, r$$

$$df_z = \frac{F_z - F_{z0}}{F_{z0}}$$

$$C_y = p_{C_{y1}}$$

$$D_y = \mu_y F_z, \quad \mu_y = p_{D_{y1}} + p_{D_{y2}} df_z$$

$$E_y = p_{E_{y1}} + p_{E_{y2}} df_z$$

$$K_y = p_{K_{y1}} F_{z0} \sin\{2\tan^{-1}[F_z / (p_{K_{y2}} F_{z0})]\}$$

$$B_y = K_y / (C_y D_y)$$

(2.5)

This 3-DOF model is able to capture most of the lateral dynamic behaviors in practice. The nonlinear variations of lateral force with respect to tire-side angle and load transfer, which are very critical to vehicle handling behavior, are accurately modeled by the well-known Magic Formula. However, the model requires a large computational effort due to its complexity, and generally prohibitive if not impossible to design controllers based on it. In practice, this nonlinear model is only used for full vehicle

simulation and controller-performance verification. Linear models suitable for controller-design purpose will be derived in the following section.

2.2 Linear Models

2.2.1 Linear 2-DOF and 3-DOF Models and Comparison

A simplified vehicle model used for controller-design purpose can be derived by linearizing the nonlinear model with respect to an operating point of interest, which is usually (β=0, r=0) for the 2-DOF model and (β=0, r=0, φ=0) for the 3-DOF model. Assuming small perturbations, a linear relationship between lateral fire force (F_y) and slip angle (α) can be established around the operating point:

$$F_{y_i} = C_i \alpha_i$$
$$i = f, r \tag{2.6}$$

where, C_i (cornering stiffness) is the slope of lateral tire force-slip angle curve (Figure **2-3**) at zero slip angle.

Taking small angle approximations, the nonlinear formulae for slip angles in Eq. **2.3** can be simplified as:

$$\alpha_f = \beta + \frac{a}{v}r - \delta_f$$
$$\alpha_r = \beta - \frac{b}{v}r \tag{2.7}$$

Substitute Eqs. **2.6** and **2.7** into Eq. **2.1** and assume constant longitudinal velocity U, the linear 2-DOF model can be derived as:

$$\begin{cases} mU\left(\dot{\beta}+r\right)=\left(C_f+C_r\right)\beta+\left(C_f a+C_r b\right)\dfrac{r}{U}-C_f\delta \\[2mm] I_{zz}\dot{r}=\left(C_f a-C_r b\right)\beta+\left(C_f a^2+C_r b^2\right)\dfrac{r}{U} \end{cases}$$

or   **(2.8)**

$$\begin{bmatrix} \dot{\beta} \\ \dot{r} \end{bmatrix}=\begin{bmatrix} -\dfrac{C_f+C_r}{mU} & -1-\dfrac{a\,C_f-bC_r}{mU^2} \\[3mm] -\dfrac{aC_f-bC_r}{I_{zz}} & -\dfrac{a^2C_f-b^2C_r}{I_{zz}v} \end{bmatrix}\begin{bmatrix} \beta \\ r \end{bmatrix}+\begin{bmatrix} \dfrac{C_f}{mU} \\[3mm] \dfrac{aC_f}{I_{zz}} \end{bmatrix}\delta_f$$

Following the same procedures, the state-space representation for the linear 3-DOF vehicle model can also be derived:

$$\begin{bmatrix} \dot{\beta} \\ \dot{r} \\ \dot{\phi} \\ \ddot{\phi} \end{bmatrix}=\begin{bmatrix} -\dfrac{C_f+C_r}{mU} & -1-\dfrac{a_f C_f-a_r C_r}{mU^2} & \dfrac{m_s h_s K_\phi I_{zz}+m_s^2 h_s^2 g I_{zz}}{U(m_s^2 h_s^2 I_{zz}+I_{zz}^2 m+I_{xx}I_{zz}m)} & \dfrac{m_s h_s C_\phi I_{zz}}{U(m_s^2 h_s^2 I_{zz}+I_{zz}^2 m+I_{xx}I_{zz}m)} \\ -\dfrac{a_f C_f-a_r C_r}{I_{zz}} & \dfrac{a^2 C_f-b^2 C_r}{I_{zz}U} & \dfrac{I_{zz}K_\phi I_{zz}+I_{zz}m_s h_s g I_{zz}}{m_s^2 h_s^2 I_{zz}+I_{zz}^2 m+I_{xx}I_{zz}m} & \dfrac{I_{zz}C_\phi m}{m_s^2 h_s^2 I_{zz}+I_{zz}^2 m+I_{xx}I_{zz}m} \\ 0 & 0 & 0 & 1 \\ \dfrac{m_s h_s I_{zz}C_f+m_s h_s I_{zz}bC_r+I_{zz}ma^2 C_f+I_{zz}mb^2 C_r}{m_s^2 h_s^2 I_{zz}+I_{zz}^2 m+I_{xx}I_{zz}m} & \dfrac{m_s h_s I_{zz}aC_f-m_s h_s I_{zz}bC_r+I_{zz}ma^2 C_f+I_{zz}mb^2 C_r}{U(m_s^2 h_s^2 I_{zz}+I_{zz}^2 m+I_{xx}I_{zz}m)} & \dfrac{-C_\phi}{I_{xx}} & \dfrac{m_s gh-K_\phi}{I_{xx}} \end{bmatrix}\begin{bmatrix} \beta \\ r \\ \phi \\ \dot{\phi} \end{bmatrix}+\begin{bmatrix} \dfrac{C_f}{mU} \\ \dfrac{aC_f}{I_{zz}} \\ 0 \\ 0 \end{bmatrix}\delta_f$$

   (2.9)

Substitute the vehicle parameters (**Appendix A**) of a 40-foot bus for the coefficients in Eq. **2.9**, yielding:

$$\begin{bmatrix} \dot{\beta} \\ \dot{r} \\ \dot{\phi} \\ \ddot{\phi} \end{bmatrix}=\begin{bmatrix} -9.4634 & -1.0005 & \underset{a_{13}}{0.0781} & \underset{a_{14}}{0.3413} \\ 0.0226 & -10.7213 & \underset{a_{23}}{0.02950} & \underset{a_{24}}{1.2884} \\ 0 & 0 & 0 & 1 \\ 5.1029 & 2.1445 & -7.3738 & -32.2091 \end{bmatrix}\begin{bmatrix} \beta \\ r \\ \phi \\ \dot{\phi} \end{bmatrix}+\begin{bmatrix} 3.2998 \\ 15.2941 \\ 0 \\ -4.8397 \end{bmatrix}\delta_f$$

   (2.10)

It can be observed that the coupling terms, a_{13}, a_{14}, a_{23}, and a_{24}, between yaw-plane motions (β, r) and roll motion φ are much smaller than the dominant terms in the same row. Therefore, the effects of roll motion on yaw-plane motions are negligible in a

linear model. In other words, the simulation results for yaw-plane dynamics (yaw rate and side-slip angle) from the 2-DOF and 3-DOF linear models will be nearly the same. The eigenvalues of the 2-DOF and 3-DOF models are compared in Figure **2-5**. As the plot shows, the eigenvalues for the yaw modes from these two models are very close, implying similar yaw dynamical characteristics. The frequency responses for side-slip and yaw rate angle from the 2-DOF and 3-DOF models are compared in the following figure, which demonstrates the similarity of 2-DOF and 3-DOF models in yaw-plane dynamics estimation. Since this thesis focuses on yaw-plane dynamics enhancement, the 2-DOF linear model is selected hereafter for linear system analysis and controller design purposes.
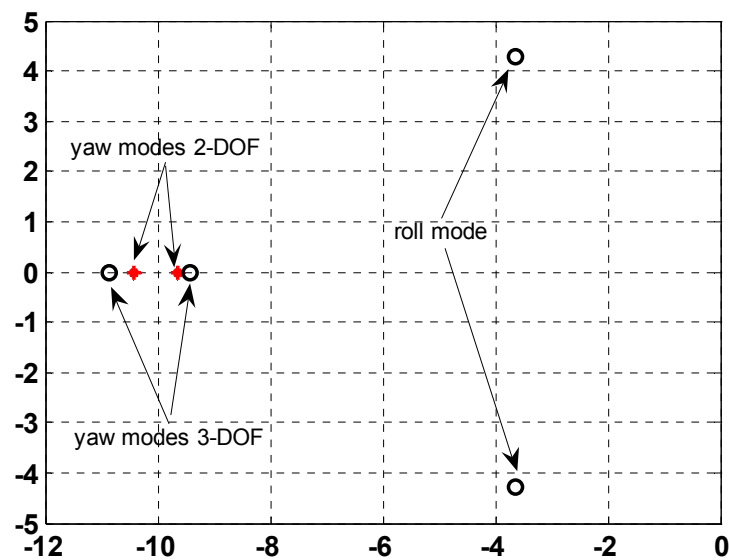
Figure **2-5**: Comparison of yaw-mode eigenvalues for 2-DOF and 3-DOF linear models
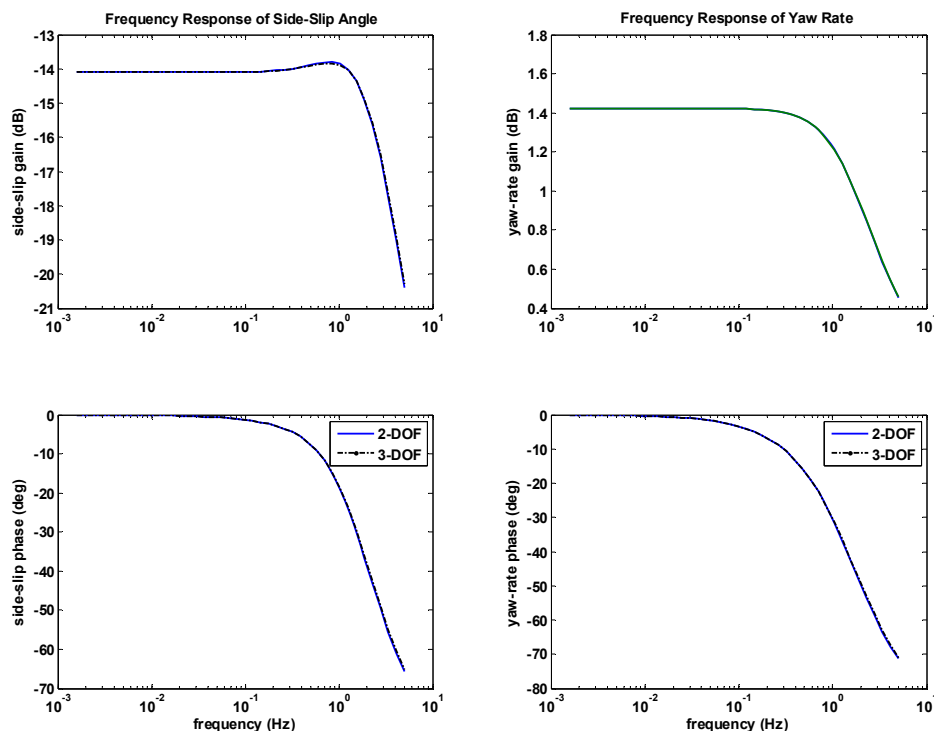
Figure **2-6**: Comparison of the frequency responses for the 2-DOF and 3-DOF models

2.2.2 Linear Models for Beyond the Linear Operating Range

The 2-DOF linear model derived in **2.2.1** by linearizing the nonlinear model with respect to the operating point (β=0, r=0) is valid only when the vehicle is subjected to small perturbations around this equilibrium. Alternatively speaking, the model is applicable for vehicle in the linear operating region, in which the lateral acceleration is less than a specific level (0.4 g for cars, 0.23 g for buses). Beyond this linear region, the nonlinear model needs to be linearized about a new operating point other than (0, 0) in order to accurately describe the vehicle's handling behaviors.

The following linearization procedure is adapted from a pervious publication (Sharp 1973).

Assume hereafter that (β_0, r_0) is the equilibrium operating point, which is by default a steady-state solution to the nonlinear equations of motions Eq. **2.1**. Apply a small perturbation $\Delta\delta$ to steering input δ_0, the steering angle then becomes:

$$\delta = \delta_0 + \Delta\delta \tag{2.11}$$

As a result, the state variables of the vehicle are perturbed to:

$$\beta = \beta_0 + \Delta\beta$$
$$r = r_0 + \Delta r \tag{2.12}$$

And, the slip angles of the front and rear tires are increased to:

$$\alpha_f = \alpha_{f0} + \Delta\alpha_f$$
$$\alpha_r = \alpha_{r0} + \Delta\alpha_r \tag{2.13}$$

Following Eq. **2.8**, the equations of motions at the perturbed states are:

$$\begin{cases} mU\left[\dfrac{d}{dt}(\beta_0 + \Delta\beta) + (r_0 + \Delta r)\right] = Y_f(\alpha_{f0}) + C_f'\Delta\alpha_f + Y_r(\alpha_{r0}) + C_r'\Delta\alpha_r \\ I_z\dfrac{d}{dt}(r_0 + \Delta r) = \left[Y_f(\alpha_{f0}) + C_f'\Delta\alpha_f\right]a - \left[Y_r(\alpha_{r0}) + C_r'\Delta\alpha_r\right]b \end{cases} \tag{2.14}$$

Since (β_0, r_0) are steady-state solutions, the following equations are valid.

$$\begin{cases} mUr_0 = Y_f(\alpha_{f0}) + Y_r(\alpha_{r0}) \\ Y_f(\alpha_{f0})a = Y_r(\alpha_{r0})b \end{cases} \tag{2.15}$$

Substitute Eq. **2.15** into Eq. **2.14**,

$$\begin{cases} mU\left[\left(\dot{\beta}_0 + \Delta\dot{\beta}\right) + \Delta r\right] = C_f'(\alpha_{r0})\Delta\alpha_f + C_r'(\alpha_{r0})\Delta\alpha_r \\ I_z\left(\dot{r}_0 + \Delta\dot{r}\right) = C_f'\Delta\alpha_f a - C_r'\Delta\alpha_r b \end{cases}$$

$$\Rightarrow \begin{cases} mU\left(\Delta\dot{\beta} + \Delta r\right) = C_f'(\alpha_{r0})\Delta\alpha_f + C_r'(\alpha_{r0})\Delta\alpha_r \\ I_z\Delta\dot{r} = C_f'\Delta\alpha_f a - C_r'\Delta\alpha_r b \end{cases} \qquad (2.16)$$

$$\Rightarrow \begin{bmatrix} \Delta\dot{\beta} \\ \Delta\dot{r} \end{bmatrix} = \begin{bmatrix} -\dfrac{C_f' + C_r'}{mU} & -1 - \dfrac{aC_f' - bC_r'}{mU^2} \\ -\dfrac{aC_f' - bC_r'}{I_{zz}} & -\dfrac{a^2C_f' - b^2C_r'}{I_{zz}U} \end{bmatrix} \begin{bmatrix} \Delta\beta \\ \Delta r \end{bmatrix} + \begin{bmatrix} \dfrac{C_f'}{mU} \\ \dfrac{aC_f'}{I_{zz}} \end{bmatrix} \Delta\delta_f$$

The linear model (Eq. **2.16**) derived for the high lateral acceleration situations are similar to that for the low lateral acceleration condition, except that $C_f{}'$ and $C_r{}'$ are "local cornering stiffness" measured at a large slip angle, typically larger than 5° (Fancher et al. 1986; Gillespie 1992; Yih 2005). Therefore, model-wise, conducting stability analysis and controller design for a vehicle at the high lateral acceleration region would be similar to the case at the low lateral acceleration region.

2.2.3 Linear Models for Low-Friction Conditions

Tire-road friction is one of the most critical factors that determine vehicle-handling dynamics. It is always desirable to include the effect the friction condition in the linear models. As a common practice, taking friction condition into consideration by multiplying tire cornering stiffness C by road-friction coefficient μ (i.e. $C_\mu = \mu C$) is frequently seen in vehicle modeling (Guldner et al. 1996; Guvenc et al. 2004; Mammar

and Koenig 2002; Ono et al. 1996). Nevertheless, the assumption behind this modeling approach appears to be incorrect.

According to the Magic Tire Formula shown in Eq. **2.5**, tire-road friction μ_y plays a role in tire-force variation through the coefficient D_y, which represents the peak magnitude of the tire force. Meanwhile, tire cornering stiffness is represented by K_y in the Magic Tire Formula, which is affected only by constants P_{ky1} and P_{ky2}. Therefore, tire-road friction condition and cornering stiffness are independent to each other (Sienel 1997). Therefore, the influence of friction condition on the tire force cannot be modeled simply by varying cornering stiffness.

The effects of friction condition and cornering stiffness variations on the tire force are illustrated in Figure **2-7**. When the tire-road friction is lowered ($\mu_y = 0.4$) for the sample truck tire, its tire force saturates faster with respect to the slip angle, but the cornering stiffness (the slope at the origin) remains unchanged. Similar results were obtained from previous experiments (Balderas and Fancher 1988). It was found that varying friction condition introduced noticeable changes at slip angles higher than 4°. When the cornering stiffness is reduced ($K_y = 0.4$) for the tire, the rate at which the tire force grows with respect to the slip angle becomes lower than the sample tire. However, the tire with the lowered cornering stiffness still approaches to the same peak tire force as the sample tire.
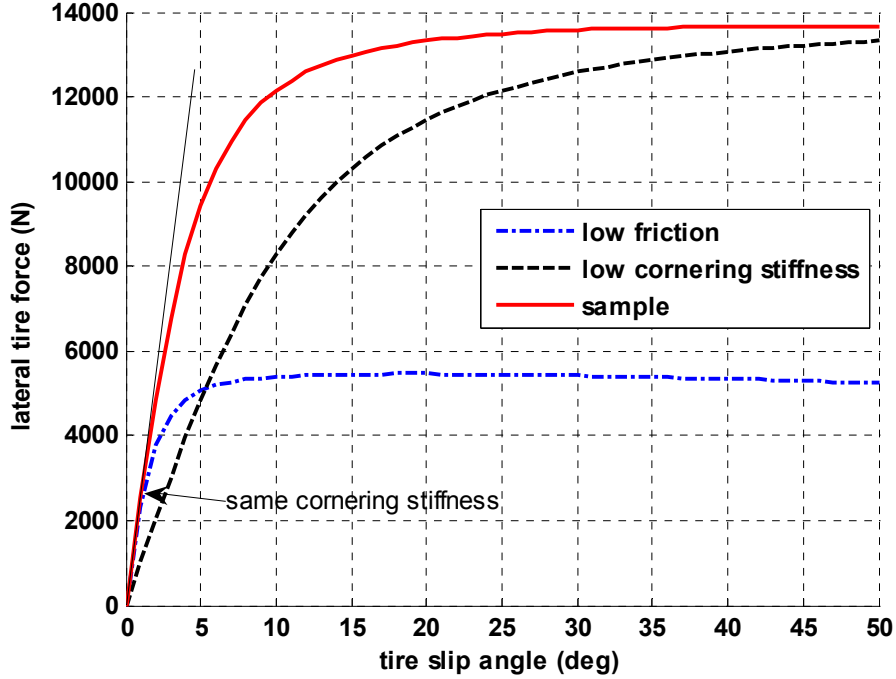
Figure **2-7**: Effects of tire-road friction and cornering stiffness on tire force

Modeling tire force on low-friction surfaces by $C_\mu = \mu C$ corresponds to the second case, though it intends to approximate the first case.

The misinterpretation in the relationship between tire-road friction and tire force during the modeling can be further realized by the following analysis.

Following the mistaken approach, multiply the cornering stiffnesses C_f and C_r by μ for the linear 2-DOF model in Eq. **2.8** to take into account the effect of tire-road friction condition:

$$\begin{bmatrix} \dot{\beta} \\ \dot{r} \end{bmatrix} = \begin{bmatrix} -\dfrac{\mu C_f + \mu C_r}{mU} & -1 - \dfrac{a\mu C_f - b\mu C_r}{mU^2} \\ -\dfrac{a\mu C_f - b\mu C_r}{I_{zz}} & -\dfrac{a^2\mu C_f - b^2\mu C_r}{I_{zz}v} \end{bmatrix} \begin{bmatrix} \beta \\ r \end{bmatrix} + \begin{bmatrix} \dfrac{\mu C_f}{mU} \\ \dfrac{a\mu C_f}{I_{zz}} \end{bmatrix} \delta_f \qquad (2.17)$$

Substitute 0.4 (the tire-road friction coefficient on slippery roads) for μ in Eq. **2.17**,

$$\begin{bmatrix} \dot{\beta} \\ \dot{r} \end{bmatrix} = \begin{bmatrix} -\dfrac{0.4C_f + 0.4C_r}{mU} & -1 - \dfrac{a(0.4C_f) - b(0.4C_r)}{mU^2} \\ -\dfrac{a(0.4C_f) - b(0.4C_r)}{I_{zz}} & -\dfrac{a^2(0.4C_f) - b^2(0.4C_r)}{I_{zz}v} \end{bmatrix} \begin{bmatrix} \beta \\ r \end{bmatrix} + \begin{bmatrix} \dfrac{0.4C_f}{mU} \\ \dfrac{a(0.4C_f)}{I_{zz}} \end{bmatrix} \delta_f \quad \textbf{(2.18)}$$

Obviously, the vehicle model for the slippery road condition ($\mu = 0.4$) shown in Eq. **2.18** would be identical to the one in Eq. **2.8** (which is derived for the dry road condition), if the cornering stiffnesses are lowered to $0.4C_{f,r}$ for the latter. The identity simply implies that the behavior of a vehicle on the slippery roads can be approximated by that of the vehicle on the dry road with lowered cornering stiffnesses.

If two systems behave similarly under the same input, they should at least have similar stable steady-state solutions. If they don't even satisfy this condition, their behaviors will not be close to each other. The steady-state solutions for a vehicle with lowered cornering stiffnesses on the dry road and the same vehicle with normal cornering stiffness on the slippery road are calculated using numerical continuation method (Dhooge et al. 2003) and graphically presented using the bifurcation diagram in Figure **2-8** for a series of steering inputs. As shown, the regions where stable steady-state solution exists are different for the two cases. With the same speed, the vehicle with a lowered cornering stiffness on the dry road is able to maintain stability for larger steering angles (higher lateral acceleration) than the same vehicle with normal cornering stiffness on the slippery road does. The plots suggest that the behavior of the vehicle on slippery roads cannot be approximated by the vehicle with lowered tire cornering stiffness on dry roads.

Therefore, modeling vehicle behavior on slippery roads by just lowering tire cornering stiffness in the linear model to μC is not appropriate.
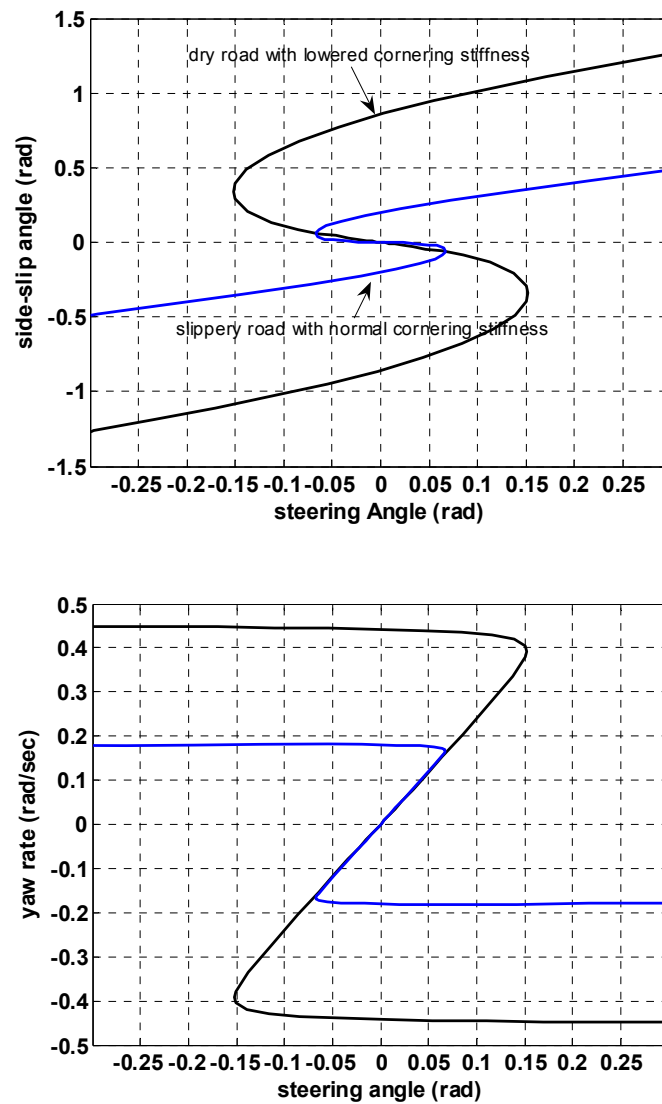
Figure **2-8**: Bifurcation diagrams

If changing tire cornering stiffness to μC is not an appropriate modeling approach, how should tire-road friction condition be taken into account? Before this question can be answered, it is necessary to know how tire-road friction affects vehicle handling.

Tire-road friction cannot change cornering stiffness, which is a physical property of the tire itself, for a tire. It is the changing rate of the cornering stiffness with respect to the slip angle that the road-friction condition really affects. In other words, lower road friction makes the tire force saturate faster on the slipper road than on the dry road. Therefore, it is the operation point, not the cornering stiffness itself, that makes vehicle handling more difficult on the slippery roads than on the dry roads. This argument agrees with our common sense – the vehicle would behave differently on dry roads and on slippery roads even though its tire cornering stiffness remains the same. It can be further illustrated by Figure **2-9** that with the same local cornering stiffness (slope of the curve), the operating point on the slippery curve is already close to saturation while the operating point on the dry curve is still distant away from saturation. Of course, the vehicle is more difficult to handle in the former despite the cornering stiffness values are the same in both cases. It is the rate at which the tire force approaching saturation induces different vehicle-handling characteristics on different road-surface conditions. Alternatively speaking, tire-road friction plays a role in vehicle handling by influencing the operating point of the vehicle.
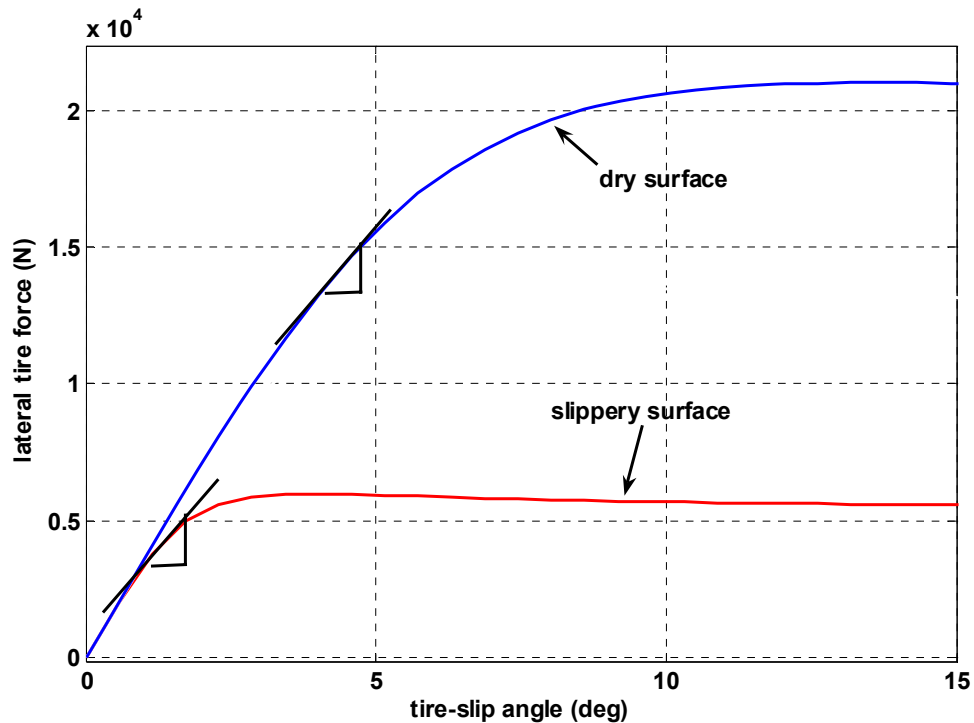
Figure **2-9**: Comparison of operating points with the same local cornering stiffness

Knowing how tire-road friction affects vehicle handling, the possibility of taking friction condition into linear model when building a linear vehicle model can now be discussed. As explained in **2.2.3**, the linear models for different operating points would assume the same form and same coefficient values, except for the local cornering stiffnesses. Otherwise stated, the models that are linearized with respect to different operating points would look the same if their local cornering stiffnesses are the same. Therefore, limited by the nature of linearization process, we would not be able to differentiate a low-friction model from a high-friction model and it is impossible to incorporate tire-road friction information in the linear model.

2.3 Comparison between the nonlinear and linear models

It was stated in previous publications (Milliken and Milliken 1995; Segel 1956b; Segel 1965) that the linear vehicle model can closely approximate the nonlinear model up to 0.4 g, where the lateral tire force starts to vary in a nonlinear fashion with respect to slip-angle change. While this statement has been proved to be true for cars, its validity for heavy-duty buses remains to be seen. In the rest of this section, the nonlinear 3-DOF model will be studied to obtain a lateral acceleration level up to which it can be approximated by the 2-DOF linear model.

Figure **2-10** shows the understeer gradient curves by simulation for the nonlinear 3-DOF models. As can be observed, the understeer gradient (slope of the curve) remains fairly constant up to about 0.25 g. Beyond this lateral acceleration level, the understeer gradient of the nonlinear model starts to deviate from a constant value and varies nonlinearly. Therefore, the nonlinear model can just be approximated by the linear model up to around 0.25 g for the best case.
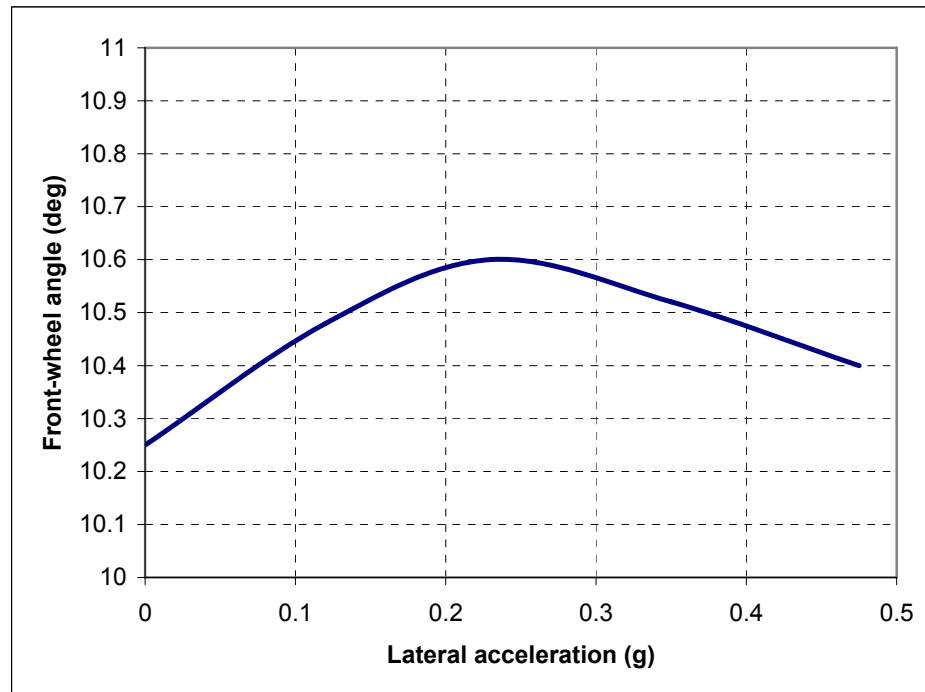
Figure **2-10**: Understeer gradient of the nonlinear 3-DOF model

The responses of the linear and nonlinear models to a series of step-steer inputs having different magnitude are presented in Figure **2-11**. As expected, the linear model is capable of a decent approximation of the nonlinear model up to about 0.23 g. When the lateral acceleration level goes beyond 0.23 g, the nonlinearity caused by lateral load transfer starts to play an role and the discrepancy between the linear and the nonlinear models become noticeable. As the lateral acceleration level approaching the tire-road friction limit, which is 0.65 g for the bus/truck tire, the steady-state of the side-slip angle of linear model is more than 100% that of the nonlinear model.
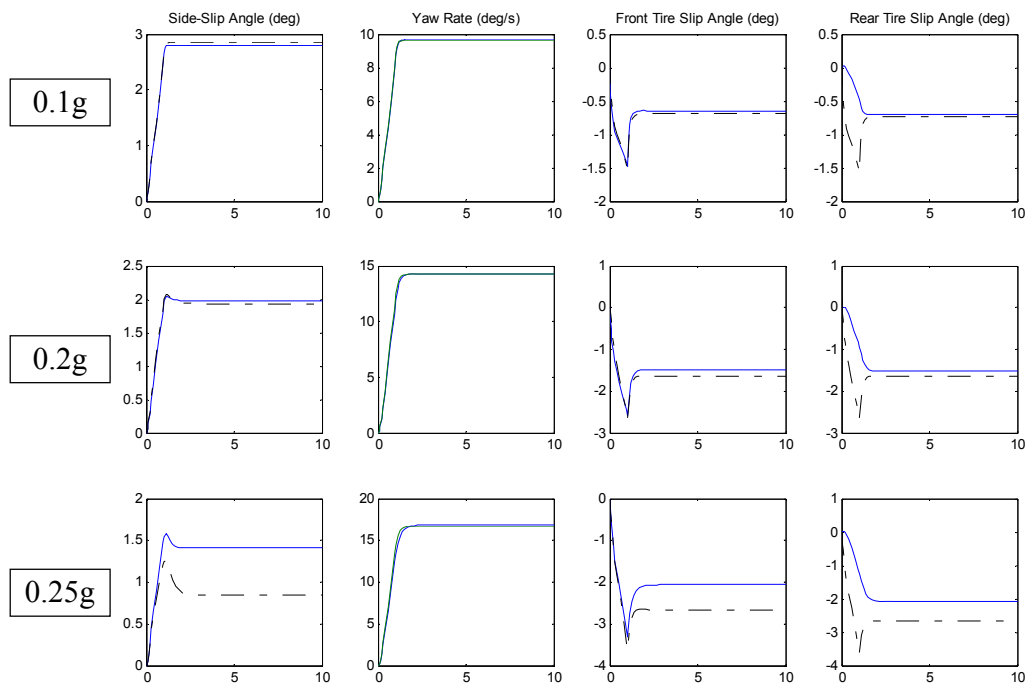
Figure **2-11**: Comparison of linear and nonlinear models for step-steer response

Upon the above comparison, the linear model, which is the linearization of the nonlinear model at (β=0, r=0), can closely approximate the behaviors of the nonlinear model up to around 0.23 g. When the lateral acceleration level is higher than 0.23 g, a linearization with respect to a new operation point other than (β=0, r=0) is necessary in order to obtain a decent approximation. This conclusion will be further confirmed in chapter 4 with testing data.

2.4 Implications for Controller Design

2.4.1 The Nominal Model for Controller Design

As a common practice, a nonlinear vehicle model is usually simplified by linearization to facilitate the controller-design process. However, as discussed in the last section, the linear model of the bus, which is linearized with respect to (β=0, r=0) is only able to approximate the nonlinear vehicle behavior up to 0.23 g on the dry road. Since the linear model assumes a constant tire cornering stiffness, the lateral tire forces unrealistically grow at a constant rate without saturations as such that the vehicle can always obtain enough lateral tire force to avoid skid-induced spinning or drifting. Consequently, while the controller designed based on this linear model works fairly well for most of the situations on the dry road with a lateral acceleration up to 0.23g, it would fail to effectively regulate vehicle behavior at other lateral acceleration levels and/or road-friction conditions where the nonlinear characteristics of the tire force start to play a significant role.

In order to preserve the fundamental dynamics for the vehicle in different operating ranges, the nonlinear model would need to be linearized correspondingly at different operating points for different operating conditions. It has been shown in **2.2.2** that the state-space representations of the models linearized at different operating points are nearly the same, except for the different local cornering stiffnesses. Therefore, it is possible that the controller designed from a linear vehicle model can be successfully

applied to the nonlinear model if the performance of the controller is robust with respect to the variation of the local tire cornering stiffness (Khalil 2002).

2.4.2 The Effect of Road Friction on the Operating Range

As discussed in **2.2.3**, the linear model is not capable of incorporating the effect of road-friction condition. Therefore, the design model, design process, and the derived controller would be the same for both dry road and slippery road cases. However, the controller would have different operating ranges for the two cases. The operating range on the slippery road is narrower than on the dry road.

References

1. Armstrong, E. (1993). "Robust controller design for flexible structures using normalized coprime factor plant descriptions." *NASA Technical Paper 3325*.

2. Bakker, E., Pacejka, H. B., and L, L. (1989). "A new tire model with an application in vehicle dynamics studies." *SAE 890087*.

3. Balderas, L., and Fancher, P. S. (1988). "Representation of truck tire properties in braking and handling studies." *UMTRI-88-29*.

4. Dhooge, A., Govaerts, W., and Kuznetsov, Y. A. (2003). "Matcont: A Matlab package for dynamical systems with applications to neural activity."

5. Fancher, P. S., Ervin, R. D., Winkler, C. B., and Gillespie, T. D. (1986). "A factbook of the mechanical properties of the components for single-unit and articulated heavy trucks." The University of Michigan Transportation Research Institute.

6. Gillespie, T. D. (1992). *Fundamentals of Vehicle Dynamics*, Society of Automotive Engineers, Warren, Pa.

7. Guldner, J., Tan, H. S., and Patwardhan, S. (1996). "Analysis of Automatic Steering Control for Highway Vehicles with Look-down Lateral Reference Systems."

8. Guvenc, B. A., Bunte, T., Odenthal, D., and Guvenc, L. (2004). "Robust two degree-of-freedom vehicle steering controller design." *IEEE Transactions on Control Systems Technology*, 12(4).

9. Khalil, H. K. (2002). *Nonlinear System 3rd Ed.*, Prentice Hall, Upper Saddle, NJ.

10. Maciejowski, J. M. (1989). *Multivariable feedback design*, Addison-Wesley.

11. Mammar, S., and Koenig, D. (2002). "Vehicle handling improvement by active steering." *Vehicle System Dynamics*, 38(3).

12. Milliken, W. F., and Milliken, D. L. (1995). *Race Car Vehicle Dynamics*, Society of Automotive Engineers, Warren, Pa.

13. Ono, E., Hosoe, S., Tuan, H. D., and Doi, S. (1996). "Robust stabilization of vehicle dynamics by active front wheel steering control." *Proceedings of the 35th Conference on Decision and Control*.

14. SAE. (1976). *Vehicle Dynamics Terminology SAE J670e*, SAE, Warrendale, PA.

15. Segel, L. "Research in the fundementals of automobile control and stability." *Proceedings of the SAE National Summer Meeting*, Atlantic City.

16. Segel, L. (1956b). "Theoretical prediction and experimental substantiation of the response of the automobile to steering control." *Proceedings of IMECHE*, 171(7), 310-330.

17. Segel, L. (1965).

18. Sharp, R. S. (1973). "Relationship between the steady-handling charateristics of automobiles and their stability." *Journal of Mechanical Engineering Science*, 15(5).

19. Sienel, W. (1997). "Estimation of the tire cornering stiffness and its application to active car steering." *Proceedings of the 36th Conference on Decision & Control*.

20. Takano, S., Nagai, M., Taniguchi, T., and Hatano, T. (2003). "Study on a vehicle dynamics model for improving roll stability." *JSAE Review*.

21. TNO. (2001). "MF-Tyre User Manual v5.2."

22. Weir, D. H., Shortwell, C. P., and Johnson, W. A. (1968). "Dynamics of the automobile related to driver control." *SAE 680194*.

23. Willumeit, H. P., Neculau, M., Vikas, A., and Wohler, A. "Mathematical models for the computation of vehicle dynamic behaviour during development." *FISITA Congress*, London.

24. Yih, P. (2005). "Steer-By-Wire: Implications for Vehicle Handling and Safety," Stanford University.

Chapter 3

Understeer/Oversteer – An Essential Characteristic of Vehicle Handling

3.1 Definition for Understeer/Oversteer

In order to evaluate the handling characteristics of a vehicle, objective criteria are required. Understeer/Oversteer is probably the single most important handling characteristic of the vehicle. It describes how steering angle needs to be changed to maintain different lateral accelerations while the vehicle is turning. One way to quantify this characteristic is to define a term known as the *understeer gradient* (Bundorf 1976; Gillespie 1992; Olley 1946):

$$K_{us} = (\frac{W_f}{C_f} - \frac{W_r}{C_r})/g \qquad (3.1)$$

$C_{f,r}$ the effective cornering stiffness of front/rear axle.

g the acceleration of gravity 9.8m/s^2

K_{us} understeer gradient

$W_{f,r}$ front/rear axle weight

As indicated by Eq. **3.1**, the understeer gradient includes the vehicle parameters that influence handling properties: vehicle weight, weight distribution, and the effective tire cornering stiffness (**Appendix B**) at each axle. Theoretically, a vehicle is said to be understeering if it has a positive understeer gradient, neutral steering if its understeer gradient is zero, and oversteering if the understeer gradient is negative. Note that the

cornering stiffnesses are assumed to be constants in Eq. **3.1**. Therefore, understeer/oversteer by this definition is valid only for the linear operating region of the vehicle.

One of the fundamental differences among understeering, neutral-steering, and oversteering vehicles can be most easily and safely observed during steady-state cornering. As illustrated in Figure **3-1**, for the same steering angle and vehicle speed, an oversteering vehicle tends to turn into a tighter path than a neutral-steering vehicle. At the same time, an understeering vehicle tends to follow the widest path among the three.

understeer

neutral steer
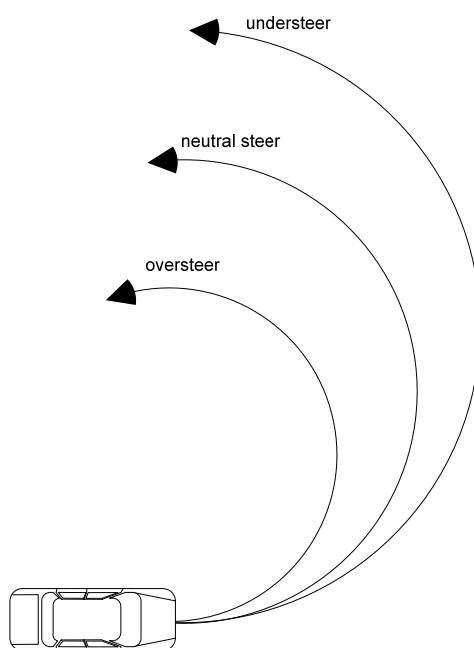
oversteer

Figure **3-1**: Understeer, oversteer, and neutral steer

As just stated, understeer gradient K_{us} determines how steering angle changes as steady-state lateral acceleration varies in the linear operation region. The relation between steering angle and lateral acceleration can be given as:

$$\delta = L/R + K_{us}a_y \qquad (3.2)$$

δ road-wheel steering angle

a_y lateral acceleration

L wheel base

R radius of the turning path

For the steady-state case, we have

$$r = \frac{a_y}{U}$$
$$R = \frac{U^2}{a_y} \qquad (3.3)$$

r yaw rate of the vehicle

U vehicle speed

Substitute Eq. **3.3** into Eq. **3.2**, the steady-state gain from steering angle to yaw rate is obtained:

$$\frac{r}{\delta} = \frac{U}{L + K_{us}U^2} \qquad (3.4)$$

It is interesting to notice in Eq. **3.4** that when the understeer gradient K_{us} is negative (oversteering), the yaw-rate response of the vehicle to an infitestimal steering input can possibly become infinite (unstable). This corresponds to the situation where the

vehicle speed is very close to the *critical speed* (U_{cr}), causing the denominator of Eq. **3.4** to become zero:

$$L + K_{us}U_{cr}^2 = 0 \quad \Rightarrow \quad U_{cr} = \sqrt{-\frac{L}{K_{us}}} \qquad (3.5)$$

According to the above discussion, open-loop (no steering corrections from the driver) yaw instability can occur when an oversteering vehicle is approaching its critical speed, even though it is running straight! Therefore, from the perspective of vehicle stability, an oversteering vehicle is usually not desirable, though it will make vehicles more responsive.

3.2 Interpretations of Understeer Gradient for Transient Response Characteristics

Although originally defined from steady-state handling, understeer gradient also has its implications for transient handling characteristics.

Rewrite Eq. **2.8** in the following form:

$$\begin{cases} mU(r + \dot{\beta}) = Y_\beta \beta + Y_r r + Y_\delta \delta \\ I_{zz}\dot{r} = N_\beta \beta + N_r r + N_\delta \delta \end{cases} \qquad (3.6)$$

where, Y_β, Y_r, Y_δ, N_β, N_r, and N_δ are the *stability derivatives* (Milliken and Milliken 1995; Segel 1956) defined as:

$$
\begin{array}{ll}
Y_\beta = C_f + C_r & N_\beta = aC_f - bC_r \\[2mm]
Y_r = aC_f - bC_r & N_r = \dfrac{b^2 C_r + a^2 C_f}{U} \\[2mm]
Y_\delta = -C_f & N_\delta = -aC_f
\end{array}
\qquad (3.7)
$$

β side-slip angle of the vehicle

a distance from the front axle to C.G.

b distance from the rear axle to C.G.

$C_{f,r}$ front/rear effective axle cornering stiffness

I_{zz} yaw moment of inertia

m vehicle weight

r yaw rate

U vehicle speed

Taking Laplace transform for the equations, the transfer functions can be obtained:

$$\frac{\beta(s)}{\delta(s)} = \frac{\dfrac{Y_\delta}{mU}s + \left(\dfrac{Y_r N_\delta}{mUI_{zz}} - \dfrac{Y_\delta N_r}{mUI_{zz}} - \dfrac{N_\delta}{I_{zz}}\right)}{\left[s^2 - \left(\dfrac{Y_\beta}{mU} + \dfrac{N_r}{I_{zz}}m\right)s + (\dfrac{N_\beta}{I_{zz}} - \dfrac{Y_r N_\beta}{mUI_{zz}} + \dfrac{Y_\beta N_r}{mUI_{zz}})\right]}$$

$$\frac{r(s)}{\delta(s)} = \frac{\dfrac{N_\delta}{I_{zz}}s + \left(\dfrac{N_\beta Y_\delta}{mUI_{zz}} - \dfrac{Y_\beta N_\delta}{mUI_{zz}}\right)}{\left[s^2 - \left(\dfrac{Y_\beta}{mU} + \dfrac{N_r}{I_{zz}}m\right)s + (\dfrac{N_\beta}{I_{zz}} - \dfrac{Y_r N_\beta}{mUI_{zz}} + \dfrac{Y_\beta N_r}{mUI_{zz}})\right]}$$

(3.8)

The two transfer functions share a common denominator, which is the characteristic equation of the system. For the 2-DOF vehicle model in Eq. **3.8**, its dynamical behavior is largely determined by the characteristic equation shown below:

$$s^2 + 2\xi\omega_n + \omega_n^2 = 0$$

where,

$$\omega_n^2 = \frac{N_\beta}{I_{zz}} - \frac{Y_r N_\beta}{mUI_{zz}} + \frac{Y_\beta N_r}{mUI_{zz}}$$

(3.9)

$$2\xi\omega_n = -\left(\frac{Y_\beta}{mU} + \frac{N_r}{I_{zz}}m\right)$$

The expressions for natural frequency ω_n can be rewritten in terms of understeer gradient and physical vehicle parameters:

$$\omega_n = \sqrt{\frac{LC_f C_r}{mI_{zz}U^2}\left(1 + \frac{K_{us}}{L}U^2\right)} \qquad (3.10)$$

For a typical 40-foot transit bus, $C_r \approx 2C_f$, $a \approx 2b$, $I_{zz} \approx mL^2/3$, the damping ratio ξ can thus be approximated by:

$$\xi = -\frac{6C_f}{mU\omega_n} \qquad (3.11)$$

Eqs. **3.10** and **3.11** show that the transient response can be affected by the understeer/oversteer characteristic of the vehicle, which basically is a steady-state consideration. According to Eqs. **3.10** and **3.11**, the higher the understeering level, the higher the natural frequency, and the lower the damping would be. As an example, the lateral acceleration responses of two vehicles with different understeering levels in a step-steer test are shown in Figure **3-2**. It can be seen from the plot, to reach the same steady-state lateral acceleration level, the vehicle with a higher understeering level ($K_{us} = 5°/g$) experienced a larger overshoot than the other one ($K_{us} = 1.8°/g$). Also, the response time of the vehicle with higher understeering level is shorter. Generally speaking, an understeering vehicle would experience a more oscillatory motion in transient state but has a higher bandwidth than an less understeering or oversteering vehicle (Milliken and Milliken 1995; Whitcomb and Milliken 1956).
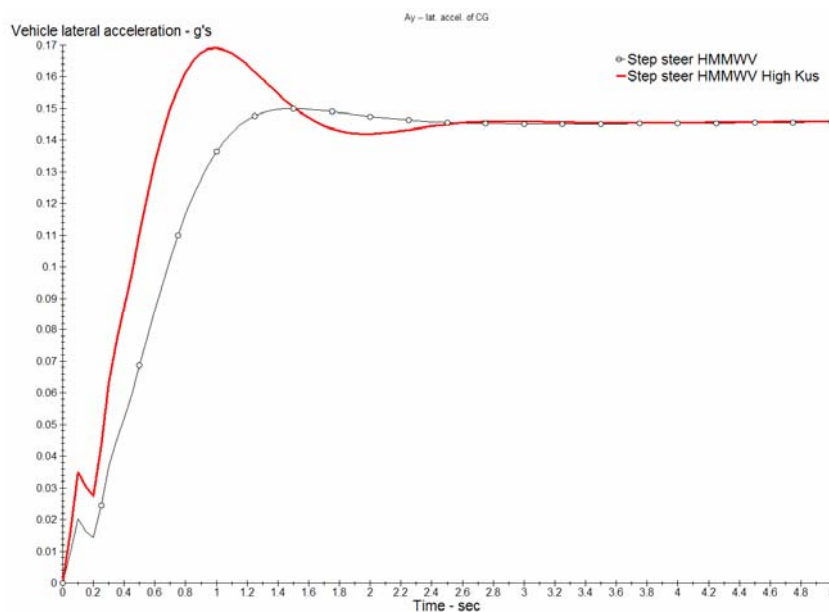
Figure **3-2**: Step responses of vehicle with different understeering levels

3.3 Extension to the Nonlinear Region and Performance Limit

3.3.1 Limit Understeer/Oversteer

While understeer/oversteer characteristic is an inherited physical property of the vehicle and largely determined by the design parameters, a vehicle can potentially experience any of the three situations, namely, understeering, neutral steering, or oversteering, given particular operating conditions such as speed, path curvature, and road friction. During normal driving, a vehicle maintains a reasonable understeering level, and almost never ventures into a nonlinear handling region. However, during emergency maneuvers, high performance driving, or on slippery roads, limit oversteer or limit understeer would become a concern. Limit oversteer describes the situation when

the rear tires of a vehicle exceed their lateral traction limits on the road before the front tires do, causing the vehicle to spin out during cornering. Under limit-oversteer situation, an understeering vehicle behaves like an oversteering vehicle. On the analogy of the definition for limit oversteer, limit understeer can be similarly defined. As discussed in **3.1**, the definition for understeer/oversteer by Eq. **3.1** is only valid for linear region. In order to quantitatively describe limit understeer/oversteer in nonlinear region, an extension of the original definition for understeer/oversteer becomes necessary.

Following Olley's classic definition (Olley 1946), a further interpretation (Pacejka 1973) of understeer gradient in terms of tire-slip angles provides more insight into the root of understeer/oversteer. In Figure **3-3**, the front and rear tire-slip angles are shown schematically for a simplified bicycle model.
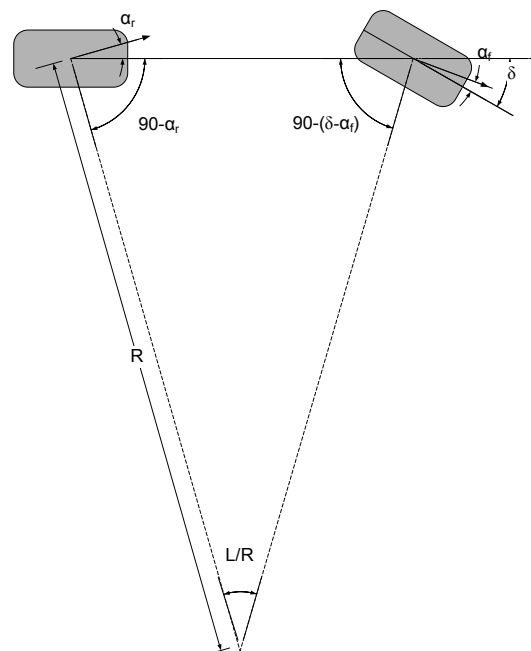
Figure **3-3**: Schematic for a simplified vehicle model

According to the geometric relations among the angles in the figure, the following equation can be derived:

$$\delta = \alpha_f - \alpha_r + L/R \tag{3.12}$$

The equation shows that the difference between the front and rear tire-slip angles is the additional steering angle to the Ackerman angle required for negotiating a path with a radius of R. Compare Eq. **3.12** to Eq. **3.2**, we have:

$$K_{us} = \frac{d\delta}{da_y} = \frac{d(\alpha_f - \alpha_r)}{da_y} \tag{3.13}$$

As represented by this equation, the understeer gradient, which describes the relationship between steering angle and lateral acceleration, can also be defined as the changing rate of the difference between front and rear slip angles with respect to lateral acceleration. Since the variables in Eq. **3.13** can be measured experimentally and there is no assumption of linearity, the definition on understeer/oversteer by Eq. **3.13** can be extended to the nonlinear operating region.

3.3.2 Final Understeer Parameter

While understeer gradient describes the steady-state handling quality of the vehicle in linear region, final understeer parameter is the counterpart of understeer gradient in the performance-limit region, which is the last 25% of the handling curve (Dixon 1987). This corresponds to the lateral acceleration level of 0.6g~0.8g for light motor vehicles and 0.3~0.6g for heavy-duty vehicles. Typical understeer diagrams for

passenger cars and heavy-duty vehicle are qualitatively shown in Figure **3-4** (Dixon 1987).
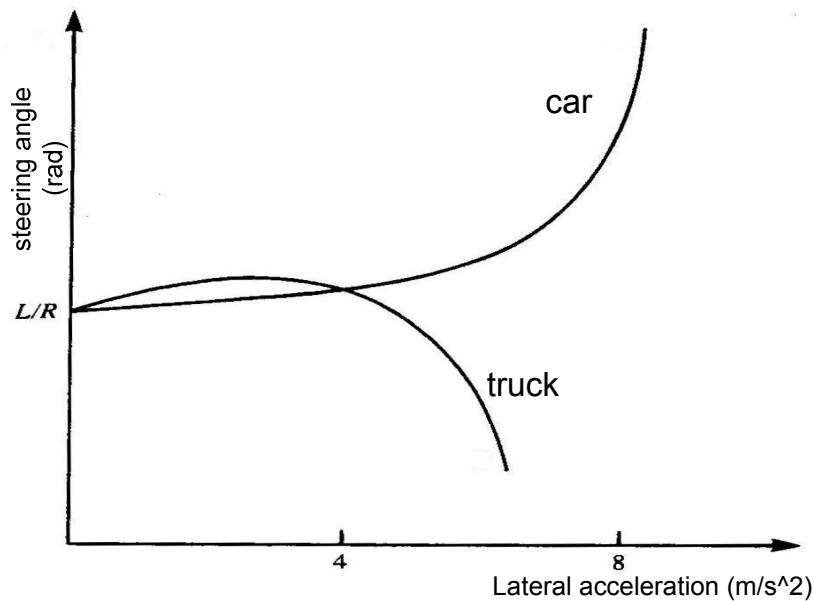
Figure **3-4**: Typical understeer diagrams for passenger cars and heavy-duty vehicles

As can be seen, the slope of the curve for cars approaches infinity in the limit region, indicating final understeer. At the same time, the slope of the heavy-duty vehicle curve goes to negative infinity when approaching performance limit, implying final oversteer. Understeer gradient is not suitable for limit cases, since it would theoretically go infinity for both final understeer and final oversteer cases. The publications (Dixon 1987; Dixon 1996) suggested using *final understeer parameter* defined as:

$$N_u = \frac{a_{y_r}}{a_{y_f}} - 1$$

(**3.14**)

Therefore, when the road-holding capacity of the rear axle is higher than that of the front axle, i.e. $a_{yr} > a_{yf}$, the front axle will saturate first at the limit condition and vehicle is final understeer. Conversely, a vehicle is final oversteer when the rear tire force saturates first. To obtain a consistent control behavior for the vehicle, final oversteer is generally not desired.

References

1. Bundorf, R. T. (1976). "The cornering compliance concept for description of directional control properties." *SAE 760713*.

2. Dixon, J. C. (1987). "Limit steady-state vehicle handling." *Proceedings of IMechE*, 201(D4).

3. Dixon, J. C. (1996). *Tyres, Suspension, and Handling*, SAE International.

4. Gillespie, T. D. (1992). *Fundamentals of Vehicle Dynamics*, Society of Automotive Engineers, Warren, Pa.

5. Milliken, W. F., and Milliken, D. L. (1995). *Race Car Vehicle Dynamics*, Society of Automotive Engineers, Warren, Pa.

6. Olley, M. (1946). "Road manners of the modern car." *Proceedings of Institute of Automobile Engineers*, v51.

7. Pacejka, H. B. (1973). "Simplified analysis of steady-state turning behaviour of motor vehicles." *Vehicle System Dynamics*, 2.

8. Segel, L. (1956). "Theoretical prediction and experimental substantiation of the response of the automobile to steering control." *Proceedings of IMECHE*, 171(7), 310-330.

9. Whitcomb, D. W., and Milliken, W. F. (1956). "Design implications of a general theory of automobile stability and control." *Proceedings of IMECHE*.

Chapter 4

Experimental Bus Handling Study and Vehicle-Parameter Identification

The handling characteristics of vehicles are closely related to driving safety. Many traffic accidents are caused by undesired and unexpected handling behaviors of the vehicle. At the same time, in order to enhance vehicle stability by automatic control, it is fundamental to understand the handling properties of vehicles. The earliest handling study of motor vehicles can be traced back to the beginning of last century (Lanchester 1907; Milliken and Whitcomb 1956). Since then, much work has been done on the measurement and analysis of handling and stability characteristics of passenger cars (Allen et al. 1990; Barter and Little 1970; Gillespie and Segel 1983; Radt and Pacejka 1963; Segel 1956a; Whitcomb and Milliken 1956). However, there is scarcity of references on the same subject for buses. In order to explore the handling characteristics of transit buses, an unladen 40-foot transit bus was tested at The Pennsylvania Transportation Institute (PTI) test track and its handling performance was evaluated based on the measurement results. The information obtained includes steady-state cornering characteristics, and the characteristics of transient responses to step and sinusoidal steering inputs in both time and frequency domains.

Transit buses are generally less maneuverable in lane change and object avoidance than cars due to their larger dimensions and higher weights. So far, little work has been published on what constitutes "good" and "bad" handling behavior for transit buses. However, based on the fact transit buses and cars operate in the same traffic

environment, it seems reasonable to expect that many of the handling evaluation criteria established for cars would be applicable to transit buses too.

The remainder of this chapter is organized as follows: First, information on the test bus and instrumentation is provided. Secondly, the test procedures and the objectives of the selected test maneuvers are detailed. Thirdly, measurement results, derived handling characteristic parameters, and their interpretations are presented followed by a summary of handling evaluation for the test bus. Finally, vehicle-parameter identification for the linear 2-DOF model based on the testing data is conducted.

4.1 The Test Vehicle

The test bus shown in Figure **4-1** is a rear engine, rear drive (RR), two-axle, 40-foot transit bus with a carrying capacity of 65 passengers. Both the front and the rear axles are solid axles equipped with air suspension systems and hydraulic dampers. The bus has dual tires on the rear axle.

Figure **4-1**: The 40-foot test bus

The dimension and weight specifications of the test bus are listed in Table **4-1**. As can be noticed, the rear-axle weight is more than twice that of the front axle. Therefore, according to Eq. **3.1**, the effective rear-axle cornering stiffness has to be more than twice that of the front axle to ensure understeering. Since the overall cornering stiffness of the dual tires at the rear axle is barely twice that of the single tire at the front, auxiliary equipment is necessary for temporal modification of tire cornering stiffnesses during turning. For the bus tested, an anti-roll bar is used at the front axle.

Table **4-1**: The specifications of the test bus

Model Year	Engine Position	Wheel Base (m)	Vehicle Weight (unladen) (kg)				Weight Distribution	
			Tire Load FL	Tire Load FR	Tire Load RL	Tire Load RR	Front	Rear
1985	Rear	6.228	2200	2048	4245	3860	34.6%	76.2%

4.2 Instrumentation and Calibration for Testing

4.2.1 Systems for Motion Measurement

Two separate systems are used in parallel for motion measurement during the testing. One is based on a VG300CB inertial measurement unit (IMU) developed by Crossbow technologies. The IMU provides pitch and roll angle measurements, along with three angular rates and three linear acceleration measurements. The analogue signals from the IMU were collected with an 8-channel data acquisition device (NI

DAQPad-6015) and post processed online using a virtual instrument (VI) created in LABVIEW®. The set-up of the Crossbow system is shown Figure **4-2**.

Crossbos IMU

steering sensor

data acquisition device
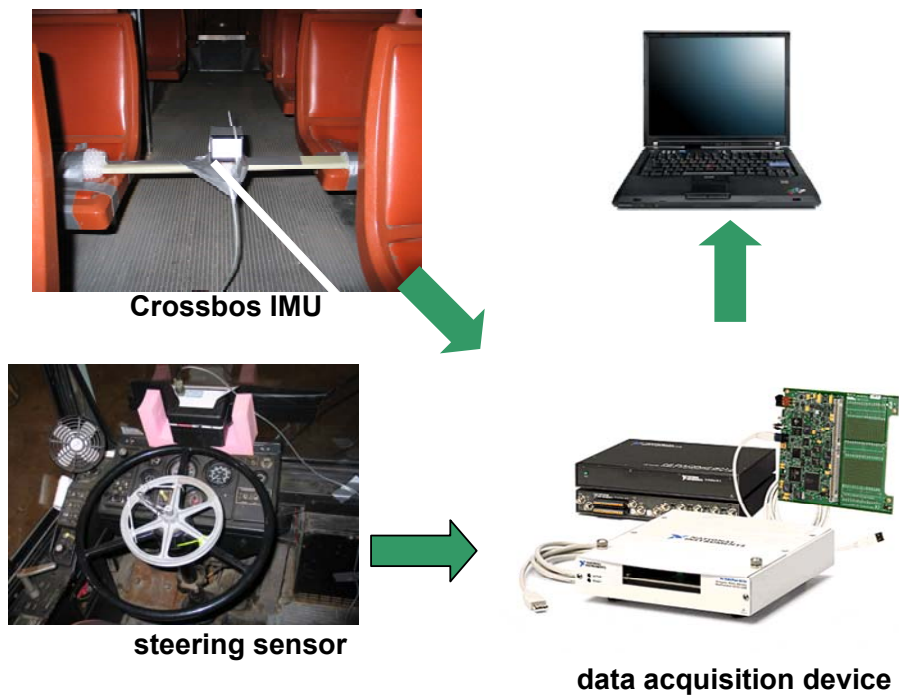
Figure **4-2**: The Crossbow data collecting system

The other measurement system is based on INS/GPS technique. The system setup is shown in Figure **4-3** (Martini 2006). It is a more advanced and complex system than the Crossbow measurement system introduced above.
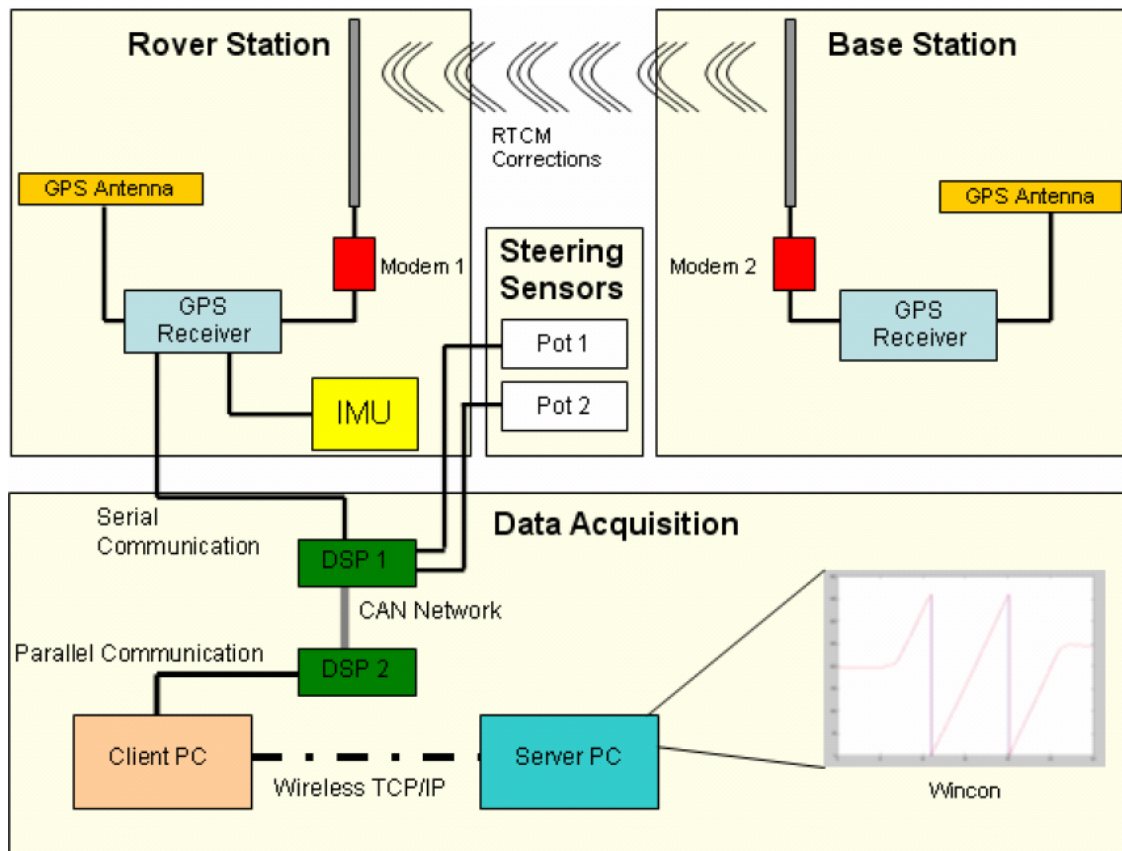
Figure **4-3**: INS/GPS sensing system

4.2.2 Steering Angle Measurement

String potentiometers were used to measure the steering angle. Two of the possible ways to measure the steering angle are: mounting the potentiometer on the windshield to the measure the circumferential displacement of the steering wheel (Figure **4-4**) or placing the potentiometer at the back of the front bumper to measure the of "linear" displacement of the swing arm (Pitman arm) of the recirculating-ball steering

machine (Figure **4-5**). Based on our experience, the latter is more favored by the drivers, because it does not interfere with driving operation.
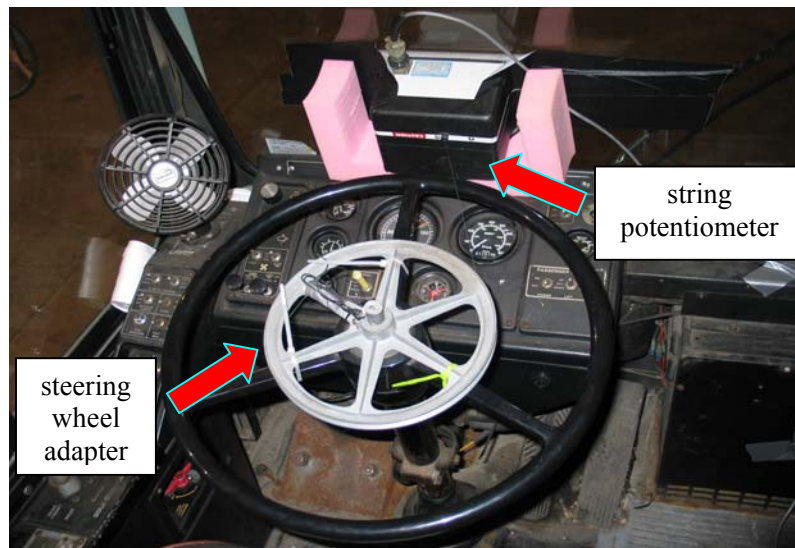
Figure **4-4**: Steering angle measurement system 1
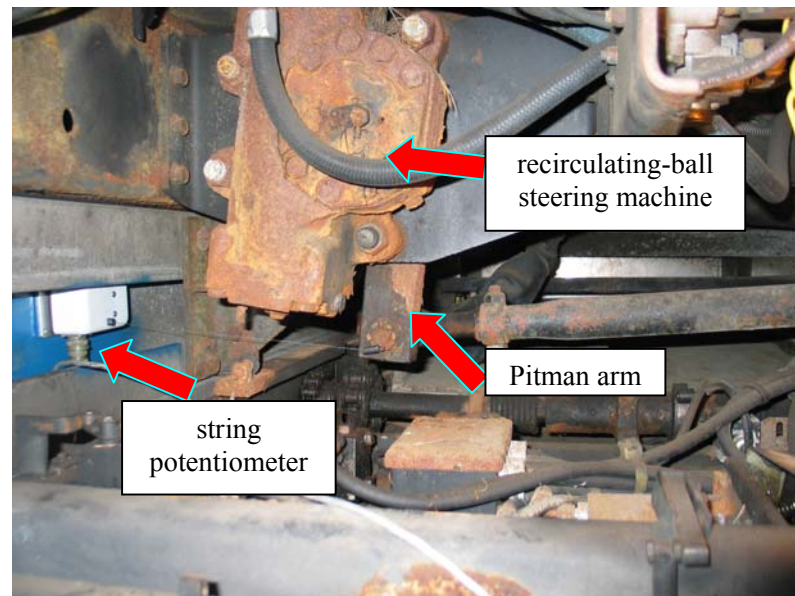
Figure **4-5**: Steering angle measurement system 2

The steering sensor was calibrated using a pair of heavy-duty slip plates as shown in Figure **4-6** (Cameron 2005).

Figure **4-6**: Wheel angle slip plate and Steering sensor calibration

The voltage outputs of the steering sensor were recorded for steering angles at a 5° interval. The recorded values were then offset by the voltage corresponding to the straight-line-running steering angle, which was measured when the bus was driven straight on flat pavement.

The calibration result representing the relationship between sensor voltage and steering angle is shown Figure **4-7**. It is clear that the sensor output varies in a linear fashion with respect to the steering angle change.
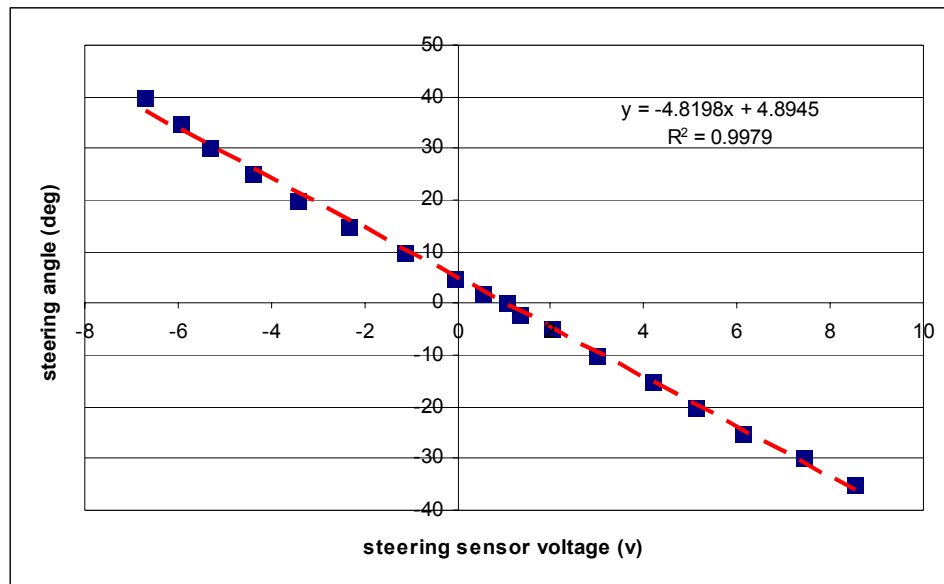
Figure **4-7**: Steering sensor calibration

4.3 Test Procedures

In order to explore both steady-state and transient response characteristics of vehicle handling for the transit bus, three test maneuvers were selected, namely, constant radius cornering (skid-pad test), step steer (J turn), and continuous sinusoidal steer. The tests were conducted following the procedures detailed in corresponding ISO standards.

4.3.1 Constant Radium Cornering

The steady-state cornering properties of the bus were measured following ISO 4138 (ISO 1982). Essentially, the test procedure consists of driving an instrumented vehicle on a circle of fixed radius at different constant speeds. The speed is incremented

from the lowest maintainable to the highest attainable at steady state. In this test, the vehicle response in terms of lateral acceleration and yaw rate were recorded. From the analysis of the recorded data, information regarding understeer characteristics can be obtained. Table **4-2** summarizes the details about the constant radius test.

Table **4-2**: Constant radius cornering test

Vehicle Loading Condition	unladen
Radius (m)	30.5
Nominal Testing Speed (mph)	5, 10, 15, 20,25
Data Recorded	lateral acceleration, yaw angle, yaw rate, heading angle, steering angle

4.3.2 Step Steer and Continuous Sinusoidal Steer

The test procedures for transient handling characteristics of the bus were adapted from ISO 14793 (ISO 2003). Step steer and continuous sinusoidal steer tests as described in standard were performed. The details on the transient response tests are summarized in Table **4-3** .

Table **4-3**: Transient response tests

	Step Steer	Sinusoidal Steer
Vehicle Loading Condition	unladen	
Nominal Testing Speed (mph)	15, 20,25	15
Steering Frequency (Hz)	n/a	0.3, 0.4, 0.5, 0.6, 0.8, 1, 1.2
Data Recorded	lateral acceleration, yaw angle, yaw rate, heading angle, steering angle	

The step-steer test was carried out to determine the sensitivity of the vehicle response to a sudden change in steering input. More specifically, it measures how promptly the vehicle reacts to a steering input and how quickly it can settle to a new equilibrium. Due to the limitation of the test track, speed of 50 mph recommended by the ISO standard for heavy-duty vehicles could not be reached. The highest safe speed achieved was 30 mph instead. The lateral acceleration during the test was purposely kept below 0.25 g to ensure linearity, which is critical for the data collected to be useful for linear model fit. The following performance evaluation specifications were extracted from the raw data:

- response times for lateral acceleration and yaw rate

- peak response times for lateral acceleration and yaw rate

- overshoot for lateral acceleration and yaw rate

The main objective for measuring vehicle responses to continuous sinusoidal steer inputs was to investigate the handling characteristics in frequency domain, essentially the frequency responses of yaw rate, lateral acceleration, and roll angle. By calculating the gains (ratios of the peak values of the response variables to steering angles) at various steering frequencies, the extent and promptness of vehicle response as a function of steering frequency can be determined.

4.4 Test Results and Discussions

The bus was tested in unladen condition on a dry asphalt pavement surface.

4.4.1 Steady-State Test

A major objective of performing the steady-state test is to determine understeer characteristics for the vehicle. There exist several conventional indicators for vehicular understeer characteristics, such as understeer gradient, stability factor, and stability margin. Each of these indicators has a unique interpretation regarding understeering property and is related to the others by design parameters of the vehicle. In order to facilitate an easy comparison with available literature, understeer gradient was adopted. In a constant-radius cornering test, the understeer gradient describes how the steering angle of the vehicle must be changed with the lateral acceleration variation. It can be identified as the slope of curve for the front wheel angle versus lateral acceleration shown in Figure **4-8**. As shown in the plots, in both clockwise and counter-clockwise turns, the steering angle increases linearly with the lateral acceleration up to about 0.23 g. Beyond 0.23 g, the changing of steering angle deviates from the linear pattern and starts to fall as lateral acceleration increases. Such a phenomenon manifests that the test bus is understeering when the lateral acceleration is lower than 0.23 g, then turns into limit oversteer beyond this lateral acceleration level. This conclusion is echoed by Figure 4-9, in which the difference between the front and rear tire-slip angles is plotted against lateral acceleration. It is shown that the slope of the curve starts to fall when the lateral acceleration exceeds 0.23 g, which implies limit oversteer for the vehicle as per Eq. **3.13**. The curve in Figure **4-8** also indicates that linear operation range of the bus is up 0.23g, which agrees with the discussion in Chapter 3.
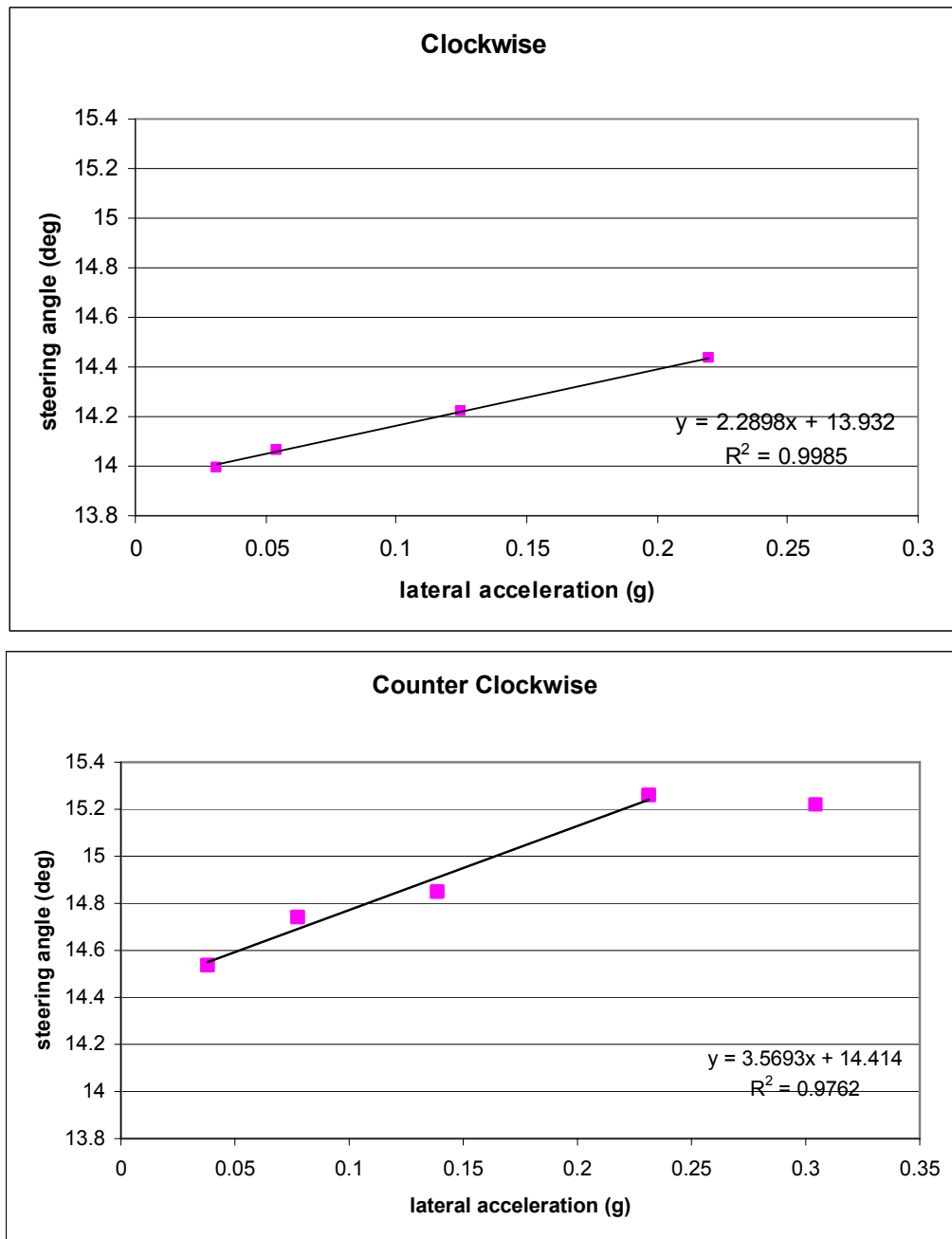
Figure **4-8**: Front wheel angle versus lateral acceleration
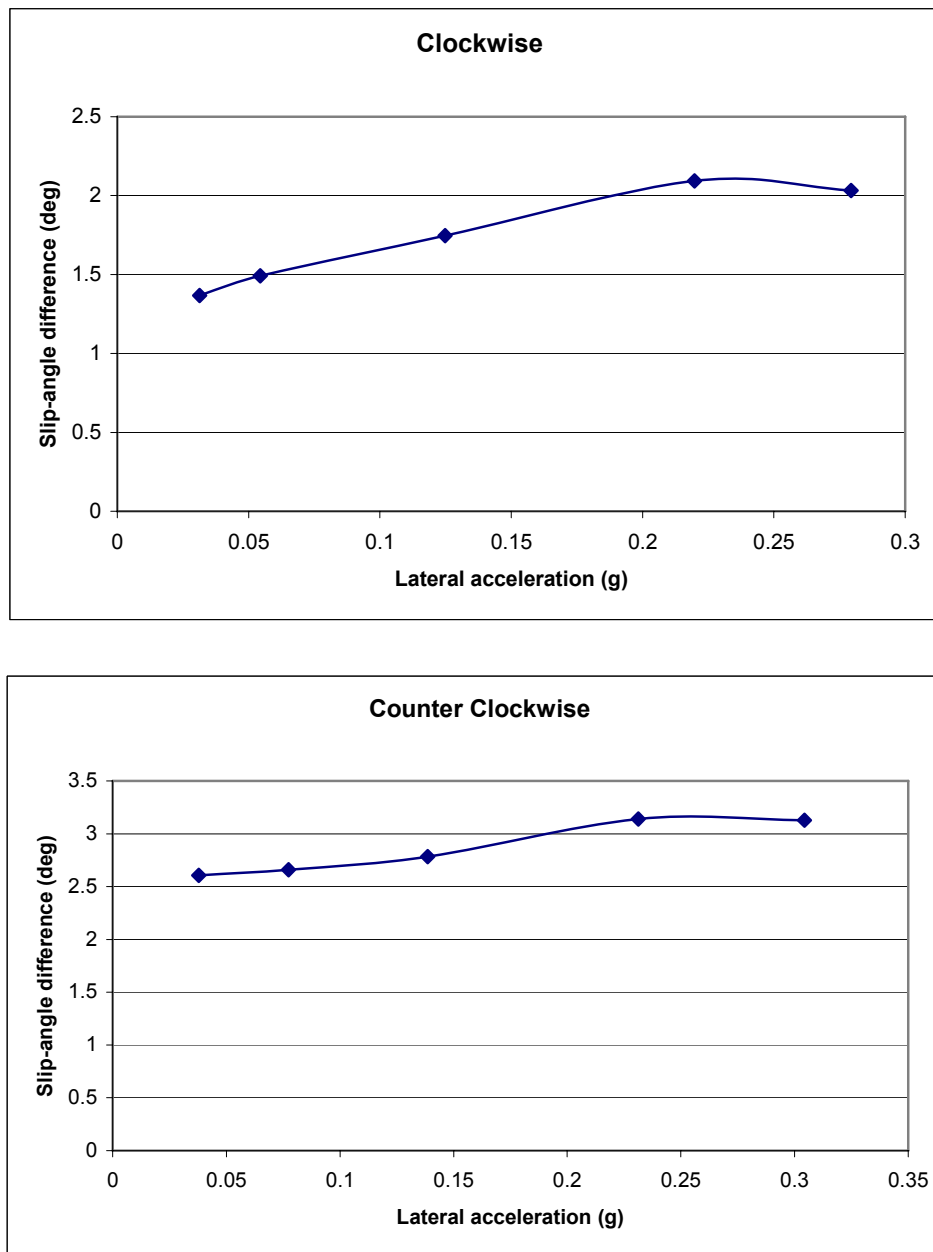
Figure **4-9**: Difference between front and rear tires at various lateral accelerations

The understeer gradients and the Ackermann angles (the interception of the curve with Y axis) are obtained by linear regression of the data points below 0.23 g. The

results for clockwise and counter-clockwise turns are reported in Table **4-4**. For comparison, the typical values for cars (Milliken and Milliken 1995a) and trucks (Sampson and Cebon 2003; Whitehead 1991) are also listed in the same table. As presented in the table, the understeer level of the tested bus is close to that of cars. If one were to judge performance based on this parameter (understeer gradient) alone, it appears that the capability of the tested bus to adapt to directional changes would be similar to that of a car for average drivers in general. The derived Ackermann angles from both directions are very close to the theoretical calculation ($\delta_{ack}=L/R=14.1°$). Since a 40-foot transit bus (or coach) has a longer wheelbase (L) than most of the other vehicles (except for articulated vehicles), its Ackermann angle should be one of the highest. Therefore, it requires a larger steering effort (angle) for the bus than for other vehicles during cornering.

Table **4-4**: Comparison of understeer gradients

	Clockwise		Counter Clockwise	
	K_{us} (°/g)	δ_{ack} (°)	K_{us} (°/g)	δ_{ack} (°)
Test Bus	2.29	13.93	3.57	14.14
Car	2~4	2~4	2~4	2~4
Truck	near neutral steer	4~13	near neutral steer	4~13

It is interesting to note that the bus exhibited a slightly higher understeering level in counter clockwise turns than in clockwise turns during the test. This phenomenon could be possibly due to asymmetric weight distribution between left and right sides of the bus, asymmetry in the steering system, different tire pressures and suspension

properties from side to side, and inconsistency in the driver operation in left and right turns may also add to the different cornering characteristics in left and right turns.

During the last three decades, steering wheel angle–side-slip angle gradient K_{ss} ($K_{ss} = \partial\delta_{sw}/\partial\beta$) has become another widely accepted steady-state handling performance criterion. K_{ss} is a more sensitive measure of vehicle directional response, which in general correlates better with subjective tests than the conventional understeer gradient (Barter 1975; Lindqvist et al. 1986). The possible reasons for this could be the inclusion of the effect of steering system and the use of side-slip angle, which is a direct measure of vehicle orientation. In addition, by deriving the changing rate of steering wheel angle with respect to the sideslip angle as a function of lateral acceleration, an insight into the transient handling behavior can also be obtained for the vehicle. The calculated K_{ss} is plotted in Figure **4-10** against lateral acceleration.
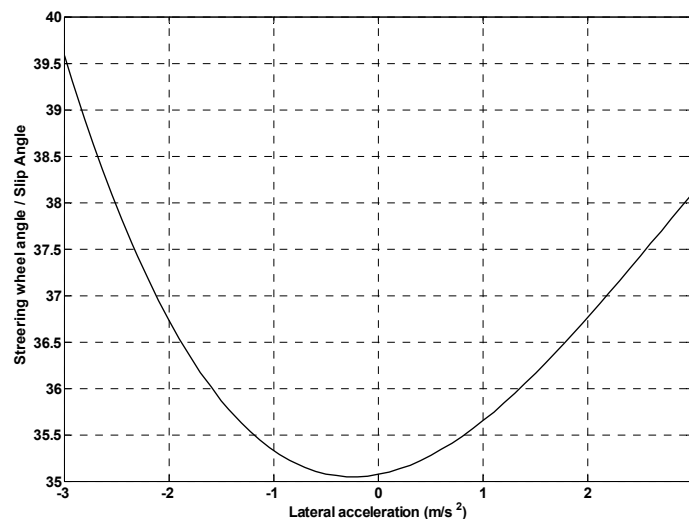
Figure **4-10**: Kss for various lateral acceleration levels

While it is not the only factor influencing "good" handling, a 'U' shaped K_{ss} versus lateral acceleration curve is usually desired, since it is accepted that good driver "feel" is associated with progressively increasing understeer level with increasing lateral acceleration (Metz 2004; Whitehead 1991). As presented in Figure **4-10**, the K_{ss} versus lateral acceleration curve derived from the bus testing measurements forms a 'U' shape and satisfies the condition mentioned above. The curve intercepts with Y axis (K_{ss} at zero lateral acceleration) at approximately 35.1. The ideal offset value for good handling is between 4 to 20 for cars (Barter 1976; Lindqvist et al. 1986). A large offset value is associated with unresponsive steering response. Hence, based on the range of reference values for cars, the steering response of the test bus would be rated as "soggy". However, the side-slip angle in daily driving rarely exceeds 5 deg (van Zanten et al. 1995). So under normal operating conditions with a K_{ss} value of approximately 35, a driver should be able to negotiate most of the curves with a steering wheel angle of less than 180 degrees (half a turn). Based on this fact, the cornering performance of the test bus seems to be acceptable.

Another usage of K_{ss} curve is for straight running performance evaluation. The higher the Y-axis interception, the better the performance is. A value of 35.1 for the test bus reflects a good straight line running performance.

4.4.2 Transient Response Tests

4.4.2.1 Step Steer

The time histories of lateral acceleration and yaw rate along with the steering input recorded at 15 mph are shown in Figure **4-11** as a sample for step-input response of the bus.
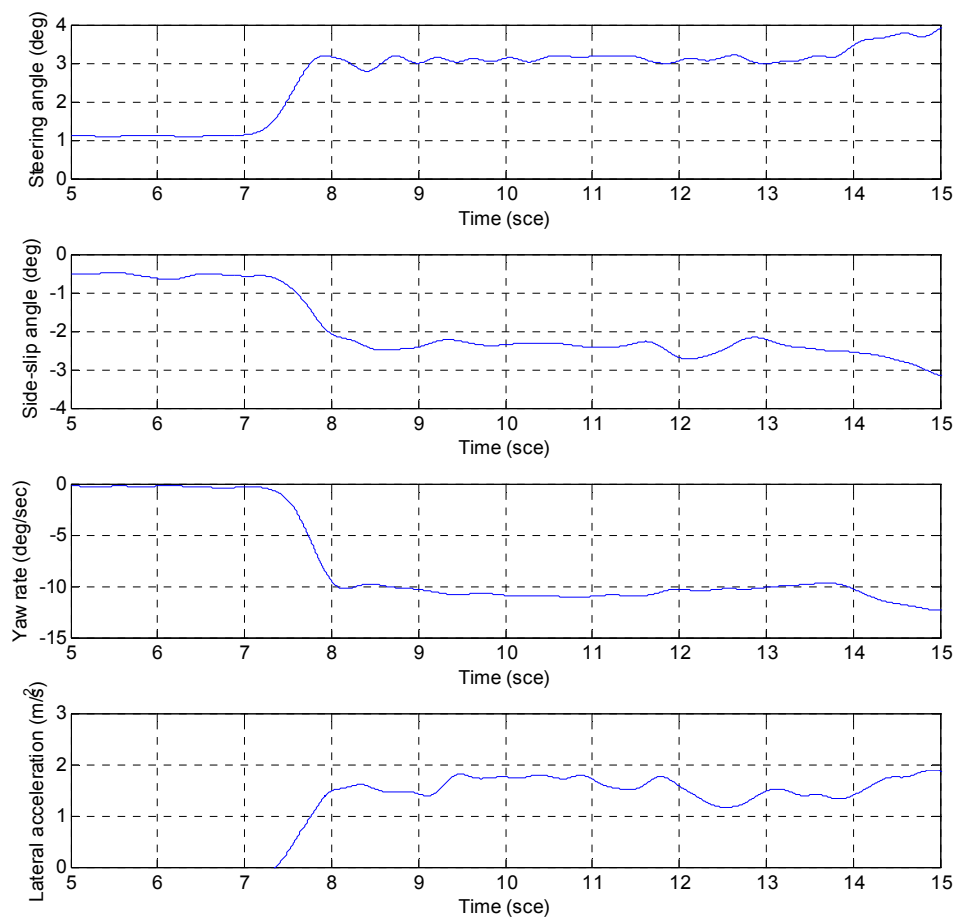
Figure **4-11**: Step-steer responses at 15mph

As displayed, a sudden change in steering wheel angle at approximately 7.3 second excited steep increases in side-slip angle, yaw rate, and lateral acceleration. Due to tire lag[2] (Heydinger et al. 1991; Milliken et al. 2003) as well as the flexibility and inertia of the vehicle system, the response had a delay with respect to the input. Since the vehicle is understeering, the yaw rate and lateral acceleration responses are underdamped (Milliken and Milliken 1995b). Consequently, oscillations around the steady-state value were observed, resulting in overshoots in measured variables.

The step-response behavior of a vehicle can be characterized by a number of parameters, typically, response time, peak response time, and overshoot. It is recommended in the literature (Good 1977), the t_{63} should be used for response time, as it is less sensitive to steering rate. However, in order to facilitate a comparison, we will use the specifications by the ISO 14793 (ISO-14793 2003).

The step-response characteristics extracted from the test measurements are reported in Table **4-5**. It is widely accepted that lateral acceleration response time to step-steer inputs is a very important criterion for handling evaluation (Jaksch 1983; Lindqvist et al. 1986). For cars and trucks, the lateral acceleration response time usually lies within $0.2 \sim 0.7$ sec (Milliken and Milliken 1995b). A vehicle with a very long response time would never seem to reach the desired heading direction, while too short a response time may be beyond a human driver's capability to comfortably cope with, and hence will also limit the vehicle's maneuverability. According to previous experiments

---

[2] Tires do not generate lateral force instantaneously in the presence of a slip angle. Instead, the tire needs to roll through a certain distance before full, steady-state lateral force is achieved, resulting a lag in lateral force generation.

(Hoffman 1976a; Hoffman 1976b; Jaksch 1983), 0.2 ~ 0.25 sec was generally found to be the ideal lower limit for lateral acceleration response time. This value was found to correspond well with favorable subjective driver ratings in severe lane change maneuvers.

Due to the differences in definitions of test criteria and in the magnitude of test parameters such as steering rate, steering input magnitude, and vehicle speed, a one-to-one comparison of the performance values obtained in this test with those found in literature is difficult. Nevertheless, the lateral acceleration response time of the test bus lies within the range mentioned in literature.

Table **4-5**: Characteristic parameters for step steer

	Response Time (s)	Peak Response Time (s)	Maximum Overshoot (%)
Lateral Acceleration	0.41	0.73	14
Yaw Rate	0.4	0.64	4.2

4.4.2.2 Sinusoidal Steer

In the context of this thesis work, the most interesting results of the transient response tests are the frequency responses of yaw rate and lateral acceleration.

The yaw rate frequency responses measured at 30 mph is presented in Figure Error! Reference source not found.. The desirable shape of the yaw rate response should be "flat" within operating frequency range. The response of the tested bus is close

to this description, showing a reasonably consistent gain level up to 1.5 Hz. Peaks in response, though unexpected for a heavy-duty vehicle, are observed at around 0.8 Hz for all testing speeds. This frequency is the damped natural frequency of yaw motion. In general, an understeering vehicle produces underdamped yaw responses (Milliken and Milliken 1995b). Therefore, the existence of response peaks is in agreement with the understeer characteristics of the vehicle.

The effect of speed on yaw rate gain can also be observed in Figure Error! Reference source not found.. It is seen that the yaw rate gain rises when vehicle speed increases. Generally, the variation of yaw rate with respect to speed is caused mainly by two factors: yaw rate sensitivity to steering rate, and yaw damping. It is worth to note, however, according to previous analysis results (Barter and Little 1970), the increase in yaw rate observed is almost entirely due to the reduction in the effect of steering rate on yaw rate at higher speeds rather than due to the reduction in yaw damping, as might be expected. Figure **4-12**
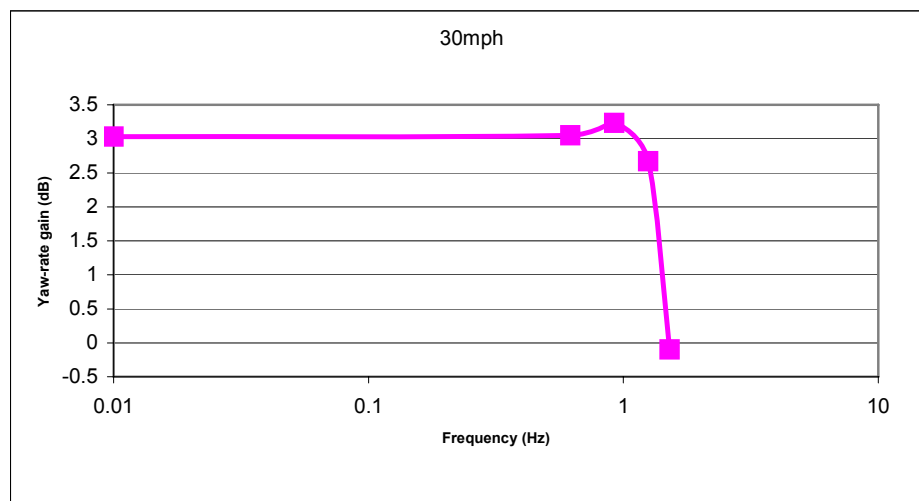
Figure **4-12**: Frequency response for yaw rate

A typical lateral acceleration frequency response plotted using the previous experimental data (Siegel 1956) for a car is shown in Figure **4-13**. As displayed, a "notch" exists within the high frequency range.   The resurging trend in lateral acceleration gain at higher frequencies is due to the increase in the acceleration component caused by the change in the turning radius (Dixon 1996; Siegel 1956). The frequency response of lateral acceleration at 15 mph is shown in Figure **4-14** . As can be seen, for the test bus, the notch in lateral acceleration response, which has been frequently encountered in previous experiments does not appear up to the peak steering frequency achievable by the driver during the test, which is near 1.5 Hz. Since this frequency limit would probably not be safely exceeded under normal operating conditions in real life, a driver is not expected to experience a fluctuating lateral acceleration gain with respect to frequency in his/her driving causing an undesirable handling feel.
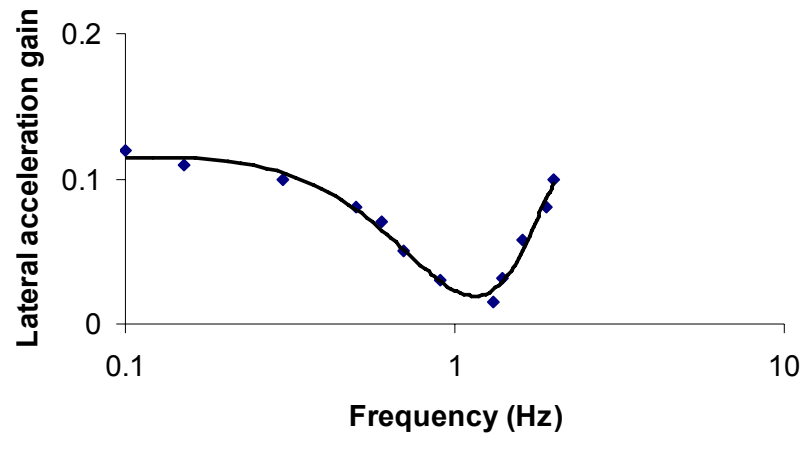
Figure **4-13**: Sample lateral acceleration frequency response for a passenger car
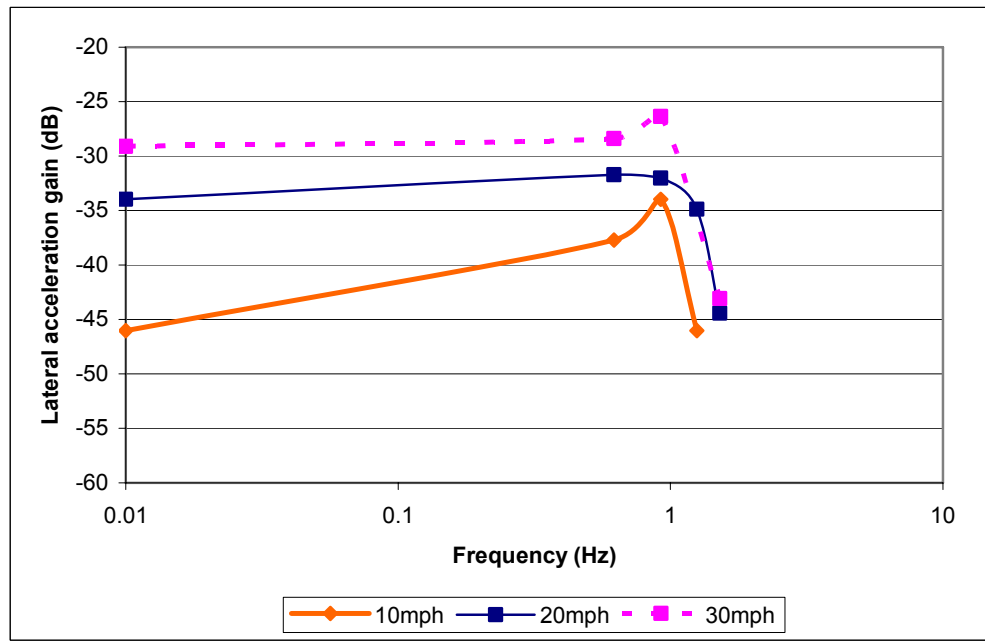
Figure **4-14**: Frequency response for lateral acceleration

As we can observe from Figures Error! Reference source not found. and **4-14**, the bandwidth of the frequency responses of yaw motion and lateral acceleration is at least 1.5 Hz. Within this bandwidth, the bus has consistent yaw rate and lateral acceleration gains with respect to steering wheel input. Compared to a modern car, which usually is able to respond to inputs as high as 3 ~ 4 Hz, the bandwidth of the test bus seems to be narrow. However, the frequency range for corrections and compensating steering in normal operations is only around 0.7 Hz (McLean and Hoffman 1973; Roland 1983). So the bandwidth of the test bus is already wide enough.

As presented in the above figures, the shapes of the frequency response curves for yaw rate, lateral acceleration of the bus are analogous to that of a car. The analogy nature reflects the similar levels of understeer achieved by the two types of vehicles at low lateral acceleration.

4.4.3 Summary

With regard to steady-state response characteristics, the test bus shows a marked improvement in performance over the models reported earlier (Rompe and Heissing 1986; Whitehead 1991; Wier et al. 1974). While a 70's bus would typically show a tendency towards oversteer in steady state, the test bus equipped with modern air suspension system remained understeer up to 0.23 g. Since vehicle lateral acceleration rarely exceeds 0.2 g on roads in North America (Jacobson 1983), the bus should remain understeering for its normal operation. The test bus achieved an understeer gradient very similar to that of passenger cars throughout its operating range. As rated by steering

wheel angle–sideslip angle gradient K_{ss}, the steady-state cornering performance is "soggy" compared to that of a car. However, it is adequate considering the lateral accelerations and side-slip angles encountered in normal bus driving.

In transient response tests, the lateral acceleration response time of the tested bus is 0.49s, which is reasonably short and even falls in the range typically achieved by passenger cars. The bandwidth of the bus is fairly wide, ensuring a consistent handling manner under different frequencies of steering inputs. In addition, the shape of the frequency response curve is similar to that of a car, reflecting the similar levels of understeer achieved by the two types of vehicles at low lateral acceleration.

4.5 Vehicle-Parameter Identification

The parameters of the bus are either directly measured or identified from the testing data. Among the parameters, vehicle mass (m), wheel base (L), and C.G. position (a, b) can be measured directly. Tire cornering stiffnesses (C_f, C_r) and yaw moment of inertia (I_{zz}) need to be numerically identified from the experimental data.

The time histories for step-steer responses of the test bus at 15 mph and 20 mph are used for parameter identification. As the lateral accelerations under these two testing speeds are less than 0.2 g, vehicle should remain in its linear operation range. The parameters (C_f, C_r, I_{zz}) are identified using model fit. During model fit, the experimental data for steering input are fed to the 2-DOF linear vehicle model described in Eq. **2.8**. At the same time, C_f, C_r, and I_{zz} are tuned such that step-steer response of the 2-DOF linear model can closely match the experimental data for the same steering input. The

parameter values cited in (Sampson 2002; Weir et al. 1974) were used as the initial values for C_f, C_r, and I_{zz}. With the parameter values listed in Table **4-6**, reasonably close fits are obtained for the testing data as shown in Figures **4-15** and **4-16**. It can be seen from the plots, the responses of the model are always ahead of the experimental data for tenths of a second. This is most possibly due to neglecting tire lag in the mathematical model.

Table **4-6**: Vehicle parameters

Vehicle Mass (kg)	12372
Wheel Base (m)	6.228
Longitudinal C.G. Position (m)	a=4.0568 b=2.1712
Front-Axle Equivalent Cornering Stiffness C_f (N/rad)	-230150*
Rear-Axle Equivalent Cornering Stiffness C_r (N/rad)	-482090*
Yaw Moment of Inertia I_{zz} (kg.m^2)	130760*

* identified from numerical model fit
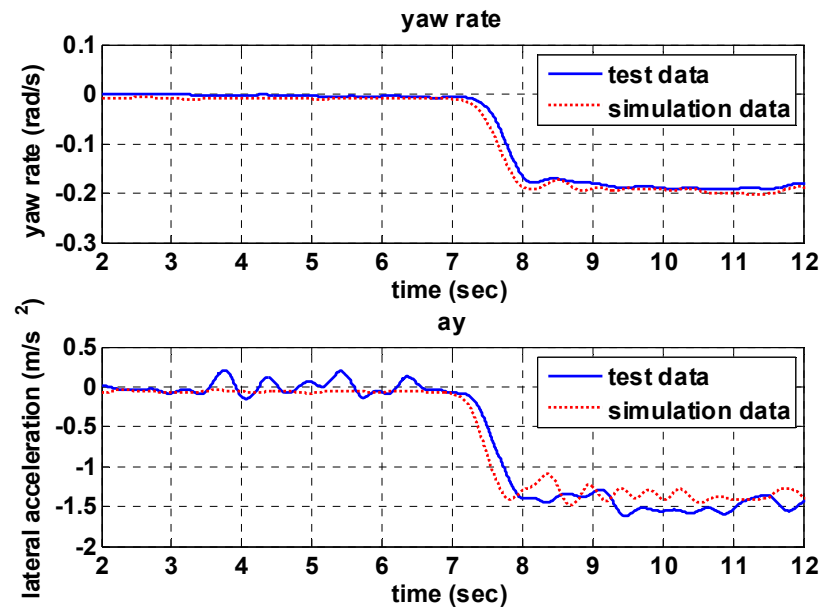
Figure **4-15**: Model fit for step-steer responses at 15 mph
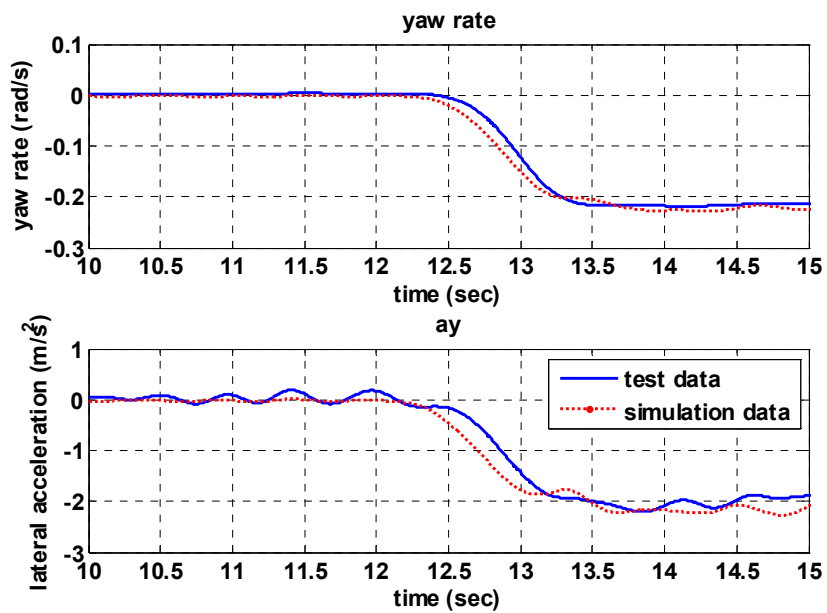
Figure **4-16**: Model fit for step-steer responses at 20 mph

References

1.   Allen, R. W., Szostak, H. T., Rosenthal, T. J., and Klyde, D. H. (1990). "Field testing and computer simulation analysis of ground vehicle dynamic stability." *SAE 900127*.

2.   Barter, N. F. (1975). "Analysis and interpretation of steady-state and transient vehicle response measurements." *Vehicle System Dynamics*, 5.

3.   Barter, N. F. (1976). "Analysis and interpretation of steady-state and transient vehicle response measurements." *Vehicle System Dynamics*, 5.

4.   Barter, N. F., and Little, J. (1970). "The handling and stability of motor vehicles." *1970/10*, The Motor Industry Research Association.

5.   Cameron, J. (2005). "Vehicle dynamic modeling for the prediction and prevention of vehicle rollover," The Pennsylvania University.

6.   Dixon, J. C. (1996). *Tires, Suspension and Handling*.

7.   Gillespie, T. D., and Segel, L. (1983). "Influence of front-wheel drive on vehicle handling at low levels of lateral acceleration." *IMechE C114/83*.

8.   Good, M. C. (1977). "Sensitivity of driver-vehicle performance to vehicle characteristics revealed in open-loop tests." *Vehicle System Dynamics*, 6.

9.   Heydinger, G. J., Garrott, W. R., and chrstos, J. P. (1991). "The importance of tire lag on simulated transient vehicle response." *SAE 910235*.

10.   Hoffman, E. (1976a). "Human control of road vehicles." *Vehicle System Dynamics*, 5.

11.   Hoffman, E. (1976b). "Human control of road vehicles." *Vehicle System Dynamics*, 5.

12.   ISO-14793. (2003). "Road Vehicles - Heavy commercial vehicles and buses - Lateral transient response test methods."

13.   ISO. (1982). "ISO 4138 - 1982." *Road Vehicles - Steady state circular test procedure ISO 4138-1982*.

14.   ISO. (2003). "ISO 14793." *Road Vehicles - Heavy commercial vehicles and buses - Lateral transient response test methods*.

15. Jacobson, M. A. (1983). "Car handling test results: response to transient inputs." *IMechE C127/83*.

16. Jaksch, F. O. (1983). "The influence of different vehicle parameter on steering controllability and stability." *IMechE C110/83*.

17. Lanchester, F. W. (1907). "Some problems peculiar to the design of the automobile." *Proceedings of Institute of Automobile Engineering*, 2.

18. Lindqvist, O., Andersson, K., and Plummer, J. (1986). "A Study of the Influence of Some Parameters on the Stability and Handling of Inter-city Coaches." *IMechE C211/86*.

19. Martini, R. (2006). "GPS/INS sensing coordination for vehicle state identification and road grade positioning," The Pennsylvania State University.

20. McLean, J. R., and Hoffman, E. (1973). "The effects of restricted preview on driver steering control and performance." *Human Factors*, 15(4).

21. Metz, L. D. (2004). "What constitute good handling?" *SAE 2004-01-3532*.

22. Milliken, D. L., Kasprzak, E. M., Meta, L. D., and Milliken, W. F. (2003). *Race Car Vehicle Dynamics - Problems, Answers and Experiments*, SAE International, Warrendale, PA.

23. Milliken, W. F., and Milliken, D. L. (1995a). *Race Car Vehicle Dynamics*, SAE International, Warrendale, PA.

24. Milliken, W. F., and Milliken, D. L. (1995b). "Race Car Vehicle Dynamics."

25. Milliken, W. F., and Whitcomb, D. W. (1956). "General introduction to a programme of dynamic research."

26. Radt, H. S., and Pacejka, H. B. (1963). "Analysis of the "steady state" turning behaviour of an automobile." *Proceedings of IMechE Symposium on Control of Vehicles*.

27. Roland, M. A. (1983). "Some aspects on suspension design parameters for improved vehicle response at the limit of adhesion." *IMechE C115/83*.

28. Rompe, K., and Heissing, B. (1986). "Test procedures and evaluation criteria for the handling characteristics of heavy commercial vehicles."

29. Sampson, and Cebon. (2003). "Active roll control of single unit heavy road vehicles." *Vehicle System Dynamics*, 40.

30. Sampson, D. (2002). "Active Roll Control of articulated Heavy Vehicles," Cambridge University.

31. Segel, L. "Research in the fundamentals of automobile control and stability." *Proceedings of the SAE National Summer Meeting*, Atlantic City.

32. Segel, L. (1956b). "Theoretical prediction and experimental substantiation of the response of the automobile to steering control." *Proceedings of IMECHE*, 171(7), 310-330.

33. Siegel, L. (1956). "In the fundamentals of automobile control and stability."

34. van Zanten, A. T., Erhardt, R., and Pfaff, G. (1995). "VDC The vehicle dynamic control system of Bosch." *SAE 950759*.

35. Weir, D. H., Teper, G. L., Hoh, R. H., Humes, R. W., Sihilling, C. S., and Hofmann, L. G. (1974). "Analysis of Truck and Bus Handling." *DOT-HS-242-2-421*, STI.

36. Whitcomb, D. W., and Milliken, W. F. (1956). "Design implications of a general theory of automobile stability and control." *Proceedings of IMECHE*.

37. Whitehead, J. P. (1991). "The handling characteristics of European intercity buses." *SAE 912678*.

38. Whitehead, J. P. (1991). "The handling characteristics of European intercity buses." *SAE 912678*.

39. Wier, D. H., Teper, G. L., and Hoh, R. H. (1974). *Analysis of Truck and Bus Handling DOT-HS-801 152*.

Chapter 5

Effects of Loading Condition on Yaw-Rate Response of Buses

5.1 Introduction

Besides the design parameters such as wheel base and tire cornering stiffness, there exist three major external factors that would most possibly influence the handling of a vehicle - speed, road friction, and loading condition. According to previous research works, speed and road friction are known to affect the handling characteristics significantly (Allen et al. 1987a; Allen et al. 1990; Barter and Little 1970; Whitcomb and Milliken 1956). However, to what extent the loading condition plays a role in affecting the handling has not been thoroughly investigated, especially for buses. During daily service, the static vehicle weight of a typical 40-foot transit bus can change by almost 50%. Consequently, the location of center of gravity, suspension compliance, tire cornering stiffness, the yaw moment of inertia, and many other vehicle parameters vary significantly. These changing parameters will directly influence the dynamical properties of the vehicle.

Since this thesis focuses on yaw-stability enhancement for buses by yaw-rate control, the effects of changes in weight and weight distribution on the steady-state as well as transient yaw-rate response of a 40-foot transit bus are investigated both analytically and numerically in the rest of this chapter. The results from such an investigation provides an answer to the question as whether it is necessary to consider

loading condition variation as an external perturbation in the linear modeling, which might deteriorate the robustness and performance of the yaw-rate controller during the controller-design process

5.2 The Variation of Loading Condition

The loading condition variation of a 40-foot transit bus in its daily service is presented Table **5-1**. Three typical loading conditions are listed: curb weight[3](C.W.), seated load weight[4](S.L.W.), and gross vehicle weight[5](G.V.W.). As can be seen, the overall weight of the bus is increased by nearly 50% when loaded from C.W. to G.V.W.. It is interesting to note, however, that while the weight of the bus is changing significantly, the weight distribution stays approximately the same. This phenomenon is fairly common for heavy-duty buses, because the C.G. (center of gravity) of the empty bus is located near the middle of the passenger area. Therefore, between weight and weight distribution, weight is the dominating factor that would affect the dynamics of the bus when loading condition is changing. Unless otherwise stated henceforth, the effects of loading condition on vehicle handling of the 40-foot test bus would be determined by studying weight change only.

---

[3] Curb Weight - vehicle weight including maximum fuel, oil and coolant; but without passengers or driver.
[4] Seated Load Weight - curb weight plus 68lb for every designed passenger seating position and for the driver.

[5] Gross Vehicle Weight - seated load weight plus 150lb for each 1.5ft^2 of free floor space.

Table **5-1**: The variation of loading condition of a bus

Loading Condition	C.W.		S.L.W.		G.V.W.	
Vehicle Weight (kg)	12395		15692		17867	
Weight Distribution (%)	Front	Rear	Front	Rear	Front	Rear
	34.98	65.02	35.98	64.02	36.47	63.53

5.3 Steady-State Characteristics

As stated in Chapter 3, one of the most important criteria that describe the steady-state handling characteristics for a vehicle is understeer gradient. The formula for calculating understeer gradient of the linear bicycle model is repeated here:

$$K_{us} = (\frac{W_f}{C_f} - \frac{W_r}{C_r})/g \tag{5.1}$$

C_f front-axle equivalent cornering stiffness

C_r rear-axle equivalent cornering stiffness

K_{us} understeer gradient

W_f front-axle weight

W_r rear-axle weight

It is obvious that the vehicle weight has a significant effect on the value of K_{us}. As we can tell from Table **5-1**, the weight carried by each axle experiences significant changes when the bus is loaded from C.W. to G.V.W.. At the same time, the cornering

stiffness will also change nonlinearly with the axle weight. The variation of cornering stiffness with vertical load can be modeled by the following formula (Fancher et al. 1986; Gillespie 1992).

$$C = k_1 F_z + k_2 F_z^2 \tag{5.2}$$

C tire cornering stiffness

F_z tire vertical load

K_i constant coefficient

Using Eq. **3.13** along with Eq. **5.2**, the understeer gradient of the bus can be calculated analytically. The results for various loading conditions are listed in Table **5-2**.

Table **5-2**: Understeer gradients for different loading conditions

Loading Condition	Kus (°/g)
C.W.	2.3
S.L.W.	2.9
G.V.W.	3.2

As can be seen, the understeering levels for C.W., S.L.W., and G.V.W. conditions are reasonably close with a maximum difference of only 0.9°/g at the front wheel, which ensures a consistent handling feel under different loading conditions a bus would typically experience during operation.

The analytical results are confirmed by the numerical simulation in Trucksim. The time histories of the required front-wheel angle for tracking a 40m-radius circle under different lateral accelerations are plotted in Figure **5-1** for the three loading

conditions. As the plot shows, the maximum difference in road-wheel steering angle is only around 0.1° at 0.2 g. The similarity in steering-angle magnitudes within linear operating range implies a similar understeer gradient. Therefore, the loading condition does not have a significant effect on steady-state handling characteristics of a bus during normal operation.
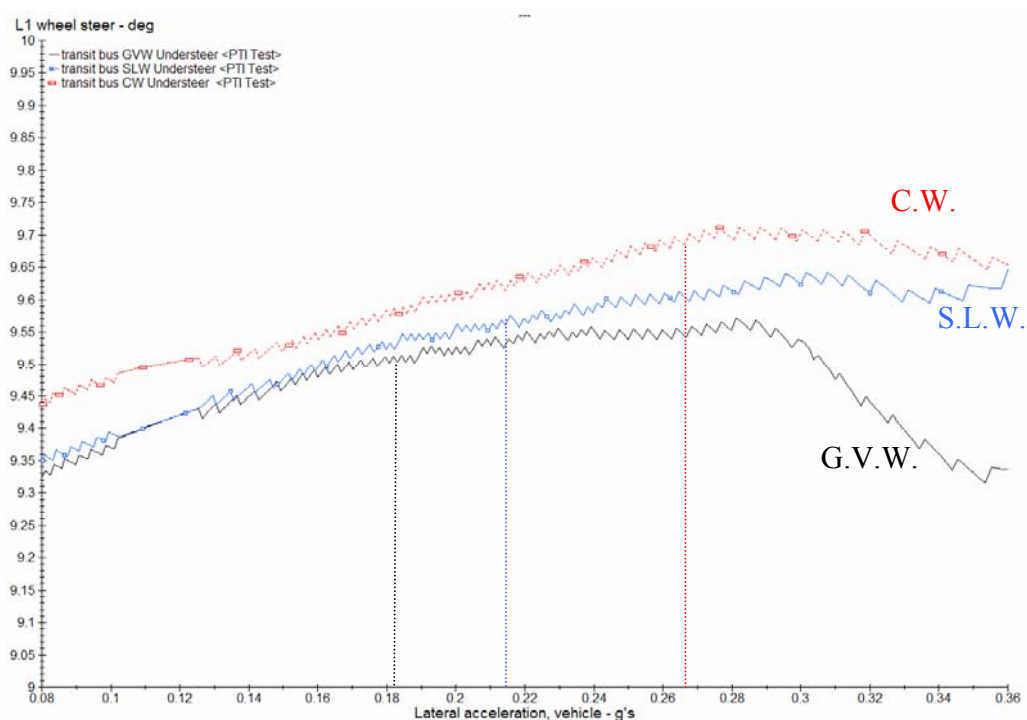
Figure **5-1**: Understeer gradient curve for different loading conditions

However, we do notice from the above plot that load condition significantly affects the linear operating range of the test bus. As shown, the linear range for C.W. is up to 0.27 g. It drops to 0.21 g and 0.18 g for S.L.W and G.V.W conditions, respectively. The change in linear operating range under different loading conditions is caused by the nonlinear variation of cornering stiffness with respect to the vertical load as illustrate by Figure **2-4** in **2.1.3**.

5.4 Transient Response Characteristics

5.4.1 Natural Frequency, Damping, and Time Constant

Since the vehicle model can be approximated by a second-order system within the linear range, its natural frequency ω_n, damping ratio ζ, and zero time constant T_L can be expressed explicitly in terms of the vehicle parameters.

$$\omega_n = \sqrt{\frac{C_f C_r L^2}{I_{zz} m U^2}[1 + \frac{mU(bC_r - aC_f)}{C_f C_r L^2}]}$$

$$\xi = (\frac{C_f + C_r}{mU} + \frac{a^2 C_f + b^2 C_r}{I_{zz} U}) \Big/ (2\omega_n) \tag{5.3}$$

$$T_L = \frac{maU}{LC_r}$$

a	distance from the front axle to C.G.
b	distance from the rear axle to C.G.
$C_{f,r}$	front/rear effective axle cornering stiffness
I_{zz}	yaw moment of inertia
L	wheelbase
m	vehicle weight
U	vehicle speed

The effects of loading conditions on the values of ω_n and ζ are presented in Figures **5-2** and **5-3**, respectively. According to the plots, while the vehicle is loaded from C.W. to G.V.W., its ω_n drops by about 10%, and ζ remains roughly the same. Usually, a system's responsiveness and oscillatory level in response would be related to

ω_n and ζ, respectively. As a result, the rise time of the bus when subject to a step-steer input would seem to increase, implying a degraded transient response performance. At the same, its overshoot level would not change significantly.
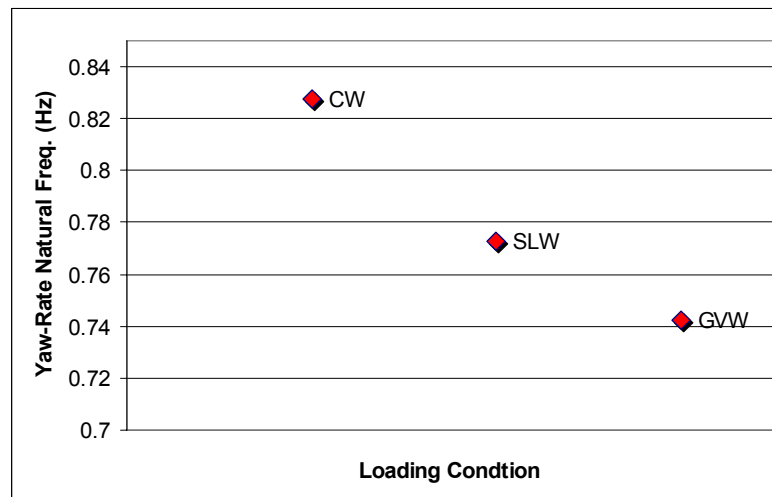
Figure **5-2**: The effect of loading condition on yaw-rate natural frequency
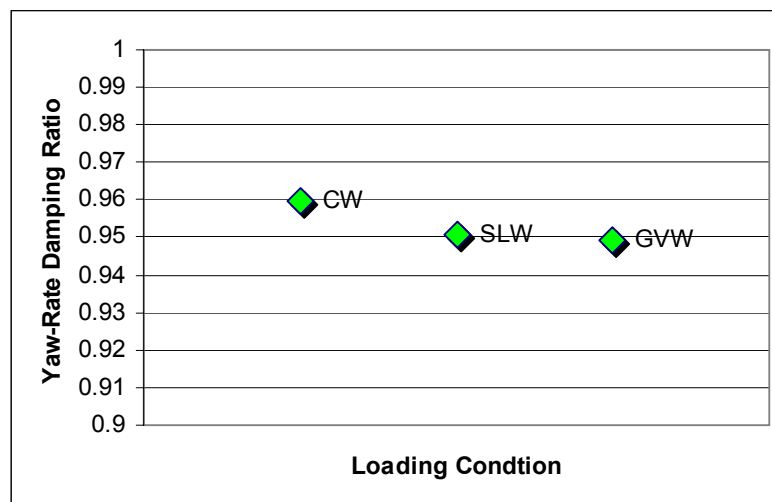
Figure **5-3**: The effect of loading condition on yaw-rate natural damping

However, the transient performance of the bus is not solely dictated by ω_n and ζ, because a vehicle is not a prototype second-order system. The time constant T_L (Shearer et al. 1996) in the numerator of the transfer function plays an equally important role as ω_n and ζ in determining the transient performance. The variation of T_L with respect to loading condition is shown in Figure **5-4**. With the bus loaded from C.W. to G.V.W., the T_L would decrease. Normally, the smaller the T_L, the shorter the rise time and the larger the overshoot will be (Kuo 1995; Ogata 2002; Shearer et al. 1996).

As per the above discussion, when the bus is loaded from C.W. to G.V.W., the corresponding variations in ω_n and ζ would tend to cause a longer response time and a marginally larger overshoot for the bus. Meanwhile, the change in T_L is likely to result in a shorter response time and a higher overshoot level. The contrasting effects of the variations in ω_n/ζ and T_L on the transient performances complicate the study. Due to lack of a comprehensive knowledge about the influence of ω_n/ζ, and T_L on transient characteristics in a closed form, it would be difficult to analytically predict transient-response performance for the test bus. Consequently, one needs to resort to numerical simulation to determine the overall effect of loading change. Nevertheless, according to previous literatures (Milliken and Milliken 1995; Whitcomb and Milliken 1956), the greater the understeering level is, the lower the damping in the yaw motion of the vehicle. Since the bus becomes more understeering when it is loaded from C.W. to G.V.W., we would tentatively expect a shorter rise time and an increased overshoot level.
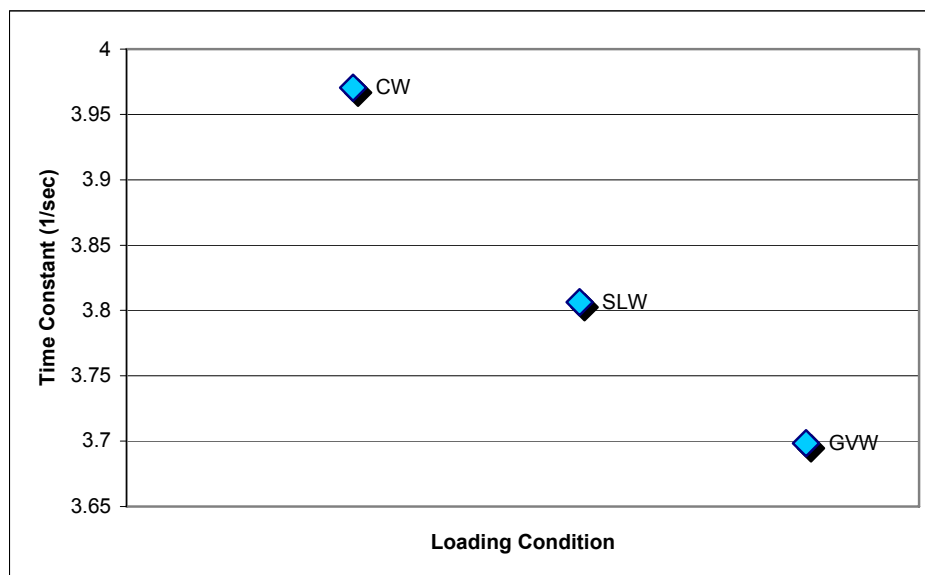
Figure **5-4**: The effect of loading condition on yaw-rate time constant

5.4.2 Step-Steer Response

The step-steer test, also known as J turn, is conducted in Trucksim to study the effects of loading conditions on transient-response performance of the test bus. The response time and the maximum overshoot for yaw-rate response will be measured during the simulated test. The "response time" refers to the "63% rise time[6]" for the step response. The "63% rise time" was selected because it was found to be insensitive to steering rate (Good 1977). The test procedure is adapted from ISO-14793 (ISO 2003). The ISO recommended testing speed of 80 km/h is used. To better approximate a step

---

[6] response time is defined as the time measured for a vehicle transient response to first reach 63% of its new steady-state value, as from the reference point when the steering-wheel angle change is 10% completed.

input, the steering input rate is set to be 500˚/sec, which is a little higher than the recommended value. The time history of the steering-wheel input for the step-steer test is shown in Figure **5-5** .
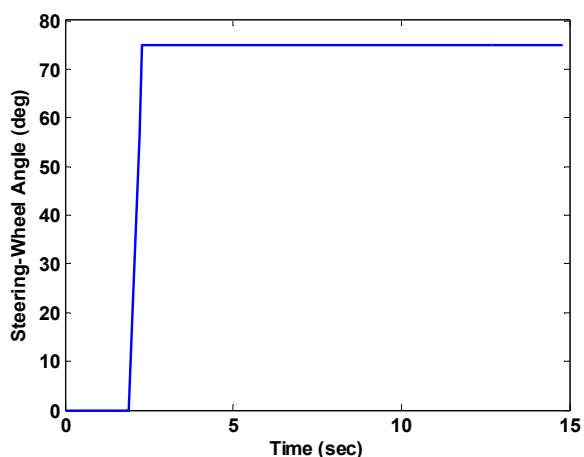
Figure **5-5**: Time history of the step-steer input

The time responses of J-turn under different loading conditions are shown in Figure **5-6** for the test bus. As can be seen, the response time is reduced and the overshoot is increased when the bus is more heavily loaded. The performance parameters of the test bus are listed in Table **5-3** for each of the loading conditions. For the three typical loading conditions, the simulated response times are all found to be around 0.4sec and overshoot level are reasonably close to each other, which implies a fairly consistent handling behavior under various loading conditions.
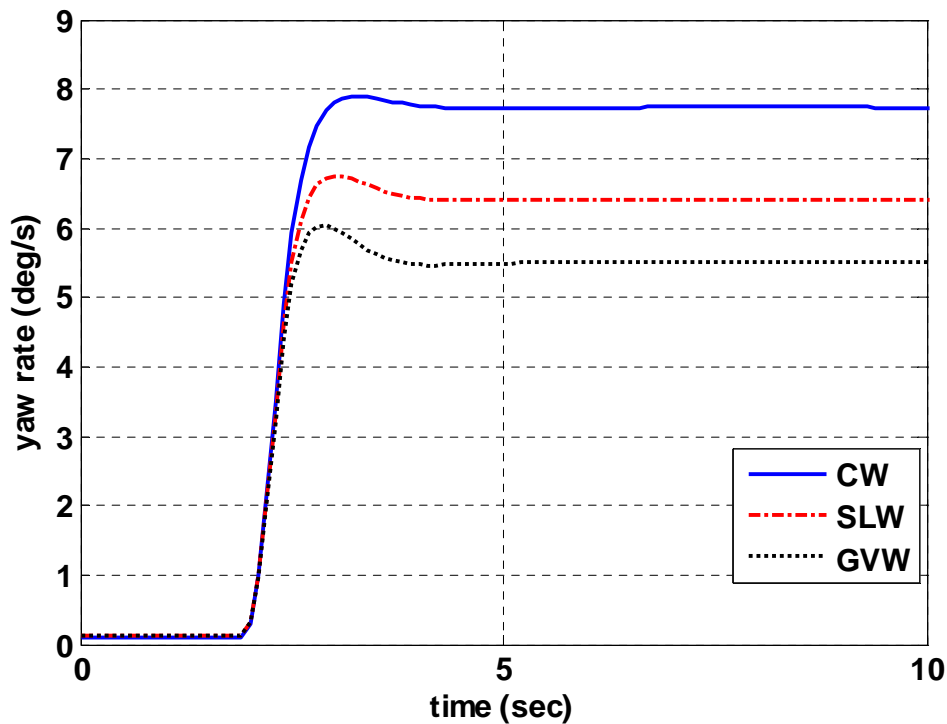
Figure **5-6**: Step-steer responses under different loading conditions

Table **5-3**: Step-steer response characteristics for different loading conditions

Loading Condition	C.W.	S.L.W.	G.V.W.
Rise Time tr63 (sec)	0.44	0.41	0.38
Overshoot (%)	3.2	5.6	8.8

Recall the discussion in the **5.4.1**, it seems that the influence of the variation in ω_n (and also ζ) on the transient performance of the bus is surpassed by the effects of the T_L. Therefore, it can be inferred that the yaw-rate dynamics is dominated by the zero time constant T_L (Allen et al. 1987b).

5.4.3 Frequency Response

The yaw-rate frequency response of the bus was first derived from the analytical transfer function. For comparison purpose, a full vehicle simulation was also conducted in Trucksim. To in obtain frequency response in Trucksim, a chirp-steer test was performed. Then, FFT was conducted on the time history of the chirp-steer test.

5.4.3.1 The Analytical Results

The Bode plots for the transfer functions from front-wheel angle to yaw rate under different loading conditions are shown in Figure **5-7**. As can be observed from the plots, the yaw-rate gain is reduced by approximately 20% at the maximum with the loading increased from C.W. to G.V.W.. At the same time, the bandwidth is very slightly broadened. The effect of loading variation on phase angle is only marginal and can be neglected in practice. As indicated by the roll-off rates of the responses, the damping ratio at C.W. is slightly higher than the other two. The results obtained from frequency analysis and step-steer test are consistent with regards to bandwidth and damping ratio variations. Since the bus has similar gain factors, bandwidth, and phase at different weights, the variation in loading condition would not cause a significant change in the frequency response.
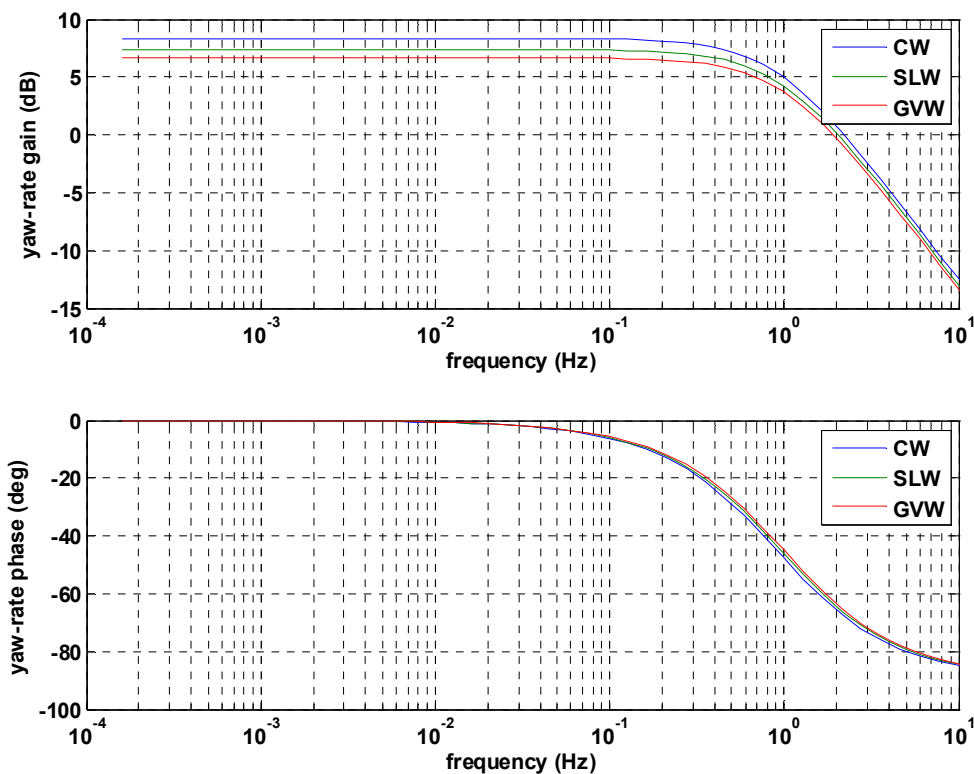
Figure **5-7**: Yaw-rate frequency response (analytical result)

5.4.3.2 Chirp-Steer Test

Chirp steer, also known as sine-sweep steer, refers to a continuous sinusoidal steering maneuver with gradually increasing frequency. The steering-wheel input for the chirp-steer test is shown in Figure **5-8**. As shown, the steering input sweeps from 0.1 to 3 Hz, while keeping a fairly constant steering magnitude. A simulated time history of yaw-rate response to the chirp-steer input at the speed of 30mph is presented for the test

bus in Figure **5-9**. The advantages of using chirp signal as the input over conducting a series of sinusoidal steer test at discrete frequencies are:

- Ideally, the frequency response can be extracted from just one time history.

- Theoretically, the frequency response of the system can be derived by simple algebraic calculations in time domain without resorting to any frequency analysis tools.

- The envelope of the time history is representative of the expected magnitude frequency response.

Usually, it requires a runway of 300-400 m to perform the chirp-steer test on a bus. Also, such a steering maneuver is very challenging for a human driver, if an automatic steering machine is not available.
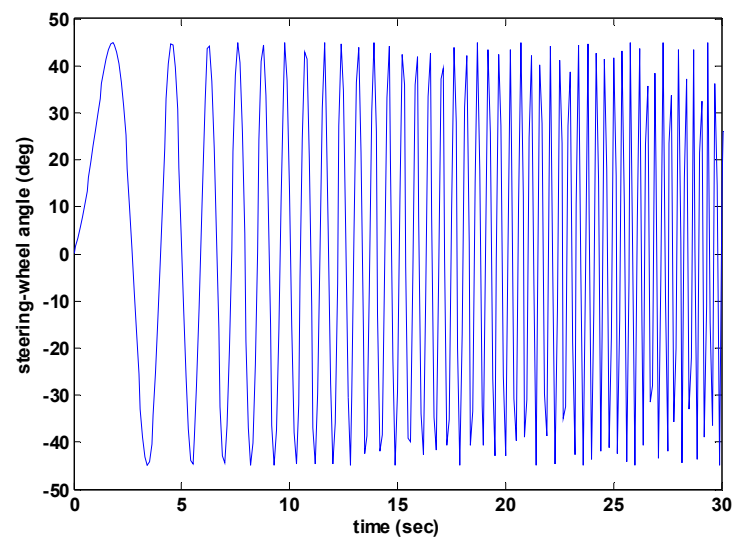
Figure **5-8**: Chirp-steer input
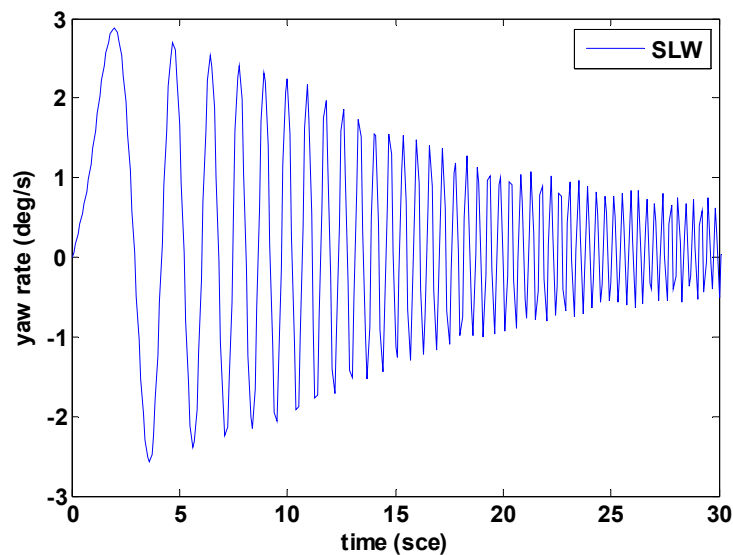
Figure **5-9**: Sample time history for chirp-steer response

5.4.3.3 Frequency Response from Trucksim

The yaw-rate frequency responses of the test bus obtained from Trucksim simulation at various vehicle loadings are displayed in Figure **5-10**. As can be seen, the results agree with those from analytical study (Figure **5-7**) very well. With the loading condition changing from C.W. to G.V.W., the gain factor is reduced while the bandwidth is increased. The roll-off rates of the curves are fairly close, indicating similar damping levels for different loading conditions. Therefore, the conclusions from the analytical study are confirmed by the numerical simulation.
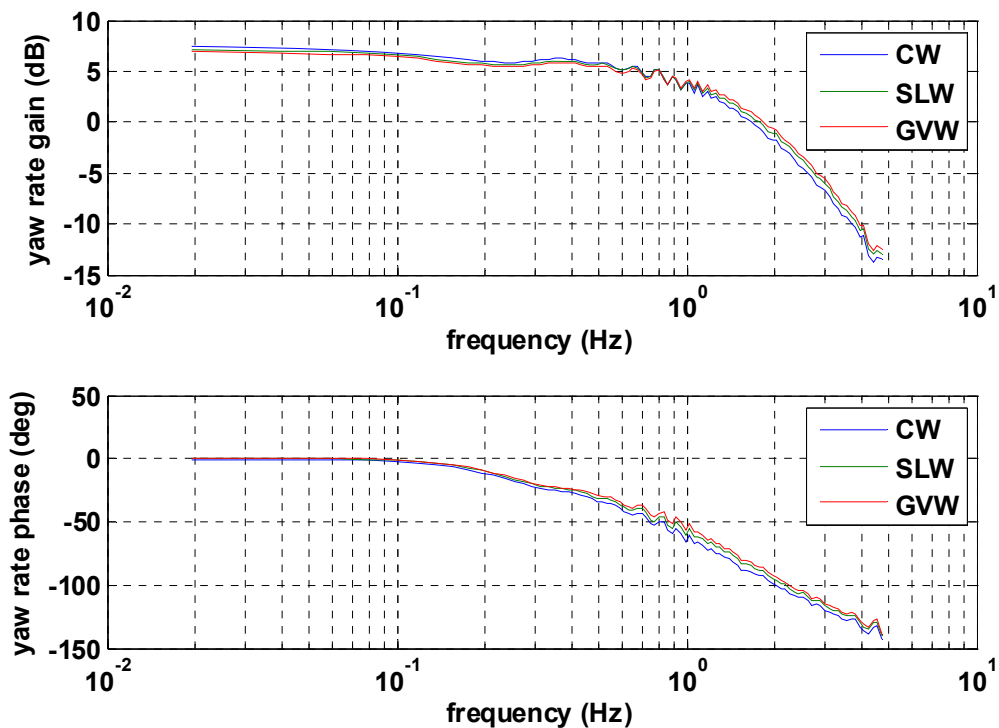
Figure **5-10**: Yaw-rate frequency response (Trucksim)

The results from both analytical study and numerical simulation show that the responses of the test bus exhibit a reasonably consistent gain level up to 1.25 Hz for all three typical loading conditions. Since the frequency range for corrections and compensating steering in the transit paths is normally less than 0.7 Hz (McLean and Hoffman 1973; Roland 1983), the bus should have reasonable yaw-rate responses to inputs at different frequencies during normal operations.

5.5 Summary

The effects of loading condition on yaw-rate response have been investigated both analytically and numerically. For the bus studied, loading condition does not have a significant effect on either the steady-state or transient-response performance within linear operating range. Therefore, it is not necessary to consider loading condition (mostly weight) as an uncertain parameter in the linear model when designing the yaw-rate controller proposed in future chapters.

References

1. Allen, R. W., J.R., T., and Szostak, H. T. (1987a). "Steady state and transient analysis of ground vehicle handling." *SAE 870495*.

2. Allen, R. W., Szostak, H. T., and Rosenthal, T. J. (1987b). "Analysis and computer simulation of driver-vehicle interaction." *SAE 871086*.

3. Allen, R. W., Szostak, H. T., Rosenthal, T. J., and Klyde, D. H. (1990). "Field testing and computer simulation analysis of ground vehicle dynamic stability." *SAE 900127*.

4. Barter, N. F., and Little, J. (1970). "The handling and stability of motor vehicles." *1970/10*, The Motor Industry Research Association.

5. Fancher, P. S., Ervin, R. D., Winkler, C. B., and Gillespie, T. D. (1986). "A factbook of the mechanical properties of the components for single-unit and articulated heavy trucks." The University of Michigan Transportation Research Institute.

6. Gillespie, T. D. (1992). *Fundamentals of Vehicle Dynamics*, Society of Automotive Engineers, Warren, Pa.

7. Good, M. C. (1977). "Sensitivity of driver-vehicle performance to vehicle characteristics revealed in open-loop tests." *Vehicle System Dynamics*, 6.

8. ISO. (2003). "ISO 14793." *Road Vehicles - Heavy commercial vehicles and buses - Lateral transient response test methods*.

9. Kuo, B. C. (1995). *Automatic Control System*, John Wiley & Sons Inc.

10. McLean, J. R., and Hoffman, E. (1973). "The effects of restricted preview on driver steering control and performance." *Human Factors*, 15(4).

11. Milliken, W. F., and Milliken, D. L. (1995). *Race Car Vehicle Dynamics*, Society of Automotive Engineers, Warren, Pa.

12. Ogata, K. (2002). *Modern Control Engineering*, Prentice Hall.

13. Roland, M. A. (1983). "Some aspects on suspension design parameters for improve vehicle response at the limit of adhesion." *IMechE C115/83*.

14. Shearer, J. L., Kulakowski, B. T., and Gardner, J. F. (1996). *Dynamic Modeling and Control of Engineering Systems*, Prentice Hall.

15.	Whitcomb, D. W., and Milliken, W. F. (1956). "Design implications of a general theory of automobile stability and control." *Proceedings of IMECHE*.

Chapter 6

PI-Controller Design for Active Front-Wheel Steering System

6.1 Overview of the Active Front-Wheel Steering System

The goal of the AFS (active front-wheel steering) system is to make the vehicle easy and intuitive to handle for the driver under potentially dangerous disturbances, such as limit oversteer/understeer[7], side-wind disturbance, and split-μ braking.

The AFS system realizes such a goal by keeping the behavior of the vehicle as close as possible to that of an ideal vehicle model through automatically front-wheel angle adjustment. This control objective can be achieved by applying model-following control strategy. The general approach is to let the controlled state variable(s) of the vehicle follow the signals generated by a reference model, which represents the desired vehicle-handling characteristics. Model-following control has been successfully applied for vehicle-dynamics control in both academic research projects (Brennan and Alleyne 1999; Chee and Tomizuka 1997; Fukao et al. 2001; Lee 1997; Nagai and Ohki 1989; van Zanten et al. 1995), and industrial applications (Krenn and Richter 2004; van Zanten et al. 1995).

The block diagram of the proposed control system is presented in Figure **6-1**. It is shown in the diagram, the controlled variable is selected to be the yaw rate (r) of the bus,

---

[7] Limit oversteer/understeer describes the situation when the rear tires of a vehicle exceed their lateral traction limits on the road before the front tires do, causing the vehicle to spin/drift during cornering.

and the input signal to the bus is the front-wheel steering angle (δ_f), producing a SISO (single-input single-output) problem. The reference signal (r_0) is generated by the ideal vehicle model according to the driver's steering put (δ_d). The error signal (e) between the reference yaw rate (r_0) and the measured yaw rate (r) from the bus actuates the AFS system. The controller in the AFS system will then adjust the steering angle based on the error signal to track the reference yaw rate.
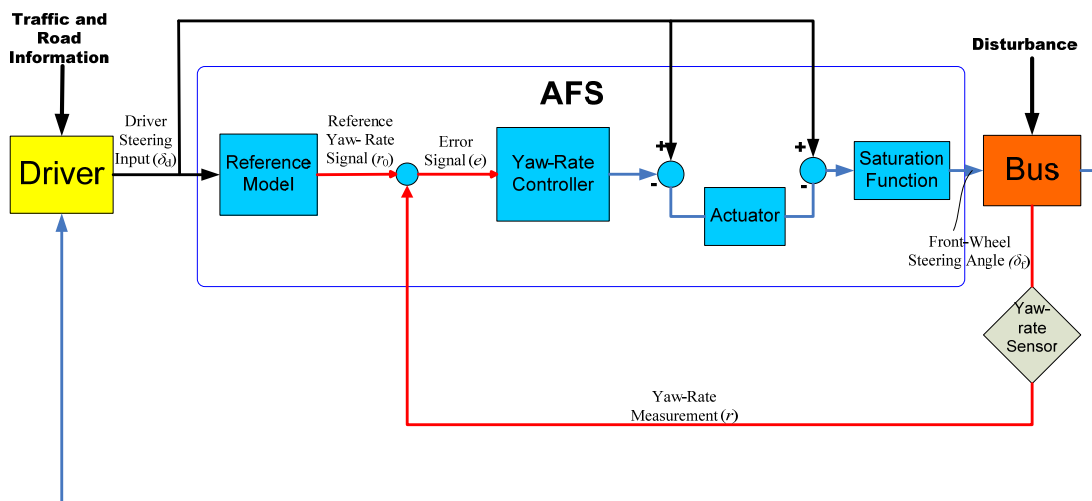
Figure **6-1**: Block diagram for the AFS (active front-wheel steering) system

The reference model is a linear bicycle model with constant tire cornering stiffness evaluated at 0° tire-slip angle on dry road. This model represents the vehicle dynamical behavior in the linear range, which is designed to be safe and predictable by most drivers. If the yaw rate of the test bus can closely follow that from the reference model regardless of external disturbances and vehicle-parameter variations, the vehicle will tend to stay stable and maneuverable to the driver.

As an essential state variable describing the vehicle's yaw dynamics, yaw rate is selected to be the controlled variable for the bus. It has been widely agreed that yaw rate is an effective and easy-to-measure controlled variable in vehicle-dynamics control (Abe et al. 1996; Anwar 2003; Ghoneim et al. 2000; Inoue and Sugasawa 1993; Ito et al. 1987; Selby et al. 2001; Yuhara and Tajima 2001; Zeyada et al. 1998). Some researchers even considered yaw rate as "the best parameter to be sensed and used for vehicle directional control" (Kasselmann and Keranen 1969). The reasons why yaw rate has become the primary control target in vehicle yaw-dynamics control were summarized in previous publications: "The vehicle's yaw rate was chosen as the primary performance output because this state is currently measured or estimated on production-vehicle control systems and because yaw-rate feedback is well known to compensate for unmodeled dynamics and unknown disturbances such as wind or road variations" (Brennan and Alleyne 2001). "Most of the vehicle disturbances, non-smooth actuator nonlinearities, unmodeled imperfections stemming from vehicle-road interactions and uncertainties regarding system parameters can be by-passed through the yaw rate measurement" (Hatipoglu et al. 1998).

6.2 Design Objectives and Specifications

The AFS system will be designed to control the yaw rate of the bus, making it track the desired signal from the reference model in the presence of external disturbances and model uncertainties. The main objectives of the AFS controller design are:

- Yaw-rate tracking - The bus equipped with an AFS system should be able to closely follow the reference yaw-rate signal with a steady-state tracking error of less than 5% (e_{ss}<5%) in the step-steer tests (described in **6.5.1**).

- Path tracking – In the simulated open-loop lane-change test (please refer to **6.5.2**), the yaw-rate controlled bus should not leave the nominal path by 0.5m laterally (van Zanten 2001).

- Disturbance attenuation – The AFS system will automatically compensate for the yaw-rate tracking error caused by the external disturbances such that the driver is able to maintain course for the bus in straight-line running under side-wind gust or split-μ braking. Considering the widths of the bus body (2.5m) and the transit path (3.6m), the maximum lateral deviation from the center line of the lane is specified to be less than 0.5m.

- System robustness with respect to tire cornering stiffness variations – With the aid of the AFS system, the bus should be able to achieve the specified yaw-rate tracking, path tracking, and disturbance-attenuation performances on the low-friction roads, including wet roads ($\mu = 0.5$) and snow packed roads (μ=0.3) (CSTRAC 2005; Marks 2005), and/or under limit-oversteer/understeer condition.

6.3 Controller-Design Strategy

A Proportional-Integral-Derivative (PID) feedback controller will be employed to implement the yaw-rate control task. PID control is selected due to simplicity in structure and undeniably dominating application in today's automatic control. More than 90% of the control loops are PID (Åström and Hagglund 2001).

The discussion in **2.4.1** implies that the controller designed from the linear bus model could possibly be applied to the nonlinear vehicle, as long as the controller performance is robust to the varying local cornering stiffness. This controller-design problem can be tackled with robust control techniques. As illustrated in Figure **6-2**, before saturation, the cornering stiffness of the tire changes between an upper bounded C_{max} and a lower bound C_{min} depending on the operation conditions. According to the robust control theory, the varying cornering stiffness can then be treated as an uncertain parameter in the model, which is represented by a linear function with a bounded uncertainty as shown in Eq. **6.1**.
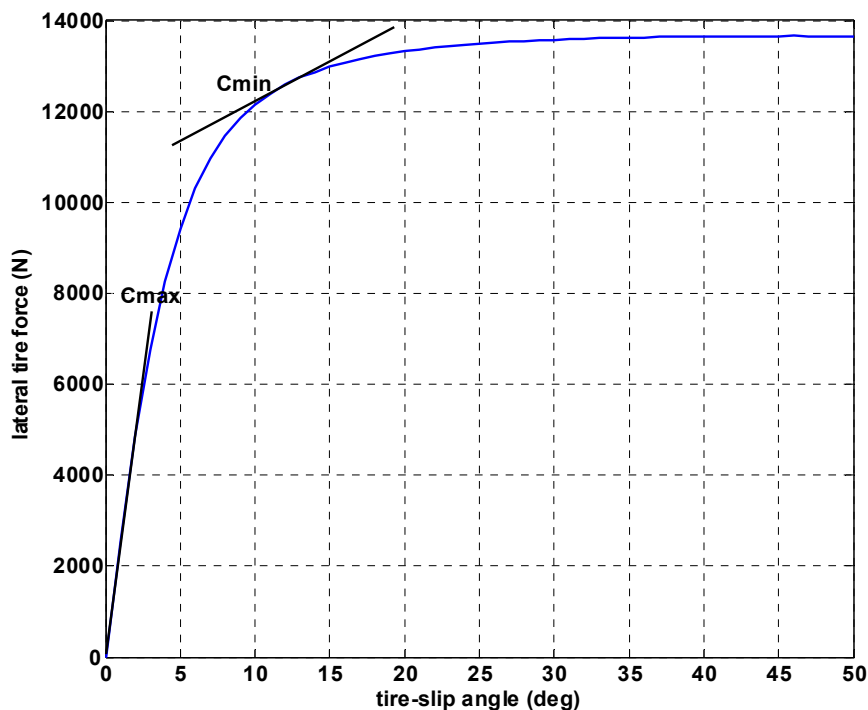
Figure **6-2**: The upper and lower bounds for the local tire cornering stiffness

$$C = C_0(1 + W\Delta) \quad (-1 \le \Delta \le 1)$$
$$C_{max} = C_0(1 + W) \quad C_{min} = C_0(1 - W)$$

(**6.1**)

C - actual cornering stiffness

C_0 - nominal cornering stiffness

W – weight

For example, assuming the local cornering stiffness of the rear tire C_r varies within $[C_{r0}(1-W), C_{r0}(1+W)]$, substitute $C_r = C_{r0}(1+W\Delta)$ into Eq. **Error! Not a valid link.** to yield:

$$
\begin{bmatrix} \dot{\beta} \\ \dot{r} \end{bmatrix} = \underbrace{\begin{bmatrix} -\dfrac{C_{f0}+C_{r0}}{mU} & -1-\dfrac{aC_{f0}-bC_{r0}}{mU^2} \\ -\dfrac{aC_{f0}-bC_{r0}}{I_{zz}} & -\dfrac{a^2C_{f0}-b^2C_{r0}}{I_{zz}U} \end{bmatrix} \begin{bmatrix} \beta \\ r \end{bmatrix} + \begin{bmatrix} \dfrac{C_{f0}}{mU} \\ \dfrac{aC_{f0}}{I_{zz}} \end{bmatrix} \delta_f}_{\text{The Nominal Model}} + \underbrace{B_1 W C_1 \begin{bmatrix} \beta \\ r \end{bmatrix} \Delta}_{\text{The Perturbation Term}}
$$
(6.2)

$$
B_1 = \begin{bmatrix} \dfrac{C_{f0}}{mU} \\ \dfrac{aC_{f0}}{I_{zz}} \end{bmatrix} \qquad C_1 = \begin{bmatrix} 1 & -\dfrac{b}{U} \end{bmatrix} \qquad -1 \le \Delta \le 1
$$

a distance from C.G. to front tire center

b distance from C.G. to rear tire center

C_{f0} nominal cornering stiffness of the front tire

C_{r0} nominal cornering stiffness of the rear tire

I_{zz} yaw moment of inertia

m mass of the vehicle

U vehicle speed

r yaw rate

β side-slip angle of the vehicle at C.G.

Comparing to the original model in Eq. **Error! Not a valid link.**, the modified model in Eq. **6.2** has an additional term introduced by the uncertain cornering stiffness. The modified vehicle model consists of two parts: a linear part representing the vehicle dynamic behavior in a particular linear operating region, called the nominal model; and a bounded uncertainty covering the cornering stiffness variation or equivalently the nonlinear characteristics of the vehicle, called the perturbation term. If a controller can regulate motions for the nominal vehicle model in the presence of the perturbation term, the same controller should possibly function well for the nonlinear vehicle model too (Ackermann 1994; Mammar and Koenig 2002; Ono et al. 1998; Sienel 1997; Stotsky and Hu 1997; You and Kim 2000).

In the following sections different controller-design techniques will be practiced. The variation ranges for C_f and C_r are [-230 KN/rad, -40 KN/rad] and [-480 KN/rad, -90 KN/rad], respectively. This cornering stiffness variation corresponds to a tire-slip angle change ranging from 0° to approximately 12°. According to Eq. 6.1, the nominal values for the uncertain C_f and C_r are: C_{f0} = -135 KN/rad, C_{r0} = -285 KN/rad.

6.4 The Steering Actuator Dynamics

One major constraint that limits the control authority of the AFS system is the dynamics of the steering actuator, which is often ignored (Fujiwara et al. 2002). With the presence of a steering actuator (Figure 6-1), the steering system cannot react to the command from the controller instantly and can only be operated at a steering rate limited by the bandwidth of the actuator. As a common practice, the actuator dynamics is assumed to be linear and can be approximated by a second-order transfer function as in Eq. 6.3, with the bandwidth ω_a = 5Hz, and damping ratio ξ = 0.707 (de Bruin 2001; Feng et al. 1998; Tai et al. 2004; Ukawa et al. 2002).

$$G_a = \frac{\omega_a^2}{s^2 + 2\xi\omega_a s + \omega_a^2}$$
(6.3)

Besides the actuator dynamics, the maximum steering angle of the vehicle is another factor that constraints the performance of the AFS system. According to the experimental measurements at PTI (The Pennsylvania Transportation Institute), the maximum steering angle of a heavy-duty bus is usually 40°. A saturation function shown in Figure 6-3 will be added to the control loop to characterize this constraint.
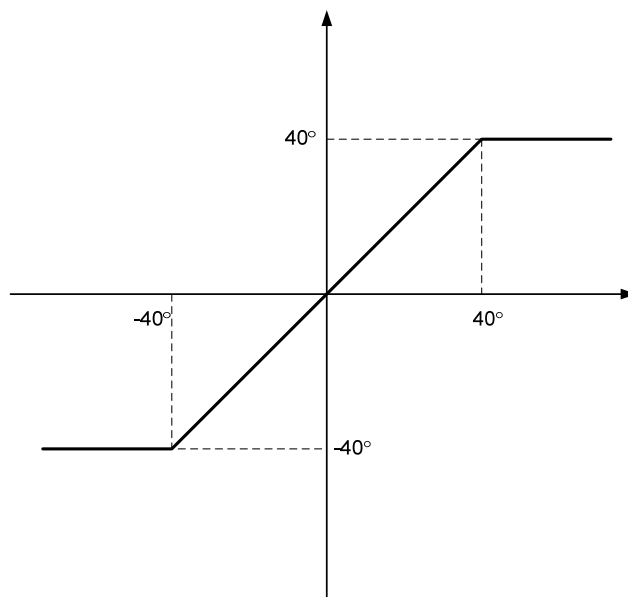
Figure **6-3**: Saturation function characterizing steering-angle limit

6.5 Introduction to Evaluation Tests

The performance of the designed AFS system will be evaluated on the nonlinear 40-foot transit bus model (Eqs. **2.4** and **2.5**, **Appendix A**) by computer simulation. The test cases are described in the following subsections. A table (Table **6-3**) is provided at the end of this section to summarize the conditions for all the test cases.

6.5.1 Step-Steer Test

The step-steer test is employed to evaluate the yaw-rate tracking performance of the bus featuring AFS. According to the specifications provided in **6.2**, the bus should be able to track the reference yaw rate with a steady-state error of less than 5%. At the same

time, in order to evaluate the robustness of the AFS controller with respect to road-friction variation, the test will be performed on low-friction road surfaces. Figure **6-4** shows the time history of the steering input at the front wheels. The testing speed is 35 mph. The following cases will be tested, representing three critical driving situations.

1. Cornering on a snow packed road with $\mu = 0.3$.

2. Cornering with limit oversteer on a wet road with $\mu = 0.5$. The limit-oversteer condition is artificially created by setting the friction at the rear tires to a level ($\mu = 0.3$) such that the rear-tire forces would saturate during the specified step-steer maneuver.

3. Cornering with limit understeer on a wet road. The limit-understeer condition is created by lowering the tire-road friction limit at the front tires in a similar manner to that in the limit-oversteer test.
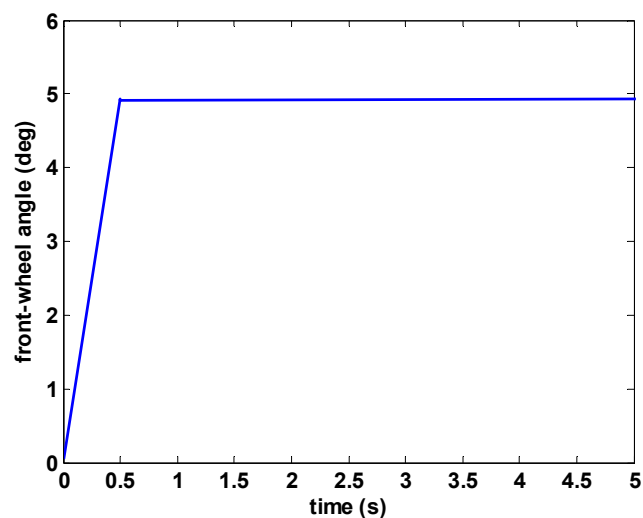
Figure **6-4**: Time history of the steering input for the step-steer test

6.5.2 Lane-Change Test (Sine-Steer Test)

Due to lack of driver-model parameters in lane-change maneuvers for transit buses, the steering input during the lane-change test is approximated by a 0.7 Hz single cycle sine wave shown in Figure **6-5**. A steering input of 0.7 Hz represents a typical high steering frequency in lane-change maneuver (Roland 1983; Tousi et al. 1991). Such a high steering frequency along with a peak steering angle of 15° represents a very severe lane-change maneuver. The test cases for the lane change will be the same as in the step-steer test. The lateral path-tracking error should be within 0.5 m (van Zanten 2001).
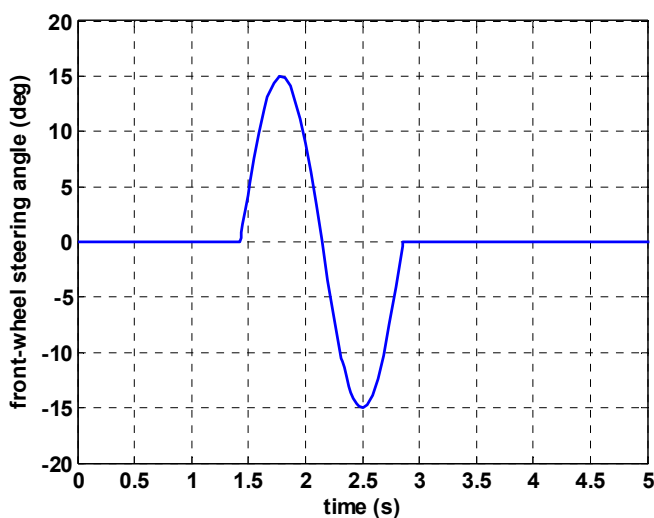
Figure **6-5**: Approximated steering input for the lane-change test

6.5.3 Side-Wind Gust Disturbance Attenuation

The significance of the AFS in assisting the driver to maintain the bus in lane under side-wind gust disturbance will be demonstrated in this test. The test will be

conducted at 35 mph on a snow packed road, with a side-wind gust applied perpendicularly to the side of bus body. The mathematical models for the wind disturbance and the driver's steering input are provided in the following subsections.

6.5.3.1 Side-Wind Gust Model

The wind-gust is modeled as a 2-second impulse (Inoue and Sugasawa 1993; Mammar et al. 2004; Nagai and Ohki 1989) with its magnitude estimated using the following equation (Milliken and Milliken 1995; Stinton 1983).

$$f_w = 0.5 \rho A C_d V_w^2 \qquad \text{(6.4)}$$

ρ density of the air

A area of the side profile of the bus

C_d aerodynamic drag coefficient

V_w wind speed

The numerical values of the parameters in the wind-force model are provided below.

Table **6-1**: Wind-gust model parameters

ρ	1.225 kg/m^3 (Stinton 1983)
A	31.5 m^2
C_d	1.28 (de Bruin 2001)
V_w	23 m/sec (50 mph)

Since the wind force acts on the geometric center of the side profile of the bus, which does not coincide with the C.G., the wind will thus not only create a side force to push the bus laterally, but also generate a torque trying to rotate the bus with respect to its C.G. The distance between the geometric center of the side body and the C.G. is approximately 1 m for a 40-foot bus.

6.5.3.2 Driver Model

A driver model for straight line running is included for the wind-gust test simulation. The classic linear preview model (Kondo and Ajimine 1968) employed to approximate the driver's steering input is described as follows. The driver first detects the lateral deviation from the desired course (which is a straight line) at an imaginary point along the view direction at a preview distance of L_p. If a deviation is detected, the driver will then make a steering correction to reduce the deviation after a delay T_r for reacting. Mathematically, the driver can be represented by the following transfer function in (Please refer to **Appendix C** for the derivation of the driver model).

$$\delta_d = G_s \frac{1 + \dfrac{L_p}{U}s}{1 + T_r s} \Delta_l \qquad (6.5)$$

δ_d steering angle from the driver

Δ_l lateral deviation from the desired path

G_s steering gain

L_p preview distance

T_r reaction time

The numerical values of the parameters in the driver model are provided as follows:

Table **6-2**: Driver-model parameters

G_s	0.02 rad/m (Harada and Iwasaki 1993)
L_p	45 m (Freedman et al. 1988)
T_r	0.3 sec (Hanke et al. 2001)

6.5.4 Split-μ braking

The effectiveness of AFS in split-μ braking is demonstrated in this test. The testing speed is 35 mph. The right-side tires of the bus are on an icy surface with $\mu = 0.1$, while the left-side tires are on a dry surface with $\mu = 0.7$. The same driver model as in the wind-gust simulation is used for this test. The perturbation caused by the split-μ braking is modeled as a 4-second impulse torque acting on the C.G. with a magnitude of 30000 N·m.

Table **6-3**: Summary for the testing conditions

Case No.	Maneuver	Vehicle Speed	Road Friction	Disturbance	Specification
1	5° step steer	35 mph	snow packed $\mu = 0.3$	n/a	steady-state Yaw-rate tracking error less than 5%
2			wet $\mu = 0.5$	limit oversteer	
3			wet $\mu = 0.5$	limit understeer	
4	lane change (15° sine steer)	35 mph	snow packed $\mu = 0.3$	n/a	lateral deviation from the center line of the lane less than 0.5m
5			wet $\mu = 0.5$	limit oversteer	
6			wet $\mu = 0.5$	limit understeer	
7	straight running	35 mph	snow packed $\mu = 0.3$	side-wind gust 50 mph	
8	straight braking	35 mph	right side: icy $\mu = 0.1$ left side: dry $\mu = 0.7$	Split-μ	

6.6 Proportional Controller (P controller) Design

P control is selected as the starting point of the controller-design process. P control is second to on/off control in simplicity (Tan et al. 1999). The only tuning parameter in a P controller is its proportional gain k_p, which is assumed to be constant within the scope of this thesis. Mathematically, P control takes the following form:

$$u = k_p \cdot e \qquad (6.6)$$

e	the error signal
k_p	proportional gain
u	controller output

Figure **6-6** shows the yaw-rate response of the uncontrolled bus during the step-steer test under limit-oversteer condition (case 2 in Table **6-3**). As the plot shows, the yaw rate of the bus cannot converge to a steady-state value, manifesting instability for the bus.
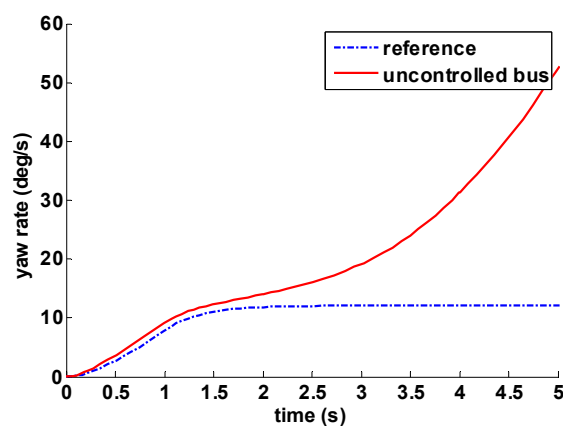
Figure **6-6**: Yaw-rate response of the uncontrolled bus

In order to stabilize the bus and yield a better tracking performance, a P controller will be employed. Generally speaking, the higher the proportional gain of a P controller, the better the performance. However, too high a proportional gain will cause stability problem for the system. In addition, the maximum proportional gain is also limited by the largest reachable steering angle. During the controller design, the proportional gain k_p is gradually increased till the yaw-rate response of the bus closely ($e_{ss}<5\%$) tracks the reference signal or the vehicle system approaches instability (response becomes oscillatory), whichever comes first.

The proportional gain iterations and the tracking errors obtained in the limit-oversteer step-steer test are listed in Table **6-4**. It is shown that when $k_p > 5$, a further increase in the gain only marginally improves the steady-state tracking error. Meanwhile, as the sample plots shown in Figure **6-7**, the step-steer response becomes oscillatory as the gain increases beyond 5. The proportional gain is finally selected to be $k_p = 5.1$, yielding a steady-state error of 16.2%. Obviously, the P controller with $k_p = 5.1$ does not meet the specified tracking performance ($e_{ss} < 5\%$) given in **6.2**. If we venture to increase k_p, the step-steer response would start to oscillate, indicating the closed-loop system is entering a limit cycle, or is approaching instability.

Table **6-4**: Proportional gain vs. Steady-state error

Proportional Gain (k_p)	Steady-State Error (e_{ss})
1	35%
3	20%
5	16.5%
5.1	16.2%
5.5	15.3%*
6	15.6%*
7	16.5%*

*measured from the mean value
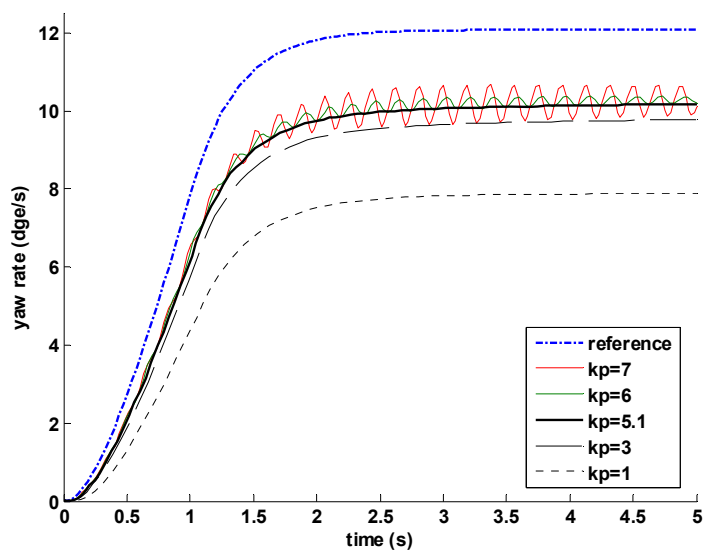
Figure **6-7**: Yaw-rate responses of the bus under P control with different gains

The P-control results suggest that a pure P control is not able to satisfy the requirements on both tracking performance and system stability. For the test bus, while a high proportional gain can be used to arguably reduce the tracking error, it will

deteriorate the stability of the vehicle system as well. Therefore, in order to achieve the desired tracking performance while maintaining system stability, a more sophisticated control strategy other than P control need to be used.

6.7 Proportional-Integral Controller (PI controller)

6.7.1 Introduction

In order to eliminate the steady-state tracking error, integral control is added to proportional control, resulting in PI control (proportional-integral control). The PI control is no doubt the most commonly used control algorithm (Åström and Hagglund 2001; Åström and Hägglund 2006; Tan et al. 1999; Yamamoto and Hashimoto 1991). In addition to steady-state elimination, another benefit of adding integral control is that the controller can be designed to be robust to a wide range of parameter perturbation (Khalil 2002).

The PI controller can be expressed in the following form:

$$u = k_p e + k_i \int_0^t e(\tau)d\tau \tag{6.7}$$

e error signal
k_p proportional gain
k_i integral gain
u controller output

The controller has two tuning parameters, k_p and k_i. There exist many methods to design a PI controller (Ogata 2002). The empirical method invented by Ziegler and

Nichols (Ziegler and Nichols 1946) is probably the most commonly used turning technique. This method has the great advantage of requiring very little information on the mathematical model of the plant. However, a fundamental drawback is that Ziegler and Nichols method inherently tends to create a very poorly damped closed-loop system (typically $\xi < 0.2$) with modest robustness to external perturbations (Åström and Hagglund 1995). The PI controller design method developed by Åström, Panagopoulos, and Hägglund (Åström et al. 1998; Panagopoulos et al. 1999) is adopted in this thesis work. The proposed method formulates the design problem as an optimization problem: optimize the disturbance attenuation with a constraint on the system robustness.

6.7.2 Design-Problem Formulation

The formulation of the Åström-Panagopoulos-Hägglund method includes characterizing design objectives in terms of controller parameters, and selecting suitable constraints for the optimization process.

6.7.2.1 Load Disturbance Attenuation

According to Åström and Hägglund (Åström and Hägglund 2006; Åström et al. 1998), for a closed-loop system with PI feedback control shown in Figure **6-8**, the response of the system to low frequency disturbances can be estimated by the transfer function in Eq. **6.8**. It is shown that for a PI controlled system under, the transfer

function between the disturbance and the output variable can be approximated by $1/k_i$.

Therefore, the integral gain k_i is a good measure of load disturbance attenuation.

$$G_{yd} = \frac{G}{1+GK} \approx \frac{1}{K} \approx \frac{s}{k_i} \qquad (6.8)$$
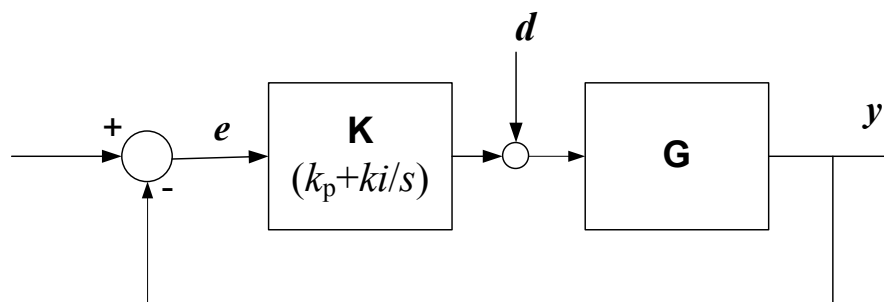
Figure **6-8**: PI feedback control system

The relationship between disturbance-attenuation performance and the integral gain k_i can also be derived through the integrated error (*IE*) (Åström and Hagglund 1995). IE^8 is an indicator for the system's tracking performance, which is defined as:

$$IE = \int_0^\infty e(t)dt \qquad (6.9)$$

where, e is the error between the output and the reference signals.

Consider the PI-control law given in Eq. **6.7**, for a stable closed-loop system subject to a step disturbance, the error e will eventually go to zero. Therefore, the following relationship between the initial and final controller outputs can be obtained:

---

[8] IE is used instead of the stricter IAE=∫│e(t)│dt, because IE is easier to deal with analytically. For a well damped system the two criteria will be close, which can be ensured by the constraint on the sensitivity function (Astrom, et al. 1998).

$$u(\infty) - u(0) = (k_p e(\infty) + k_i \int_0^\infty e(\tau)d\tau) - (k_p e(0) + k_i \int_0^0 e(\tau)d\tau) \qquad (6.10)$$

Assuming zero initial error ($e(0)=0$),

$$k_i \int_0^\infty e(\tau)d\tau = u(\infty) - u(0)$$

$$\Rightarrow IE = \int_0^\infty e(\tau)d\tau = \frac{u(\infty)}{k_i} \qquad (6.11)$$

Both Eqs. **6.8** and **6.11** imply that in order to optimize the disturbance attenuation performance, the integral gain k_i needs to be maximized within the available range.

6.7.2.2 Robustness to Parameter Uncertainties

The requirement on robustness to parameter uncertainties can be expressed in terms of the maximum value of the sensitivity function S, which is defined in Eq. **6.12**. It gives the relative sensitivity of the closed-loop system to the relative plant model error. The maximum value of the sensitivity function, M_s, is characterized by its H_∞ value $\|S\|_\infty$. Graphically, M_s can be interpreted as the inverse of the shortest distance from the Nyquist curve of the loop transfer function to the critical point (-1, 0) (Doyle et al. 1990; Skogestad and Postlethwaite 1996). Therefore, to ensure system robustness to perturbations, a small sensitivity (yielding long distance to the critical point) is generally required. Typical values of M_s are in the range of 1~2 (Åström et al. 1998; Garcia et al. 2005; Skogestad and Postlethwaite 1996).

$$S = \frac{dT/T}{dG/G} = \frac{1}{1+GC} \qquad (6.12)$$

The robustness of the closed-loop system can also be characterized by the largest value of the complementary sensitivity function T defined as:

$$T = \frac{GC}{1+GC} = 1 - S \qquad (6.13)$$

As shown by Eq. **6.13**, the complementary sensitivity function is actually the transfer function from the reference signal to the system output. The term "complementary" follows from the identity $S+T=1$. Similar to the sensitivity function, the maximum value of the complementary sensitivity function M_T is characterized by its H_∞ value $\|T\|_\infty$. Physically, the value M_T is the size of the resonance peak of the closed-loop system. Typical values of M_p are 1 to 1.5 (Åström and Hägglund 2006; Skogestad and Postlethwaite 1996).

6.7.2.3 Optimization-Constraint Selection

The design process of the PI controller can be summarized as: find the controller with the largest integral gain k_i subject to the constraints on system stability and robustness. The process can be illustrated by the following figure.
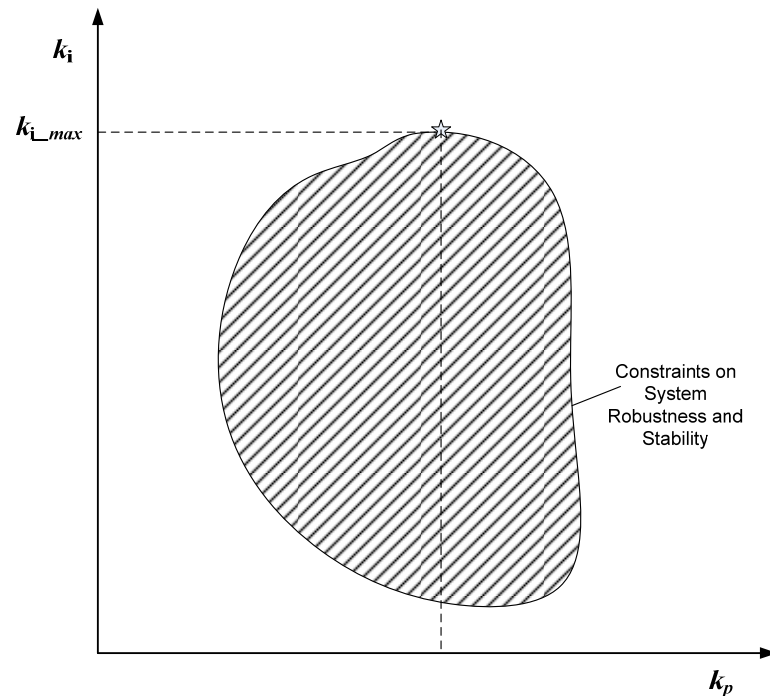
Figure **6-9**: Graphical presentation of the PI-controller design process

Since the system robustness constraint can be specified by both M_S and M_T as presented in **6.7.2.2**, it necessitates a selection between these two candidates for a suitable design parameter. It is shown by Åström et al. (Åström et al. 1998) that M_S is a better choice than M_T, because the performance (response) of the closed-loop system is more sensitive to M_S variation. Meanwhile, it is important that the resulting M_T value is not too large. Therefore, M_T also needs to be calculated when the design is completed. If M_T is too large, it is necessary to repeat the design with a smaller M_s value. In our case, a constraint on the maximum sensitivity $M_s < 2$ was found to yield a satisfactory result.

6.7.3 The Designed PI Controller and Its Robustness to Model Uncertainty

According to the discussion in **6.7.2**, a PI controller is design based on the nominal model (Eq. **6.2 Appendix A**) and the actuator model (Eq. **6.3**). Besides the maximum value of the sensitivity function (M_s), the crossover frequency ω_c is also constrained. As discussed in chapter 4, the bandwidth of yaw-rate response of a 40-foot bus is approximately 1.5 Hz. To ensure a reasonable bandwidth of the controlled vehicle system, ω_c is required to be at least 9 rad/sec ($\approx$ 1.4 Hz). Sample iteration results from the numerical optimization are presented in the following table.

Table **6-5**: Iteration results for PI-controller design

k_p	k_i	M_s	M_T	ω_c (rad/sec)
3.6	3.3	1.4737	1.0778	9.0004
3.6	6.8	1.5148	1.1824	9.1417
3.7	0.1	1.4596	1.0112	9.1998
3.7	6.7	1.5284	1.1719	9.3684
3.8	0.1	1.4749	1.0109	9.449
3.8	6.7	1.5434	1.165	9.6011
4.5	0.1	1.5886	1.0084	11.1436
4.5	5.1	1.6398	1.0961	11.2
5.0	0.1	1.667	1.0488	12.3342
5.0	2.5	1.7015	1.0857	12.3445

And, the PI controller is determined to be:

$$G_c = k_p + \frac{k_i}{s}$$
$$k_p = 3.7, \quad k_i = 6.8$$

(**6.14**)

The robustness of closed-loop system with the designed PI controller is investigated using the *v*-gap metric (Vinnicombe 2001). The *v*-gap metric, δ_v, is defined as:

$$\delta_v(G_1, G_2) = \left\| \frac{\left| G_1 - G_2 \right|}{\sqrt{1 + \left| G_1 \right|^2} \sqrt{1 + \left| G_2 \right|^2}} \right\|_\infty \tag{6.15}$$

where, G_1, G_2 are transfer functions of two linear systems. The *v*-gap metric is introduced to measure the distance between two linear systems in terms of their frequency responses G_1 and G_2. By theory if the closed-loop system consisting of the controller C and the process G_1 is stable with a generalized stability margin γ, and G_2 is another system which is close to G_1 in the sense that $\delta_v < 1/\gamma$, then the controller C is also guaranteed to stabilize and yield similar performance (as in G_1) for G_2. The generalized stability margin is defined as:

$$\gamma = \left\| \begin{bmatrix} G \\ I \end{bmatrix} (1 + GC)^{-1} \begin{bmatrix} -C & I \end{bmatrix} \right\|_\infty \tag{6.16}$$

As can be seen from Eq. **6.16**, the transfer function matrix within $\left\| \cdot \right\|_\infty$ describes how the external perturbations propagate through the system. A good closed-loop performance requires the small outputs due to perturbations, which implies γ should be small. At the same time, a small γ will also guarantee the closed-loop system to be robust with respect to model uncertainties. Usually, $\gamma < 3$ gives a reasonable robustness and performance (Åström 2005; Panagopoulos and Astrom 2000; Vinnicombe 2001).

By Eq. **6.16**, the generalized stability margin for the closed-loop system consisting of the PI controller (Eq. **6.14**) and the nominal bus model (Eq. **6.2**) is

calculated to be $\gamma = 2.78$. Since the worst-case[9] v-gap metric is $\delta_v = 0.28$, which satisfies $\delta_v < 1/\gamma$, the designed PI controller should be able to yield satisfactory results. Nevertheless, the controller is designed based on a simplified linear model, its performance and robustness on a nonlinear vehicle model remains to be proved in the tests.

6.8 PI Active Front-Wheel Steering Controller Evaluation on a 40FT Bus

The following subsections presents the performance evaluation results for the PI active front-wheel steering controller on the nonlinear bus model with the test cases listed in Table **6-3** .

6.8.1 Case 1: Step Steer on the Snow Packed Road

The bus was tested with a 5° step steer, on the snow packed road with $\mu = 0.3$, at the speed of 35 mph. The time histories of yaw rate and side-slip angle of the PI controlled bus are shown in Figure **6-10** along with those of the uncontrolled bus and the reference model. As can be seen from the plots, the yaw rate of the controlled bus followed the reference signal more closely than the uncontrolled bus, of which the yaw rate actually started to diverge towards the end of the test period and finally became unstable. The effect of the AFS is more obvious when comparing the side-slip angle

---

[9] The nominal model is perturbed by simultaneously vary its front and rear cornering stiffness, resulting different δ_v for each case. The worst case is determined by finding the largest δ_v before the model goes unstable.

responses between the controlled and the uncontrolled buses. As the plot shows, the uncontrolled bus went unstable from the beginning of the test, while the AFS system successfully contained the side-slip angle for the controlled bus to be less than 7.5°. The AFS system effectively regulated the motion of the bus, thus preventing the vehicle from becoming unstable.
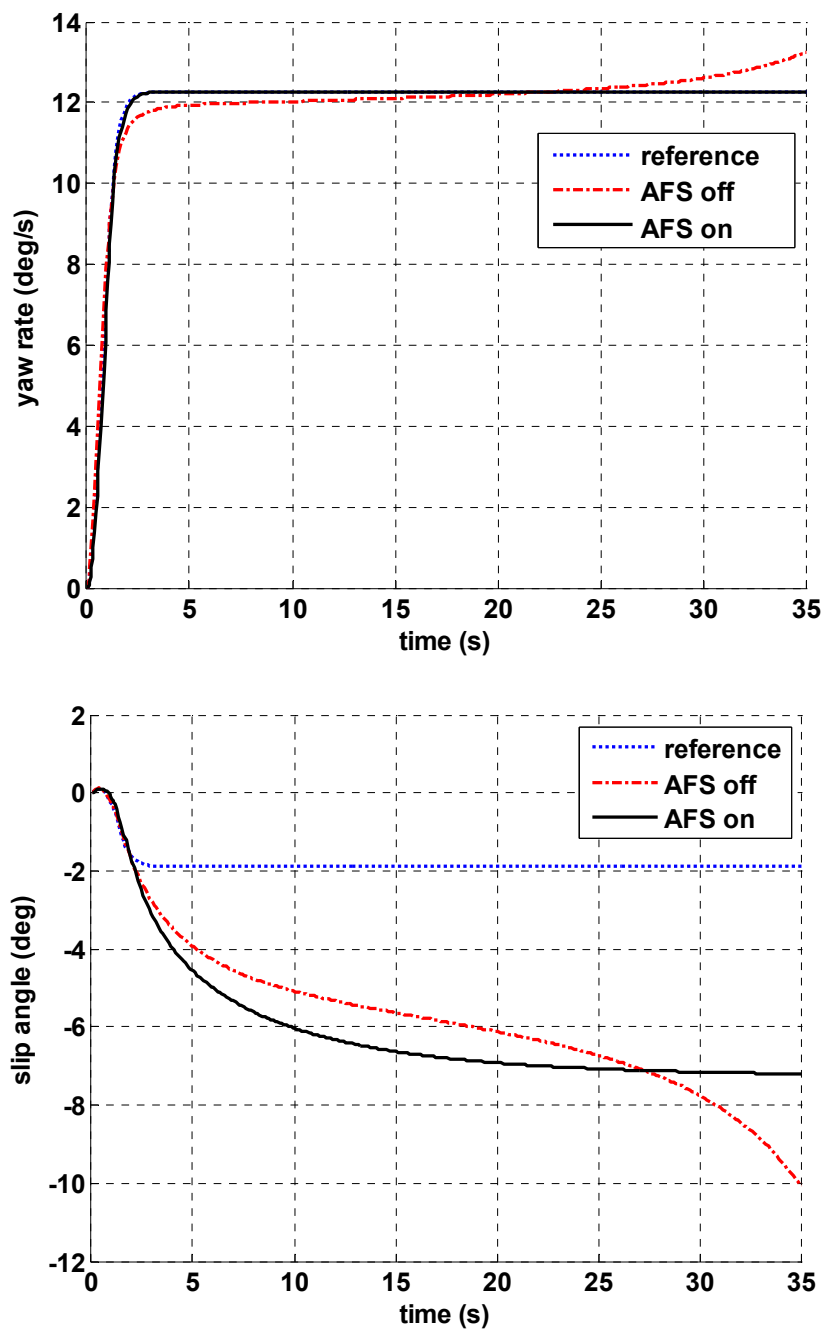
Figure **6-10**: Vehicle response in the step-steer test on the snow packed road

6.8.2 Case 2: Step Steer under Limit Oversteer on the Wet Road

The bus was tested with a 5° step steer, on the wet road with $\mu = 0.5$, at the speed of 35 mph, under limit-oversteer condition.

The responses of the state variables are displayed in Figure **6-11** for both the controlled and uncontrolled buses. As shown, while the yaw rate of uncontrolled bus diverged indefinitely, the bus equipped with AFS strictly followed the reference yaw-rate signal and remained stable in this severe test maneuver. The steering command from the AFS controller is plotted against time in Figure **6-12**. As the time history shows, the AFS controller implemented this step-steer maneuver by "counter steering", which is a "trick" possessed only by highly-skilled drivers.
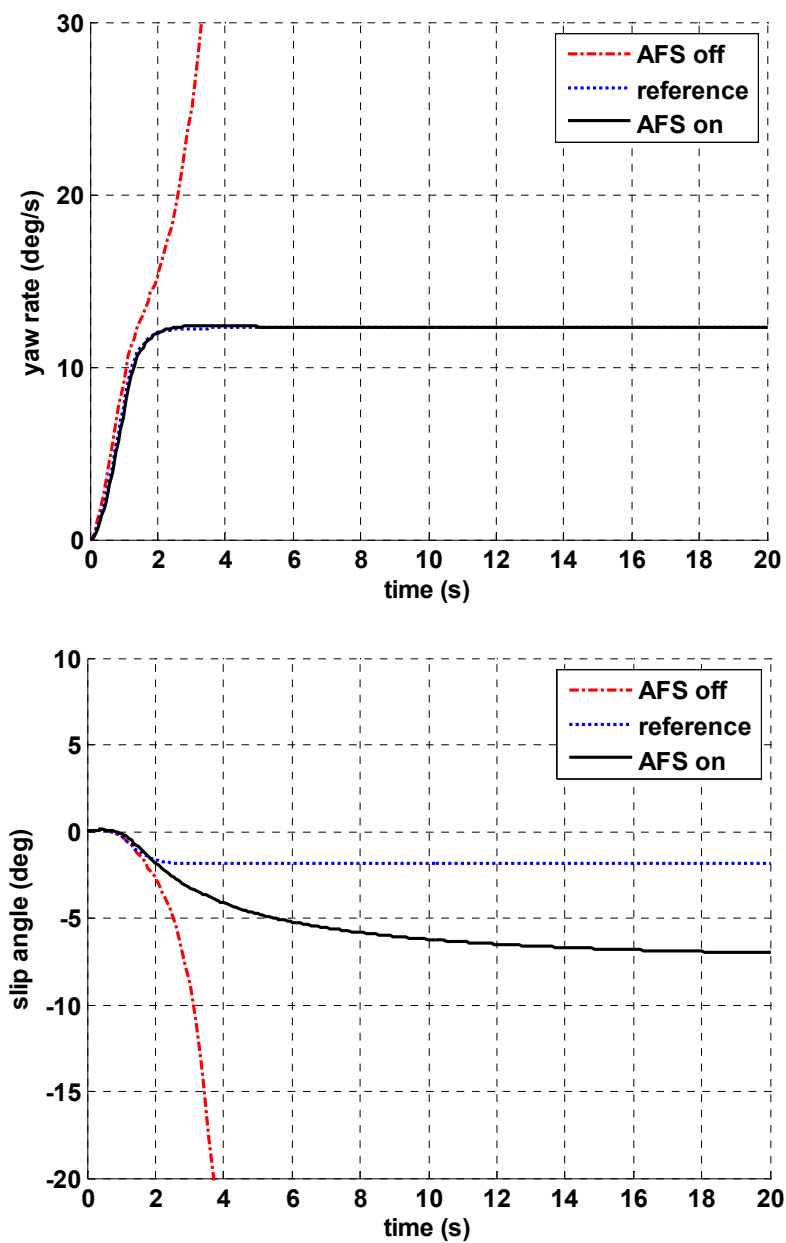
Figure **6-11**: Vehicle response in the step-steer test under limit oversteer on the wet road
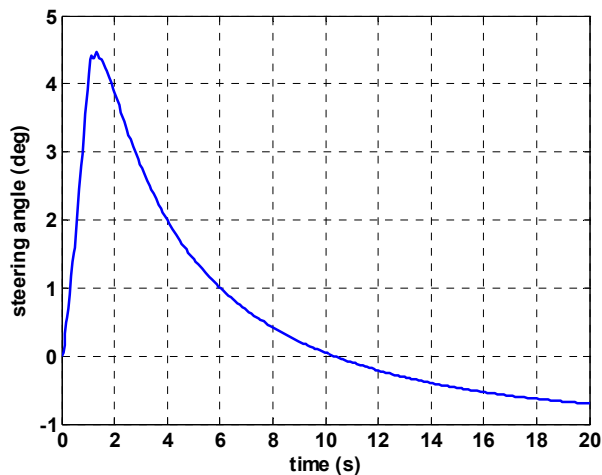
Figure **6-12**: Steering command from the AFS controller

6.8.3 Case 3: Step Steer under Limit Understeer on the Wet Road

The bus was tested under the same condition as in the limit-oversteer case, except that a limit-understeer condition is applied.

The time histories of the yaw rate and side-slip angle are displayed in Figure **6-13** for both the controlled and uncontrolled buses. As shown, while both the uncontrolled and controlled buses were stable in this test maneuver, the controlled bus was able to follow the reference yaw rate much more closely than the uncontrolled one, implying a better maneuverability for the bus with AFS. In this case, the significance of AFS can be more easily appreciated by studying the moving trajectory of the bus shown in Figure **6-14**. As can be seen, the bus featuring AFS was running closely to the nominal path, while the uncontrolled bus had strayed laterally about 10 m towards the end of the test.

Figure **6-13**: Vehicle response in the step-steer test under limit understeer on the wet road
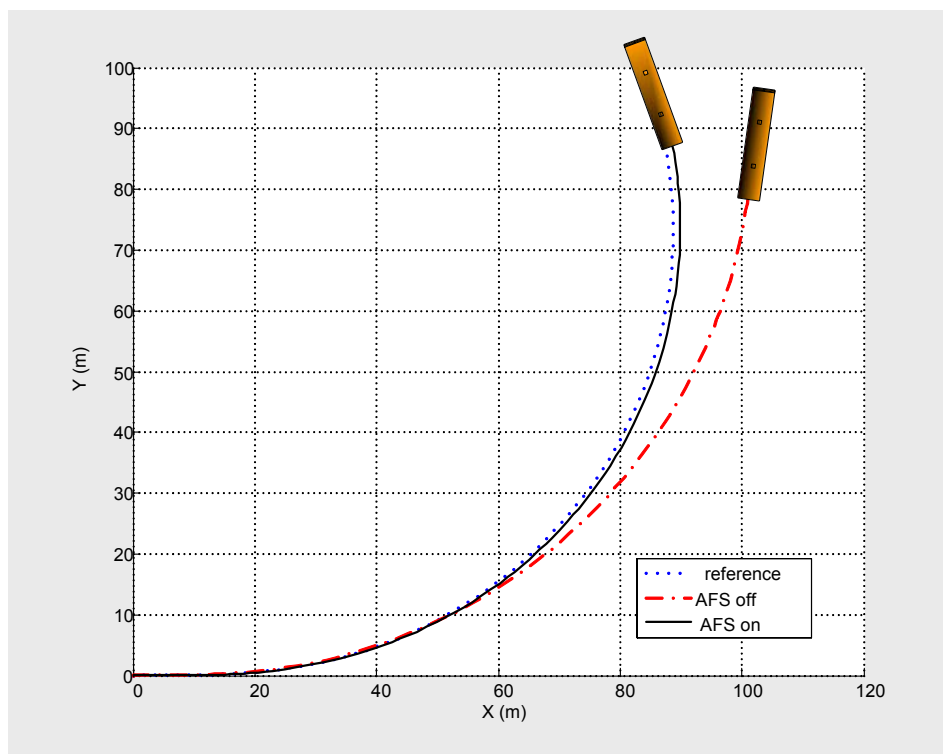
Figure **6-14**: Moving trajectory of vehicle C.G. in the step-steer test under limit oversteer on the wet road

The results from the above three step-steer tests clearly demonstrate that the AFS system improved the yaw stability of the bus in all cases. They further suggest that the stabilizing function of the AFS system is best appreciated in the limit-oversteer case than in the other two cases. This is because the AFS system generates the correcting torque using the front-tire forces, and the peak front-tire force in the specified limit-oversteer condition is the highest among all three cases.

6.8.4 Case 4: Lane Change on the Snow Packed Road

The bus was tested with a single cycle 15° 0.7 Hz sine steer, which simulates the steering input in a severe lane-change maneuver. The tire-road friction was $\mu = 0.3$, and the testing speed was 35 mph.

Figure **6-15** shows the yaw-rate and side-slip angle responses of the controlled and uncontrolled buses. Due to yaw-rate tracking of AFS, the controlled bus was able to achieve a more reasonable heading angle than the uncontrolled bus in the first turn. As a result, the bus with AFS was able to track the desired path with a deviation of less than 0.5 m, while the uncontrolled bus failed to implement the lane change (Figure **6-16**).
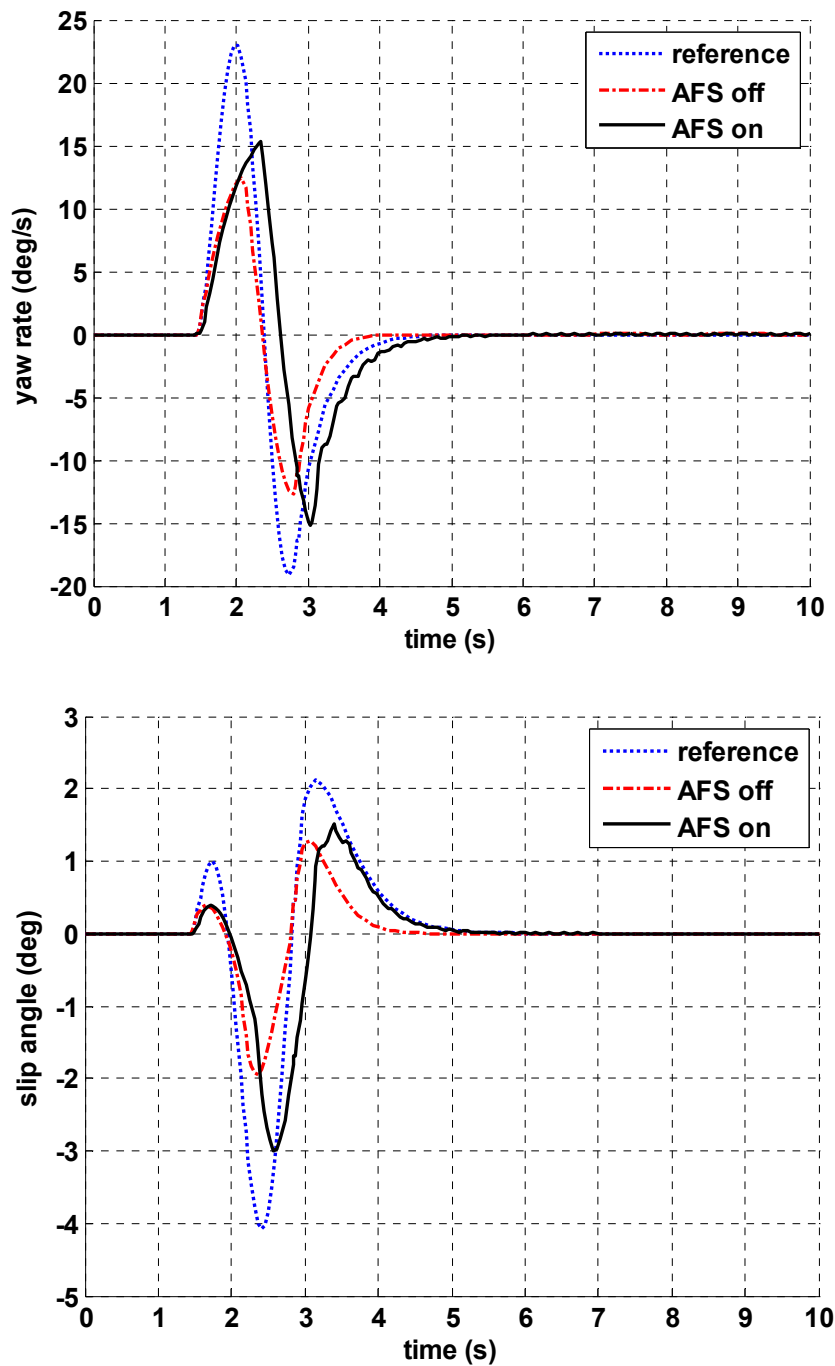
Figure **6-15**: Vehicle response in the lane-change test on the snow packed road
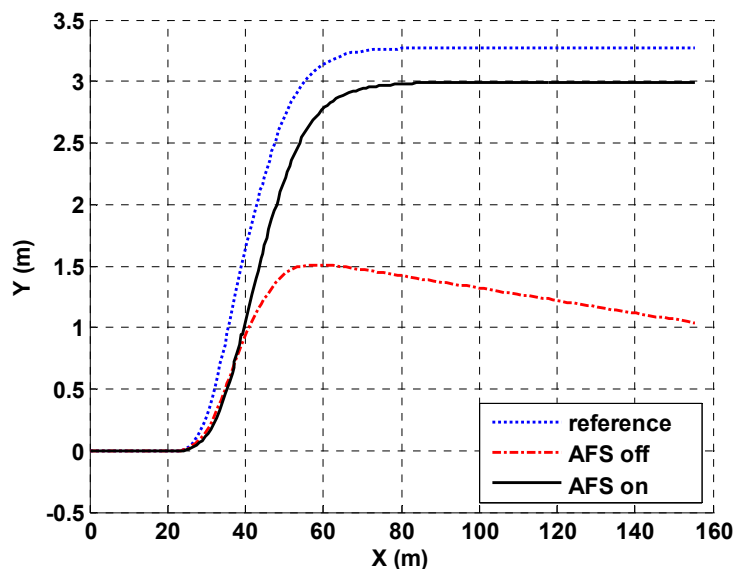
Figure **6-16**: Moving trajectory of vehicle C.G. in the lane-change test on the snow packed road

6.8.5 Case 5: Lane Change under Limit Oversteer on the Wet Road

The bus was tested with a 15° 0.7 Hz sine steer, on the wet road with μ = 0.5, at the speed of 35 mph, under limit-oversteer condition.

It is shown in Figure **6-17**, both the controlled and the uncontrolled buses could follow the reference yaw-rate signal in a reasonably close fashion, yet the tracking performance of the controlled one is slightly better during the first turn. Consequently, the heading angle of the controlled bus aligned with the desired path better than the uncontrolled one. The maximum lateral deviation from the desired path was approximately 0.35 m for the controlled bus, and 0.85 m for the uncontrolled bus (Figure **6-18**).
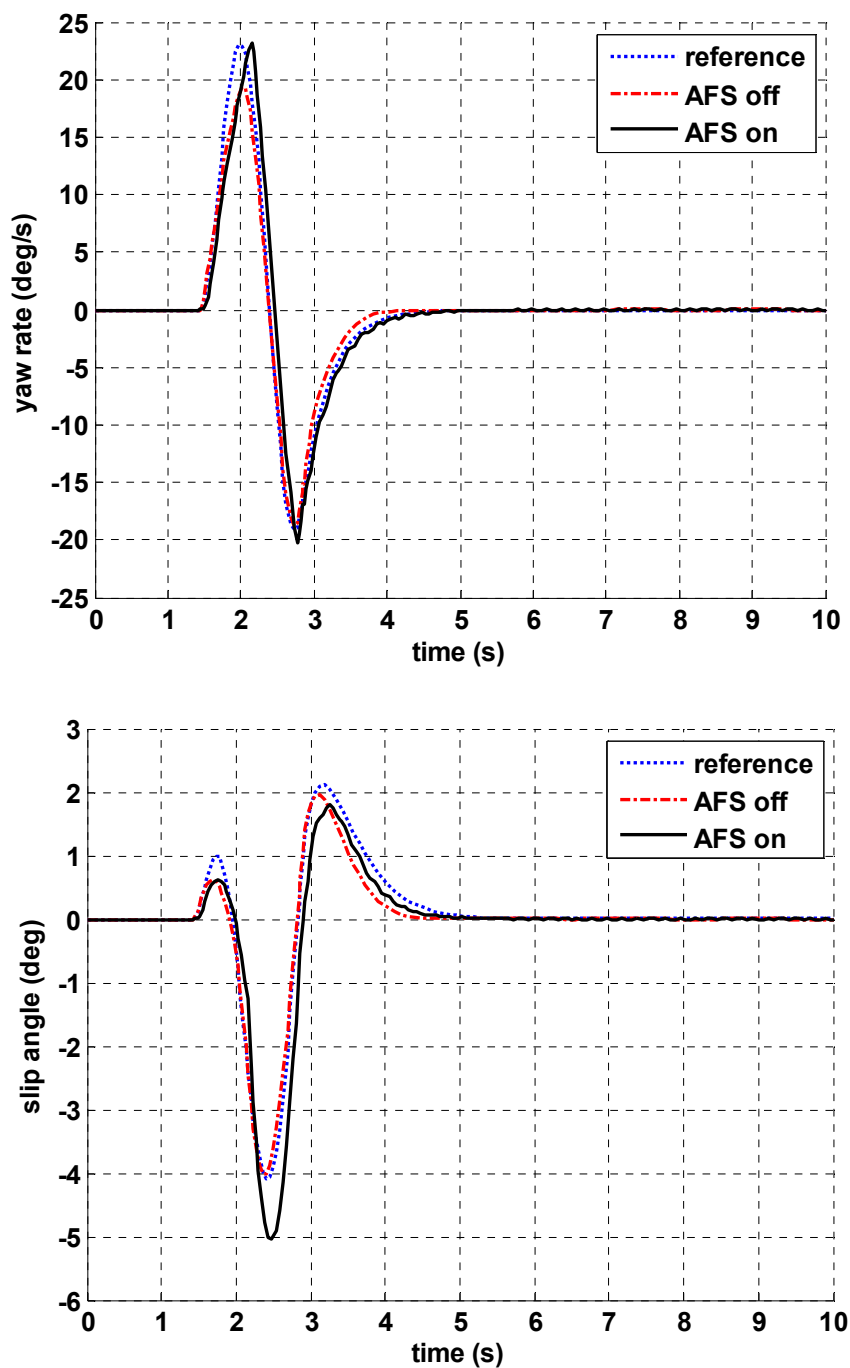
Figure **6-17**: Vehicle response in the lane-change test under limit oversteer on the wet road
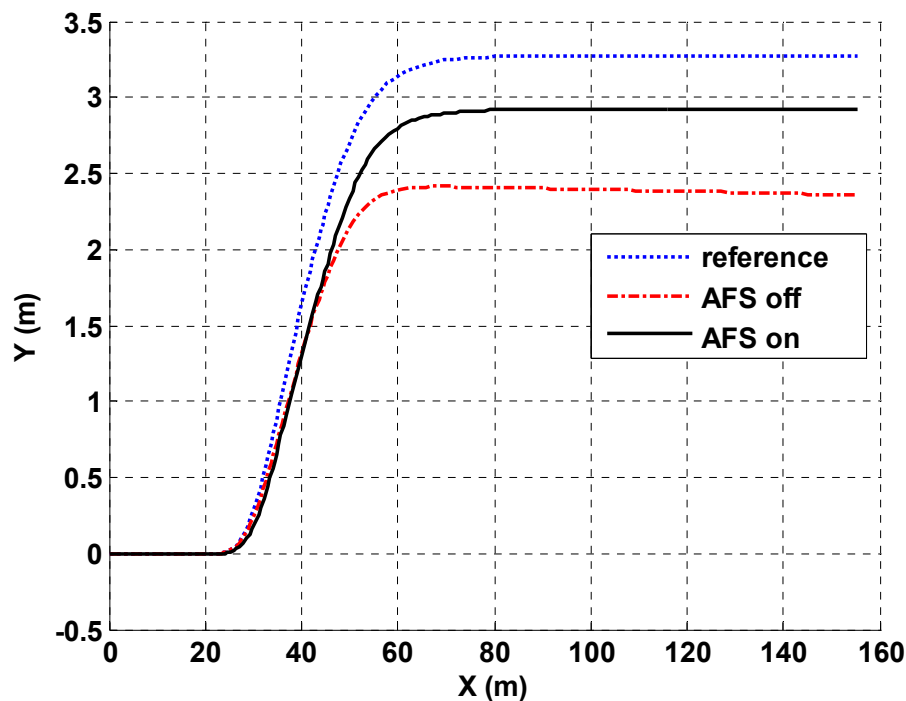
Figure **6-18**: Moving trajectory of vehicle C.G. in the lane-change test under limit oversteer on the wet road

6.8.6 Case 6: Lane-Change under Limit Understeer on the Wet Road

The bus was tested under the same condition as in limit-oversteer lane change, except that the limit-understeer condition was applied.

Similar to the other two lane-change cases (4 and 5), the AFS system automatically compensate for limit understeer, yielding a reasonable heading angle for the vehicle. Therefore, the bus with AFS was able to track the desired path with a lateral error of about 0.25 m, while the uncontrolled vehicle failed this lane-change maneuver. The results are presented in Figures **6-19** and **6-20**.
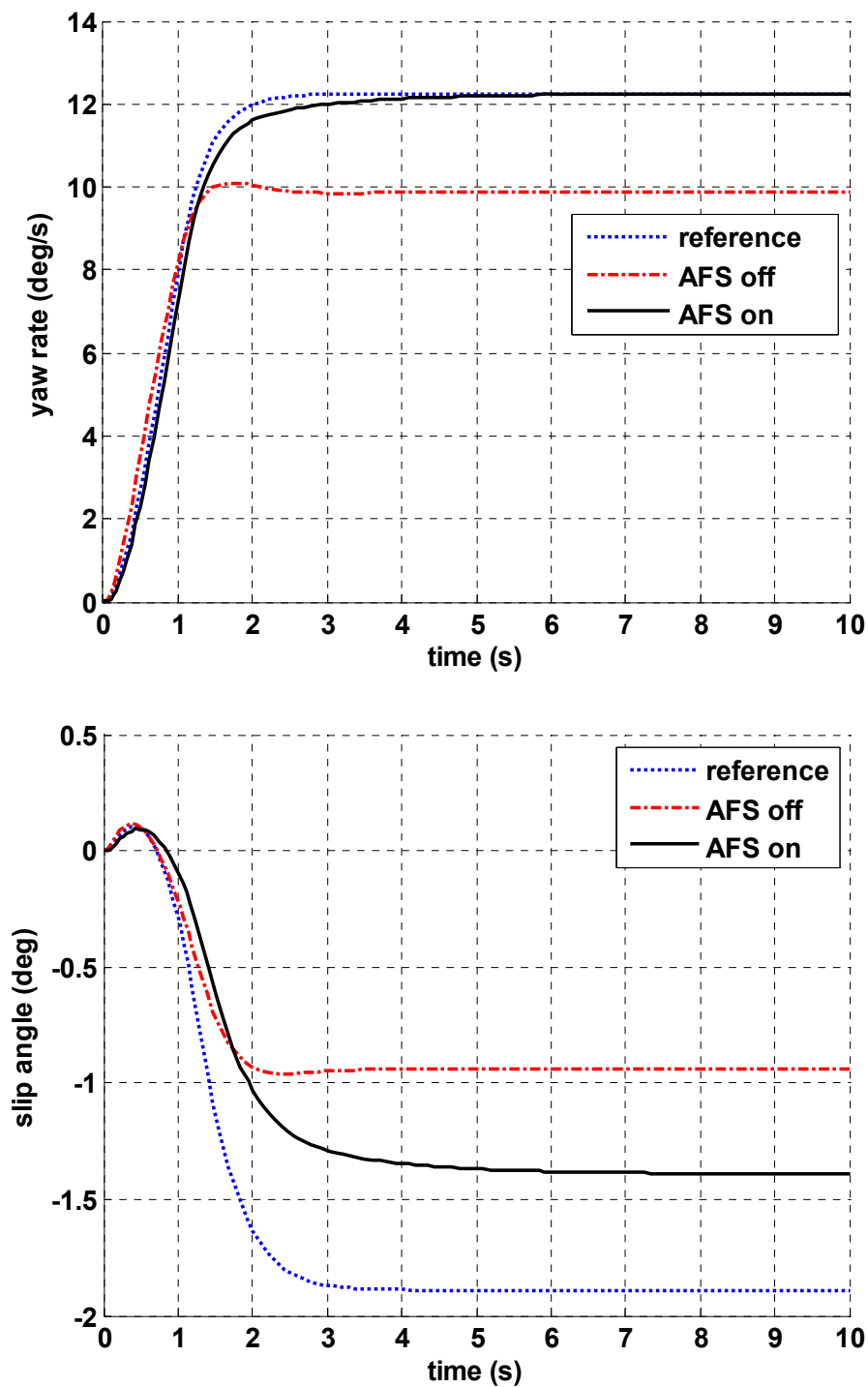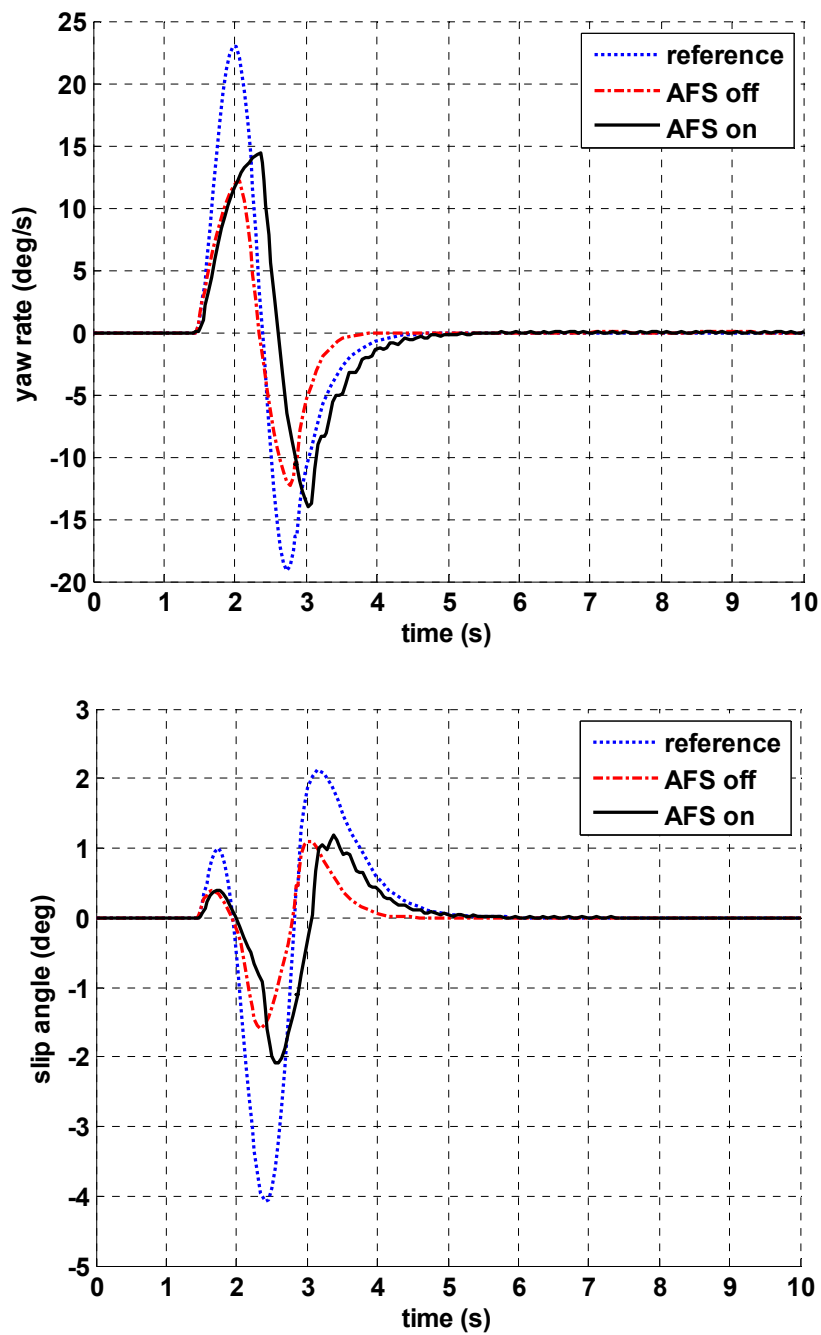
Figure **6-19**: Vehicle response in the lane-change test under limit understeer on the wet road
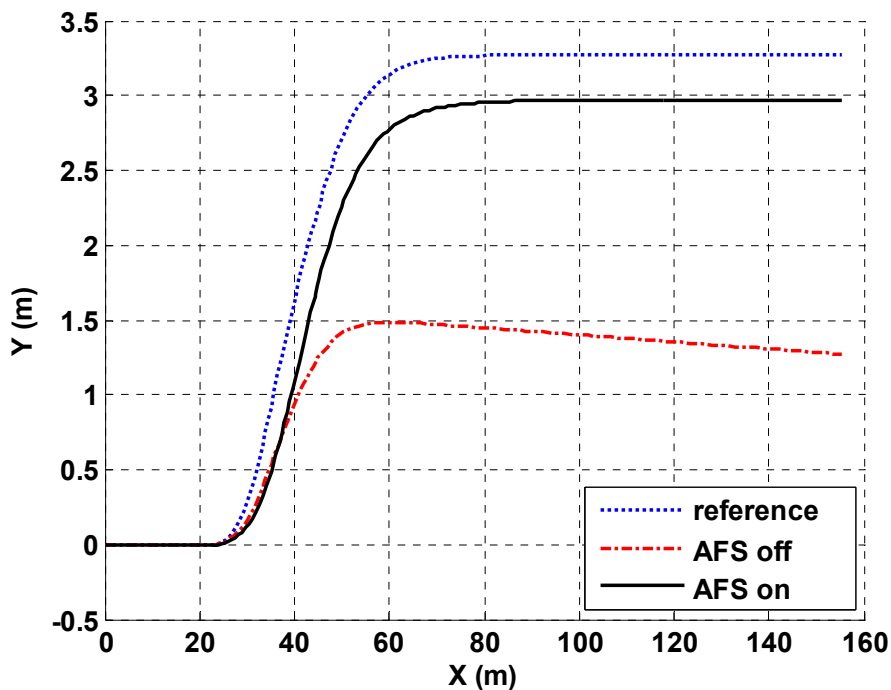
Figure **6-20**: Moving trajectory of vehicle C.G. in the lane-change test under limit understeer on the wet road

Since the lane-change tests were not as severe as the step-steer tests, the bus could maintain stability without the aid of AFS. Therefore, the stabilizing effect of AFS system in these lane-change tests did not seem to be as dramatic as in the step-steer tests. However, by looking at the moving trajectories of the vehicle, it is realized that the AFS system did improve the handling of the bus. The bus with AFS is apt to track the desired path without further steering corrections from the driver, which in fact will help to alleviate the working load and psychological stress of the driver in the critical situations.

6.8.7 Case 7: Straight Running under Side-Wind Gust on the Snow Packed Road

The bus was tested on a road with packed snow $\mu = 0.3$, at the speed of 35 mph. A side-wind gust of 50 mph was applied vertically to the side body of the vehicle.

The moving trajectories of the controlled and uncontrolled buses are shown in Figure **6-21**. The effectiveness of the AFS system can be clearly seen. As the figure shows, the largest lateral deviation of the controlled bus from the desired path (straight line in blue) is less than 0.2 m, while the bus without AFS deviated almost 0.6 m from the center line of the lane. Considering the lane width is 3.6 m and width of the bus body is about 2.6 m, the uncontrolled bus may already intrude into another lane.
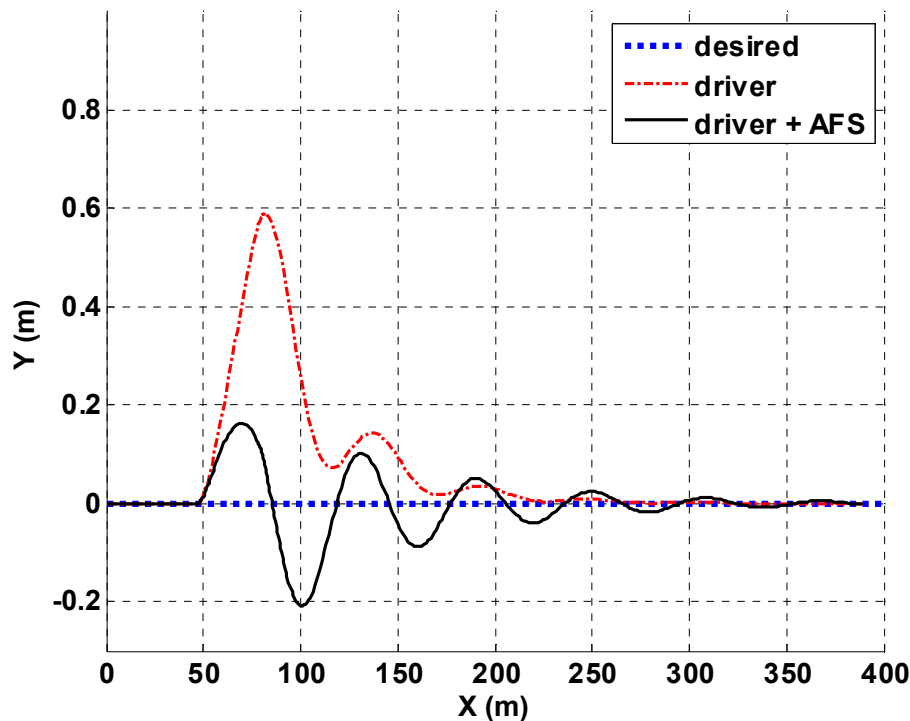
Figure **6-21**: Vehicle paths under side-wind gust disturbance

6.8.8 Case 8: Split-μ Braking

The usefulness of AFS in split-μ braking was demonstrated in this test. The bus was running at 35 mph. Its right tires were on an icy surface with $\mu= 0.1$, while its left tires were on a dry surface with $\mu = 0.7$.

The moving trajectories of the controlled and uncontrolled buses are shown in Figure **6-22**. The largest lateral deviation of the controlled bus from the desired path (straight line in blue) is less than 0.1 m. At the same time, the largest deviation of the uncontrolled bus is more than 1 m. Although the bus without AFS finally comes back to the original lane and stays stable throughout the braking period, a lateral deviation of larger than 1 m from the center line of the driving lane is absolutely not desired in any traffic environment.
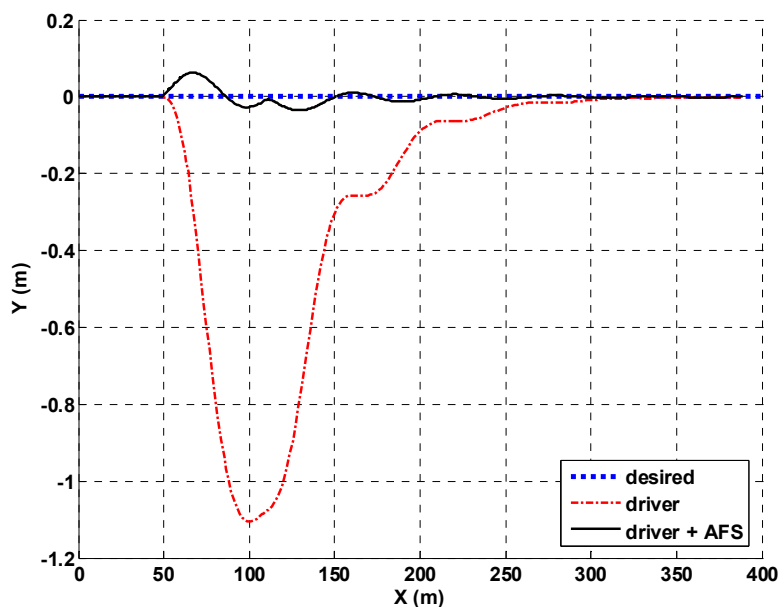
Figure **6-22**: Vehicle paths under split-μ braking

6.9 Conclusions

The simple proportional-integral AFS (active front-wheel steering) controller design based the nominal linear model performed very well on the nonlinear vehicle for the specified test cases. It is evident from test results that the AFS system based on yaw-rate control significantly improved the stability and maneuverability of the bus under various critical driving situations. In addition, as can be observed in step-steer tests, the effectiveness of AFS in stabilizing vehicle motion is most conspicuous under limit oversteer situation. In the cases where the bus can maintain stability even without automatic control system involved, the AFS system still shows its capability in assisting driver to regulate vehicle motion more effectively and more promptly.

References

1. Abe, M., Ohkubo, N., and Kano, Y. (1996). "A direct yaw moment control for improving limit performance of vehicle handling - comparison and cooperation with 4WS." *Vehicle System Dynamics Supplement*, 25.

2. Ackermann, J. (1994). "Robust decoupling, ideal steering dynamics and yaw stabilization of 4WS cars." *Automatica*, 30(11).

3. Anwar, S. (2003). "A predictive control algorithm for a yaw stability management system." *SAE 2003-01-1284*.

4. Åström, K. (2005). "Model Uncertainty and Robust Control."

5. Åström, K. J., and Hagglund, T. J. (1995). *PID Controllers: Theory Design, and Tuning*, ISA.

6. Åström, K. J., and Hagglund, T. J. (2001). "The future of PID control." *Control Engineering Practice*, 9.

7. Åström, K. J., and Hägglund, T. J. (2006). *Advanced PID Control*, ISA.

8. Åström, K. J., Panagopoulos, H., and Hägglund, T. J. (1998). "Design of PI controllers based on non-convex optimization." *Automatica*, 34(5).

9. Brennan, S., and Alleyne, A. (1999). "Driver assisted yaw rate control." *Proceedings Of American Control Conference*.

10. Brennan, S., and Alleyne, A. (2001). "A comparison of coordinated rear and torque steering MISO driver assist yaw rate controllers." *American Control Conference*.

11. Chee, W., and Tomizuka, M. (1997). "Unified Lateral Motion Control of Vehicles for Lane Change Maneuvers in Automated Highway Systems." *UCB-ITS-PRR-97-29*.

12. CSTRAC. (2005). "Investigating Officer's Traffic Accident Reporting Manual."

13. de Bruin, D. (2001). "Lateral Guidance of All-Wheel Steered Multiple-Articulated Vehicles," Technology University Eindhoven.

14. Doyle, J., Francis, B., and Tannenbaum, A. (1990). *Feedback Control Theory*, Macmillan Publishing Co.

15. Feng, K. T., Tan, H. S., and Tomizuka, M. (1998). "Automatic steering control of vehicle lateral motion with the effect of roll dynamics." *Proceedings of the American Control Conference.*

16. Freedman, M., Staplin, L. K., Gilfillan, D. P., and Byrnes, A. M. (1988). "Noticeability Requirements for Delineation on Non-Illuminated Highways." *FHWA-RD-88-028.*

17. Fujiwara, Y., Masakazu, Y., and Shuichi, A. "Automated steering control system design for passenger vehicle in consideration of steering actuator dynamics." *Proceedings of the American Control Conference.*

18. Fukao, T., Miyasaka, S., Mori, K., Adachi, N., and Osuka, K. "Active steering systems based on model reference adaptive nonlinear control." *Proceedings Of IEEE Intelligent Transportation Systems Conference 2001*, Okland, CA.

19. Garcia, D., Karimi, A., and Longchamp, R. (2005). "PID controller design with specifications on the infinity-norm of sensitivity functions." *Proceedings Of IFAC 2005.*

20. Ghoneim, Y. A., Lin, W. C., Sidlosky, D. M., Chen, H. H., Chin, Y. K., and Tedrake, M. J. (2000). "Integrated chassis control system to enhance vehicle stability." *International Journal of Vehicle Design*, 23(1).

21. Hanke, O., Bertram, T., and Hiller, M. (2001). "Analysis and control vehicle dynamics under crosswind conditions." *Proceedings of 2001 IEEE/ASME International Conference on Advanced Intelligent Mechatronics.*

22. Harada, H., and Iwasaki, T. (1993). "Stability criteria and objective evaluation of a driver-vehicle system for driving in lane change and against crosswind." *Vehicle System Dynamics Supplement (Proceedings of 13th IAVSD Symposium).*

23. Hatipoglu, C., Remill, K., and Ozguner, U. (1998). "Automated lane change: theory and practice." *Proceedings of IFAC Advances in Automotive Control.*

24. Inoue, H., and Sugasawa, F. (1993). "Comparison of feedforward and feedback control for 4WS." *Vehicle System Dynamics*, 22.

25. Ito, K., Fujishiro, T., Kanai, K., and Ochi, Y. (1987). "Four wheel steering system synthesized by model matching control." *6th IEE/IMechE Automotive Electronics Conference.*

26. Kasselmann, J., and Keranen, T. (1969). "Adaptive steering." *Bendix Technical Journal*, 2.

27. Khalil, H. K. (2002). *Nonlinear System 3rd Ed.*, Prentice Hall, Upper Saddle, NJ.

28. Kondo, M., and Ajimine, A. (1968). "Driver's sight point and dynamics of the driver-vehicle system related to it." *SAE 680104*.

29. Krenn, M., and Richter, T. (2004). "Active Steering - BMW's approach to modern steering technology."

30. Lee, A. Y. (1997). "Matching vehicle responses using the model-following control method." *SAE 970561*.

31. Mammar, S., and Koenig, D. (2002). "Vehicle handling improvement by active steering." *Vehicle System Dynamics*, 38(3).

32. Mammar, S., Raharijaona, T., Glaser, S., and Duc, G. (2004). "Lateral driving assistance using robust control and embedded driver-vehicle-road model." *vehicle System Dynamics Supplement*, 41.

33. Marks, C. (2005). "Pavement skid resistance measurement and analysis in the forensic context." *Proceedings of International Conference on Surface Friction Roads and Runways*.

34. Milliken, W. F., and Milliken, D. L. (1995). *Race Car Vehicle Dynamics*, Society of Automotive Engineers, Warren, Pa.

35. Nagai, M., and Ohki, M. (1989). "Theoretical study on active four-wheel-steering system by virtual vehicle model following control." *International Journal of Vehicle Design*, 10(1).

36. Ogata, K. (2002). *Modern Control Engineering*, Prentice Hall.

37. Ono, E., Hosoe, S., Tuan, H. D., and Doi, S. (1998). "Bifurcation in vehicle dynamics and robust front wheel steering control." *IEEE Transactions on System Technology*, 6(3).

38. Panagopoulos, H., and Astrom, K. J. (2000). "PID control design and H∞ loop shaping." *International Journal of Robust and Nonlinear Control*, 10.

39. Panagopoulos, H., Astrom, K. J., and Hagglund, T. J. (1999). "Design of PID controllers based on constrained optimization." *Proceedings Of American Control Conference*.

40. Roland, M. A. (1983). "Some aspects on suspension design parameters for improve vehicle response at the limit of adhesion." *IMechE C115/83*.

41. Selby, M., Manning, W. J., Brown, M. D., and Crolla, D. A. (2001). "A coordination approach for DYC and active front steering." *SAE 2001-01-1275*.

42. Sienel, W. (1997). "Estimation of the tire cornering stiffness and its application to active car steering." *Proceedings of the 36th Conference on Decision & Control*.

43. Skogestad, S., and Postlethwaite, I. (1996). *Multivariable Feedback Control: Analysis and Design*, JOHN WILEY & SONS.

44. Stinton, D. (1983). *The Design of the Aeroplane*, Van Nostrand Reinhold.

45. Stotsky, A., and Hu, X. (1997). "Stability analysis of robustly decoupled car steering system with nonlinear tire model." *Proceedings of the 36th Conference on Decision and Control*.

46. Tai, M. H., Hingwe, P., and Tomizuka, M. (2004). "Modeling and Control of Steering System of Heavy Vehicles for Automated Highway Systems." *IEEE/ASME Transactions on Mechatronics*, 9(4).

47. Tan, K. K., Wang, Q. G., Hang, C. C., and Hagglund, T. J. (1999). *Advances in PID Control*, Springer.

48. Tousi, S., Bajaj, A. K., and Soedel, W. (1991). "Finite disturbance directional stability of vehicles with human pilot considering nonlinear cornering behavior." *Vehicle System Dynamics*, 20.

49. Ukawa, H., Idonuma, H., and Fujimura, T. (2002). "A study on the autonomous driving system of heavy duty vehicle." *International Journal of Vehicle Design*, 29(1).

50. van Zanten, A. T. (2001). "Bosch ESP systems: 5 years of experience." *SAE 2000-01-1633*.

51. van Zanten, A. T., Erhardt, R., and Pfaff, G. (1995). "VDC The vehicle dynamic control system of Bosch." *SAE 950759*.

52. Vinnicombe, G. (2001). *Uncertainty and Feedback: H∞ loop-shaping and γ-gap metric*, Imperial College Press, Cambridge, UK.

53. Yamamoto, S., and Hashimoto, I. "Present status and future needs: The view from Japanese industry." *Proceedings of the 4th International Conference on Chemical Process Control*.

54. You, S., and Kim, H. S. (2000). "Later dynamics and robust control synthesis for automated car steering." *Proceedings of IMECHE, part D*, 215.

55. Yuhara, N., and Tajima, J. (2001). "Advanced steering system adaptable to lateral control task and driver's intention." *Vehicle System Dynamics*, 26(2).

56.   Zeyada, Y., Karnopp, D., El-Arabi, M., and El-Behiry, E. (1998). "A combined active-steering differential-braking yaw rate control strategy for emergency maneuvers." *SAE 980230*.

57.   Ziegler, J. G., and Nichols, N. B. (1946). "Optimum settings for automatic controllers." *Transactions of ASME*, 64.

Chapter 7

Controller Design with H_∞ Loop Shaping – An Extension to PI Control

In this chapter, an alternative yaw-rate controller to the one introduced in Chapter 6 will be designed using H_∞ loop shaping for the AFS (active front-wheel steering) system of the transit bus. H_∞ loop shaping is an advanced robust control technique, which usually results in more comprehensive and more sophisticated control systems than a PI controller. It is of our interest to study how the simple PI controller compares to the advanced H_∞ controller in terms of stability and performance robustness.

7.1 Introduction

The H_∞ loop-shaping design procedure was first proposed by McFarlane and Glover (McFarland and Glover 1988). The method is a combination of classical loop shaping and H_∞ robust stabilization. H_∞ loop shaping is essentially a two-stage design process (Skogestad and Postlethwaite 1996). First, the open-loop plant is augmented by pre and post-compensators to give a desired shape to the singular values of the open-loop frequency responses. Then the resulting shaped plant is robustly stabilized against uncertainties in the form of normalized coprime factor descriptions using H_∞ optimization.

During the last twenty years, H_∞ loop-shaping technique has been tested and proved effective in many applications, such as flight control (Hyde and Glover 1993;

Mammar and Duc 1992; Prempain and Postlethwaite 2004), vehicle dynamic control (Hingwe et al. 2000), combustion instabilities stabilization (Chu et al. 2003), and precise servo control (Choi et al. 1995). Besides its success in various industrial fields, H_∞ loop-shaping design method is selected for this thesis research due to its easiness and intuitiveness in use:

- In other methods, the designer needs to take care of both performance requirements and closed-loop stability at the same time. H_∞ loop shaping provides a way to decouple these two tasks to some extent. It allows the designer to concentrate on fulfilling the performance requirements by adding compensators in the first design step, resulting in a shaped plant, and then let the computer do an automatic synthesis of the stabilizing controller K_∞[10] for the shaped plant during the second step.

- No problem dependent uncertainty or weight selection is required during H_∞ optimization in the second step.

---

[10] Note that the optimal robustness K_∞ can achieve is pre-determined by the shaped plant designed during the first step.

7.2 Theoretical Background on H_∞ Loop Shaping

7.2.1 Uncertainty Representation in Coprime Factors

One of the fundamental elements in robust control theory is the modeling of uncertainties. Plant uncertainties can be modeled in three common ways (Vidyasagar and Kimura 1986). Let a transfer matrix G_0 represent the nominal plant, and Δ_G denote the uncertainty to G_0. The uncertainty is called "additive uncertainty" if the perturbed plant G is written as:

$$G = G + \Delta_G \tag{7.1}$$

The uncertainty is named "multiplicative perturbation" if G is represented by:

$$G = (I_p + \Delta_G)G_0 \quad or \quad G = G_0(I_m + \Delta_G) \tag{7.2}$$

The third method of modeling plant uncertainty involves the use of coprime factorizations. The nominal system G_0 is written in coprime factor form, and the system uncertainties are defined in terms of additive perturbations to the respective coprime factors. For a nominal system G_0 with left coprime factors representation:

$$G_0 = M^{-1}N \quad (M \in RH_\infty, \ N \in RH_\infty) \tag{7.3}$$

the perturbed system G is then given by:

$$G = (M + \Delta M)^{-1}(N + \Delta N) \quad ([\Delta M, \Delta N] \in RH_\infty) \tag{7.4}$$

Compared to additive and multiplicative uncertainty representations, writing uncertainty in the coprime factor form has an engineering significance. As illustrated by

the following example (Glover et al. 1992), coprime factor uncertainty does not require the perturbed system and nominal system to have the same number of right-half-plane (RHP) poles and zeros, which is pre-requisite for using additive or multiplicative uncertainty representations.

Example

Define the nominal plant G_0, and the perturbed plant G, respectively as:

$$G_0 = \frac{1}{s+a} \ , \ G = \frac{1}{s-a}$$

Write the perturbation in additive form,

$$\Delta_G = \frac{2a}{s^2 - a^2},$$

or in multiplicative form,

$$\Delta_G = \frac{2a}{s-a}$$

Apparently, the perturbations represented in the above two forms are unstable (have RHP poles), thus the perturbed system cannot be written in the form of additive or multiplicative uncertainty. However, using coprime factor, the nominal and the perturbed plants can be well represented, respectively by:

$$G_0 = M^{-1}N \ , \ \begin{bmatrix} N \\ M \end{bmatrix} = \frac{1}{s+\sqrt{1+a^2}} \begin{bmatrix} 1 \\ s+a \end{bmatrix}$$

$$G = (M+\Delta M)^{-1}(N+\Delta N) \ , \ \begin{bmatrix} \Delta N \\ \Delta M \end{bmatrix} = \frac{1}{s+\sqrt{1+a^2}} \begin{bmatrix} 1 \\ s-a \end{bmatrix}$$

As can be seen from the above example, the coprime factor model provides a more generalized uncertainty representation than either additive or multiplicative form. Any (stable or not) transfer function matrix G can be represented in terms of a pair of asymptotically stable, real-rational, proper transfer function matrices that are coprime (Armstrong 1993).

7.2.2 Robust Stabilization Problem

The process of using feedback to stabilize and control a perturbed system G can be posed as a general robust stabilization problem (Skogestad and Postlethwaite 1996).

Taking G as a family of perturbed systems for a given perturbations Δ_G with

$$\left\| \Delta_G \right\|_\infty < \varepsilon \tag{7.5}$$

By theory (McFarland and Glover 1990), a single controller K should exist that is able to stabilize not only the nominal plant G_0 (i.e. G with $\Delta_G = 0$) but also all members in the G family, if

1. K stabilizes the nominal plant G_0

2. $\left\| F_l(P,K) \right\|_\infty < \varepsilon^{-1}$

where, P is the generalized plant involving G_0, and $F_l(P,K)$ is the lower linear fractional transform (LFT) given by:

$$F_l(P,K) = P_{11} + P_{12}K(I - P_{22}K)^{-1}P_{21} \tag{7.6}$$

The parameter ε in the theorem can be viewed as the stability margin for a given closed-loop system. As illustrated by Figure **7-1**, for a system with coprime-factor representation defined by Eq. **7.4**, the generalized plants P is given by Eq. **7.7**.
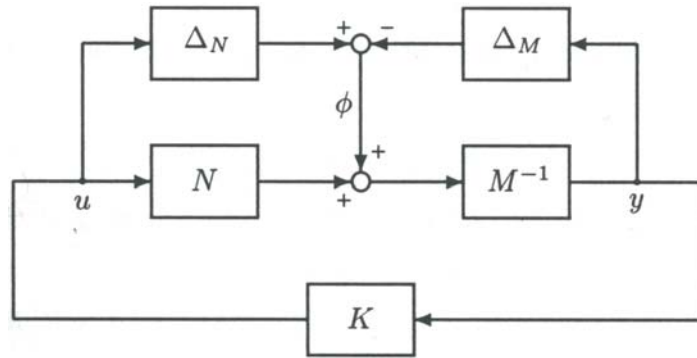
Figure **7-1**: System with coprime factor uncertainty

$$\begin{bmatrix} u \\ y \\ y \end{bmatrix} = P \begin{bmatrix} \phi \\ u \end{bmatrix}$$

$$\Rightarrow P = \begin{bmatrix} \begin{bmatrix} 0 \\ M^{-1} \end{bmatrix} & \begin{bmatrix} I \\ G \end{bmatrix} \\ M^{-1} & G \end{bmatrix}$$

(7.7)

Substituting Eq. **7.7** into Eq. **7.6**, the condition for the existence of robust controller K_∞ can be rewritten for the plants with coprime factor perturbations:

$$\gamma = \left\| F_l(P, K) \right\|_\infty = \left\| \begin{bmatrix} K \\ I \end{bmatrix} (I - GK)^{-1} M^{-1} \right\|_\infty \leq \varepsilon^{-1}$$

(7.8)

7.2.3 Optimal Robust Stabilization Problem for Plants with Coprime Factor Representation

After defining the condition for the existence of robust controller K, the next step in the robust stabilization problem is to find a feedback controller K_∞ to maximize the stability margin ε of the closed-loop system under the uncertain perturbations.

A significant feature of coprime factor representation is that, when the coprime factors in Eq. **7.3** are normalized, i.e. M and N satisfy

$$M\,M^* + N\,N^* = I$$
$$M^*(s) = M^T(-s) \quad N^*(s) = N^T(-s)$$

(7.9)

where, the superscript T stands for transpose matrix. Then, the maximum achievable stability margin $(\varepsilon^{-1})_{max}$ has an explicit closed form (Glover and McFarland 1989):

$$\gamma_{min} = (\varepsilon^{-1})_{max} = (1 - \left\| [N,M] \right\|_H^2)^{-1/2} = (1 + \rho(XZ))^{1/2}$$

(7.10)

where, subscript H refers to the Hankel norm, $\rho(\cdot)$ denotes the largest eigenvalue, and Z is the unique positive definite solution to the algebraic Riccati equation in the following.

$$(A - BS^{-1}D^TC)Z + Z(A - BS^{-1}D^TC)^T - ZC^TR^{-1}CZ + BS^{-1}B^T = 0$$
$$R = I + DD^T, S = I + D^TD$$

(7.11)

X is the unique positive definite solution to another algebraic Riccati equation.

$$(A - BS^{-1}D^TC)^T X + X(A - BS^{-1}D^TC) - XBS^{-1}B^T X + BS^{-1}B^T = 0$$

(7.12)

A controller K_∞ guarantees the optimal/suboptimal robust stability condition stated in Eq. **7.8** for a specified $\gamma > \gamma_{min}$ is given by:

$$K_\infty = \begin{bmatrix} A + BF + \gamma^2 (L^T)^{-1} ZC^T (C + DF) & \gamma^2 (L^T)^{-1} ZC^T \\ B^T X & -D^T \end{bmatrix}$$
$$F = -S^{-1}(D^T C + B^T X)$$
$$L = (1 - \gamma^2)I + XZ$$

(7.13)

The significance of Eqs. **7.10** and **7.13** are that, since γ_{min} can be computed from Eqs. **7.10**, the explicit solutions for the optimal/suboptimal K_∞ can be obtained by simply solving Eq. **7.13**.

To summarize the above discussion, there exist two important features of normalized coprime factor uncertainty descriptions:

1. Coprime factor descriptions do not require the perturbed plant and nominal plant to have the same number of right-half-plane (RHP) poles and zeros. It enables us to describe perturbed plants with different unstable modes other than the nominal plant.

2. The use of normalized coprime factor plant descriptions leads to a closed-form expression for the optimal stability margin. The optimal stability margin can be computed directly in terms of the design model parameters, thus allowing optimal or suboptimal robust compensators to be found without the γ-iteration seen in the standard H_∞ design, which significantly facilitates the design process (Skogestad and Postlethwaite 1996).

7.2.4 Loop-Shaping Procedure within Normalized Coprime Factorization Robust Stabilization Structure

Solving a robust stabilization problem alone is of little practical significance, because the performance requirements cannot be specified (Skogestad and Postlethwaite 1996). To implement performance specifications, MacFarland and Glover proposed adding pre- and post-compensators to the nominal plant G_0 to shape the open-loop singular values prior to robust stabilization of the "shaped" plant. Accordingly, the design process can be essentially divided into two stages. First, following the approach of classic loop-shaping design, add pre- and post-compensators to the plant according to the performance requirements. Second, robustly stabilize the "shaped" plant as described in **7.2.3**.

The loop-shaping procedure can be illustrated by Figures **7-2** and **7-3**. Let W_1 and W_2 be system pre- and post-compensators, respectively. These two compensators are used to shape the original plant G_0 according to the performance requirements. As shown in Figure **7-2**, an augmented plant G_A is then defined by:

$$G_A = W_2 G_0 W_1 \qquad (7.14)$$

Performing a NCF (normalized coprime factorization) robust stabilization design for G_A yields a dynamic compensator K_A that robustly stabilizes G_A. Finally, a simple block manipulation as shown in Figure **7.3** yields the corresponding compensator K to be applied to the original unshaped plant G:

$$K_\infty = W_1 K_A W_2 \qquad (7.15)$$
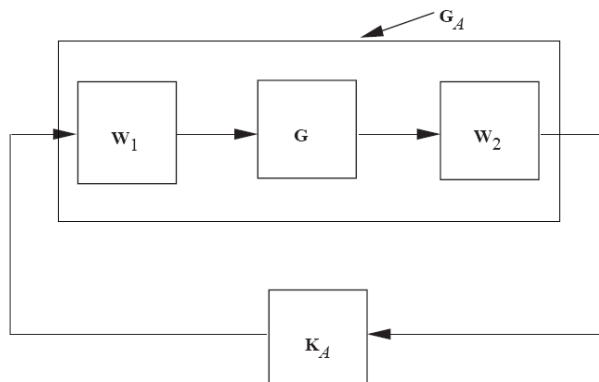
Figure **7-2**: Shaping the original plant and stabilizing the shaped plant
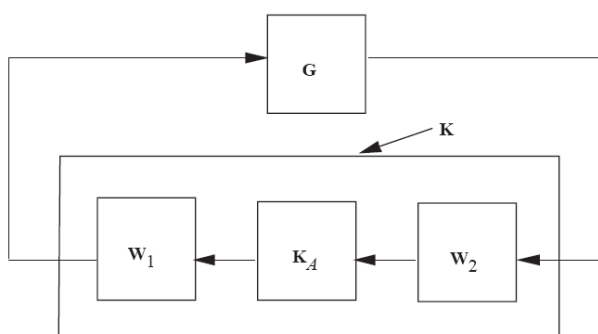
Figure **7-3**: The controller to be applied to the original plant

7.2.5 Classic Loop Shaping and Bode's Ideal Loop

As discussed in **7.2.3** and **7.2.4**, since the second step in the H_∞ loop-shaping controller synthesis follows a well-established standard optimal robust stabilization routine, the most challenging task would occur in the first step – selecting the pre- and post-compensators $W_1(s)$ and $W_2(s)$. The purpose of these two filters is to shape the open-loop gains of the nominal plant G_0 based on the performance specifications.

Usually, the pre-compensator W_1 is selected to shape G_0 to achieve the specified performance objectives, while the post-compensator W_2 is selected to reflect the relative importance of the controlled output variables and the other measurements fed back to the controller. W_2 is often chosen to be a constant found by trial and error. The selection of W_1 follows the procedures of classic loop-shaping briefly reviewed as follows.

7.2.5.1 Classic Loop Shaping

Many performance and robust stability objectives can be written as requirements on the maximum singular values of particular closed-loop transfer functions. The principle idea of "loop shaping" is that the maximum singular values of these closed-loop transfer functions can be directly determined by the singular values of the corresponding open-loop transfer function (McFarland and Glover 1990). This idea may be illustrated by analyzing the feedback control loop in Figure **7-4**. The system G is subject to exogenous inputs including reference commands r, disturbance to the output d, and measurement noise n.
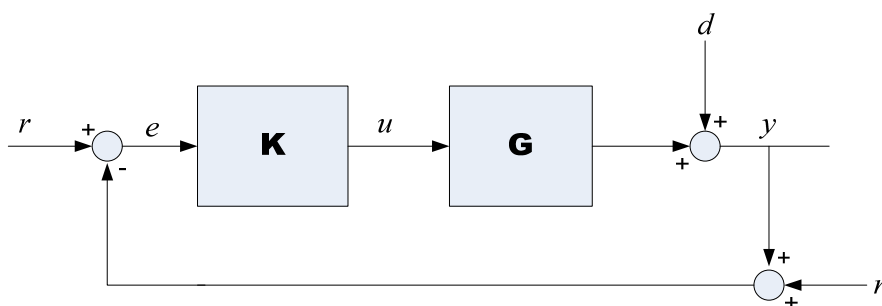
Figure **7-4**: Closed-loop system with exogenous inputs

From Figure **7-4** the following equations relating the output y and tracking error e to noise n, disturbance d, and reference r can be derived for the SISO case.

$$y = (1+GK)^{-1}GK\ n + (1+GK)^{-1}GK\ r + (1+GK)^{-1}d \qquad (7.16)$$

$$e = (1+GK)^{-1}GK\ n + (1+GK)^{-1}\ r + (1+GK)^{-1}d \qquad (7.17)$$

The effects of disturbance d on the plant output y and the tracking error can be attenuated by minimizing $\left|(1+GK)^{-1}\right|$. And, minimizing $\left|GK(1+GK)^{-1}\right|$ gives the largest stability margin. The following inequalities relate the above two closed-loop objectives to the loop transfer function GK of the system.

$$\left|(I+GK)^{-1}\right| \approx \frac{1}{|GK|} \qquad (7.18)$$
$$\text{for frequencies where } |GK| \gg 1$$

$$\left|GK(I+GK)^{-1}\right| \approx |GK| \qquad (7.19)$$
$$\text{for frequencies where } |GK| \ll 1$$

It can be seen from Eqs. **7.18** and **7.19** that the open-loop requirements for output disturbance attenuation and tracking error are in conflict with the open-loop requirement for robust stability. This fact reflects the well-known inherent trade-off between performance and stability, because $|GK|$ has to be large to satisfy the disturbance-attenuation and tracking error requirements, and at the same time the requirement on stability needs $|GK|$ to be small. Obviously, these two requirements cannot be fulfilled over the same frequency range. However, it is not necessary to achieve disturbance

attenuation and robust stability simultaneously. Normally, the disturbances are assumed to be large in magnitude only over a low-frequency range, and stability is appreciable only over a complementary high-frequency range (McFarland and Glover 1990). The controller K is typically designed to results in large $|GK|$ over low-frequency range, and small $|GK|$ over high-frequency range as shown in Figure **7-5** (Skogestad and Postlethwaite 1996).
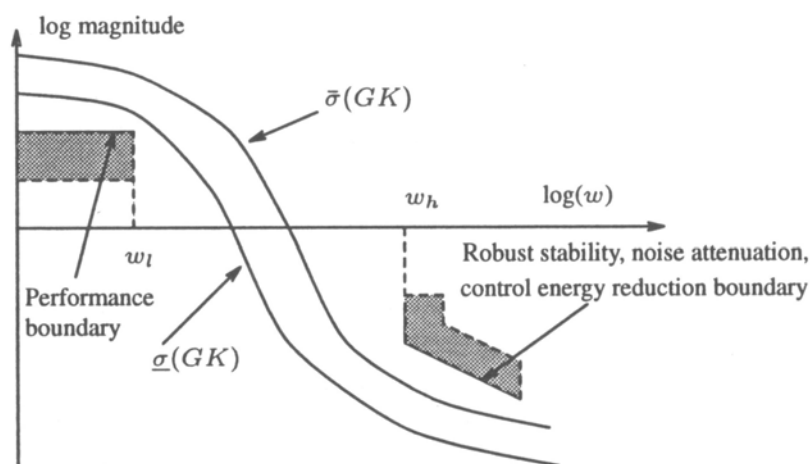
Figure **7-5**: Design trade-offs for the loop transfer function GK

7.2.5.2 Bode's Ideal Loop Transfer Function

In the last section, we have theoretically discussed how to choose a pre-compensator W_1 that can shape the loop ($L=W_1G_0$) such that the loop transfer function satisfies a given set of specifications. In practice, a simple but effective way (Le and Safonov 1992) to find W_1 is to first determine a desired loop transfer function L_d, which yields the desired performance, then obtain the pre-compensator W_1 by:

$$W_1 = L_d G_0^{-1} \tag{7.20}$$

For a plant, which is minimum phase (no right half plane poles or zeros), any loop transfer function can be obtained by proper compensation (Åström 2005). Based on Eq. **7.20**, it is then of our top priority to search for a desired loop transfer function L_d.

According to Åström (Åström 2006), Bode suggested an ideal loop transfer function (Eq. **7.21**), when working with feedback amplifiers.

$$L_{Bode} = (\frac{\omega_{gc}}{s})^n \quad (n > 0) \tag{7.21}$$

where, ω_{gc} is the specified gain cross over frequency for the ideal loop transfer function.

The Nyquist curve for the Bode ideal loop transfer function is simply a straight line through the origin with a constant phase margin ($180° - n \cdot 90°$). The reason why Bode selected this particular loop transfer function is that it gives a closed-loop system insensitive to gain changes. In other words, the phase margin stays as a constant at ($180° - n \cdot 90°$). And, the gain margin is infinite.

In addition, Bode's ideal loop yields a roll-off rate of -20 dB/dec around the gain cross-over frequency, which is typical value desired by control-system designers (McFarland and Glover 1990; Skogestad and Postlethwaite 1996).

7.2.6 Summary for H_∞ Loop-Shaping Method

In summary for the above discussion, the controller design using H_∞ loop shaping can be conducted in four steps:

1. Use pre- and post-compensators W_1 and W_2 to shape the frequency response of the nominal plant G_0.

2. Robustly stabilize the augmented plant $W_1 G_0 W_2$.

3. Check the stability margin ε against the magnitude of the largest perturbation $\|\Delta_G\|_\infty$. If $\varepsilon < \|\Delta_G\|_\infty$, the synthesis needs to be restarted from first step.

4. Verify the designed controller using a nonlinear vehicle model. The controller needs to be re-designed, if either the stability or the performance requirements cannot be satisfied with the nonlinear model.

7.3 H_∞ Loop-Shaping Controller

The nominal vehicle model G_0 is single-input-single-output (SISO). As a result, we can put full weight on the single output of the plant, the yaw rate, r, i.e. the post-compensator can simply be $W_2 = 1$.

The pre-compensator W_1 will be designed using Eq. **7.20**. Bode's ideal loop defined in Eq. **7.21** is selected as the desired loop shape for the design. Considering the bandwidth of a transit bus is about 1.5 Hz, the gain crossover frequency ω_{gc} for the desired loop is set to be 1.5 Hz. And, $n = 1$ is tentatively selected in order to obtain a rational transfer function. The resulting desired loop transfer function is:

$$L_d = \frac{10}{s} \tag{7.22}$$

If we apply the H_∞ loop-shaping method (Le and Safonov 1992; McFarland and Glover 1988) to the nominal bus model G_0 with the desired loop transfer function defined by Eq. **7.22**, the obtained controller is Eq. **7.23**, and the loop $L = G_0K_\infty$ is plotted in Figure **7-6**. As can be observed from the Bode plot, the designed controller K_∞ is able to robustly shape the plant to the desired loop L_d within the upper and lower bounds ($\approx$ +/- 3 dB) up to at least 100 rad/sec (15 Hz), as long as the system uncertainty is less than the allowable maximum perturbation, which is $v = 0.68$ as a result of the design.

$$K_\infty = \frac{0.03488s^4 + 1.628s^3 + 37.98s^2 + 104.9s + 77.49}{0.00005s^4 + 0.01645s^3 + 11.3s^2 + 19.18s} \tag{7.23}$$
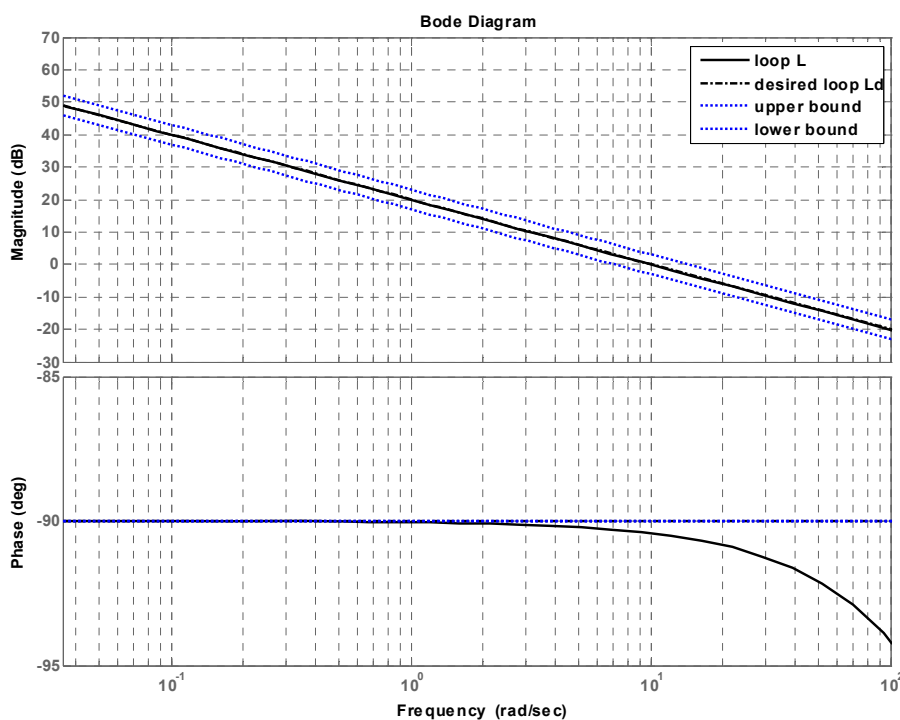
Figure **7-6**: H_∞ loop-shaping results

7.4 A Comparison between the PI Controller and the H_∞ Loop-Shaping Controller

In this section, the H_∞ loop-shaping controller is evaluated for robustness about tire-road friction reduction in the step-steer cases listed in Table **6-1**.

Since H_∞ controllers are best known for improving system robustness, it would be of special interest to see if the H_∞ loop-shaping controller yields more promising results on the low-friction surfaces than the PI controller does. A side-by-side comparison between the bus featuring a H_∞ loop-shaping controller and the bus equipped with the PI controller is presented in Figures **7-7** to **7-9**. The plots show the yaw-rate and side-slip angle responses along with steering inputs.

It can be observed from the plots that the yaw-rate and side-slip angle responses of the bus with the H_∞ loop-shaping controller are very close to those of the bus with the PI controller. In addition, if the friction coefficients are further reduced from the specified values in Table **6-1** for the step-steer cases, neither controller was able contain the stability of the bus. Therefore, in the specified testing cases, the performance and stability robustness about road-friction variation the sophisticated H_∞ loop-shaping controller can achieve is practically no better than what the PI controller can. These two controllers have similar performance in terms of yaw-stability enhancement under the critical driving situations. The advantage of the H_∞ controller is that its controller output (i.e. the steering input to the bus) is smaller and smoother than that from the PI controller. Nevertheless, we still would like to recommend the PI controller over the H_∞ loop-shaping controller for implementing the yaw-stability enhancement task on the 40-foot

transit bus, considering the structure of the PI controller is considerably less complex than the latter.
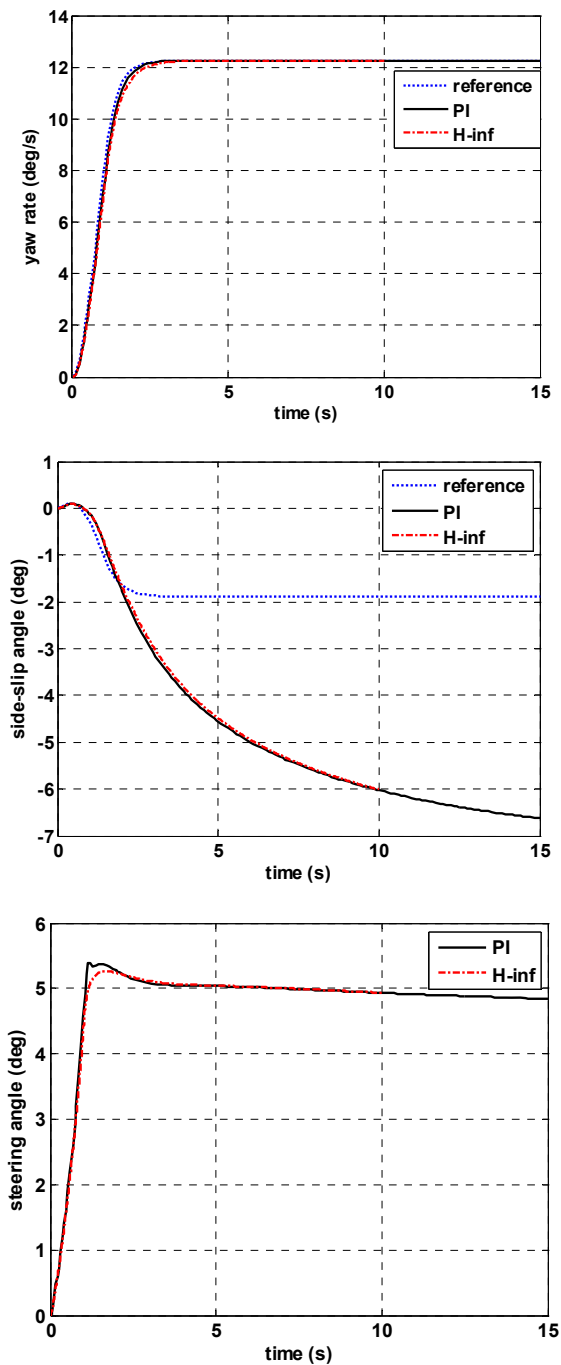
Figure **7-7**: Comparison between the PI controller and the H_∞ loop-shaping controller for the step-steer test on the snow packed road

Figure **7-8**: Comparison between the PI controller and the H_∞ loop-shaping controller for the step-steer test under limit oversteer on the wet road

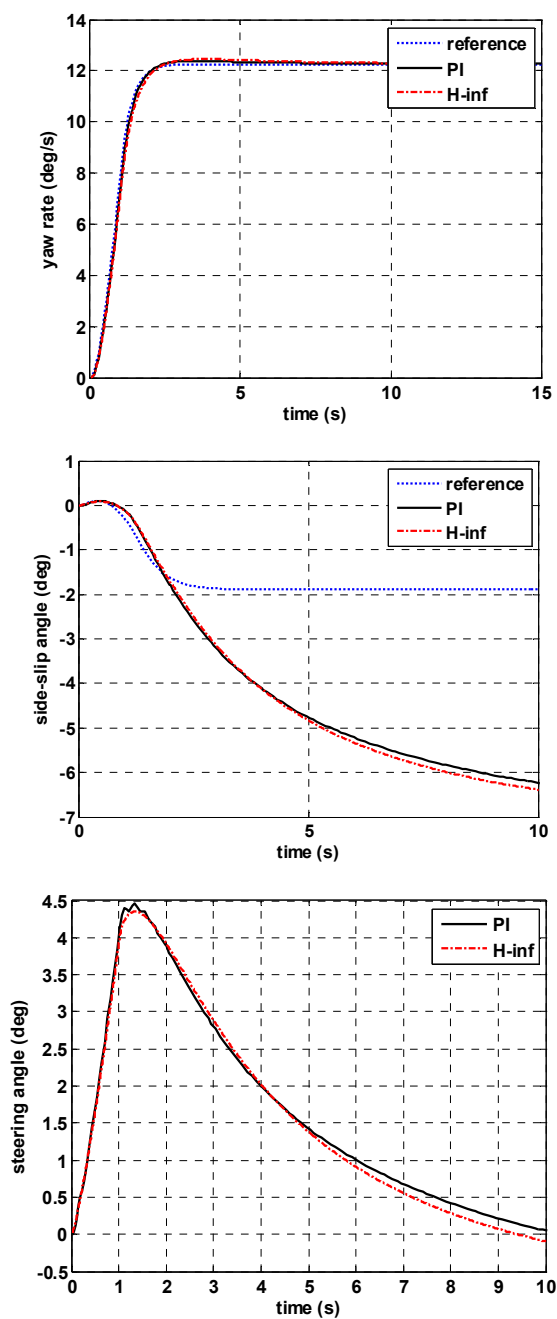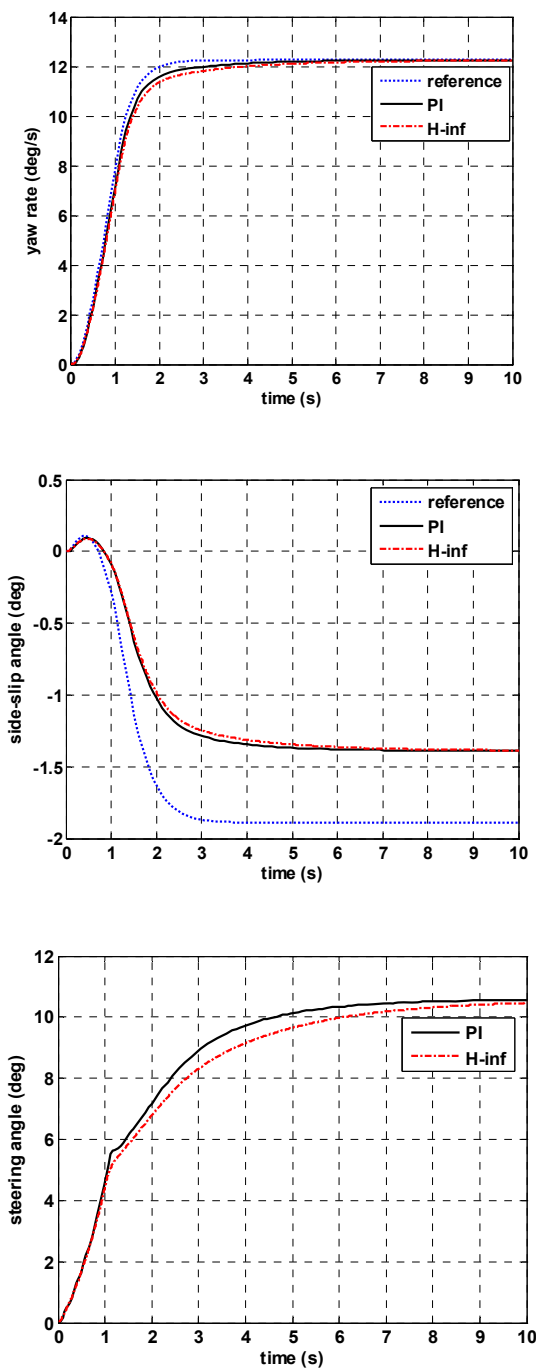Figure **7-9**: Comparison between the PI controller and the H_∞ loop-shaping controller for the step-steer test under limit understeer on the wet road

References

1.   Armstrong, E. (1993). "Robust controller design for flexible structures using normalized coprime factor plant descriptions." *NASA Technical Paper 3325*.

2.   Åström, K. (2005). "Model Uncertainty and Robust Control."

3.   Åström, K. (2006). "Feedback Systems - An Introduction for Scientists and Engineers."

4.   Choi, C. T., Kim, J. S., and Peak, K. N. (1995). "Robust loop shaping H∞ control of servo systems." *IEEE*.

5.   Chu, Y. C., Glover, K., and Dowling, A. P. (2003). "Control of combustion oscillations via H∞ loop-shaping, Mu-analysis and integral quadratic constraints." *Automatica*, 39.

6.   Glover, K., and McFarland, D. (1989). "Robust stabilization of normalized coprime factor plant descriptions with H_∞ bounded uncertainty." *IEEE Transactions on Automatic Control*, 34(8).

7.   Glover, K., Sefton, J., and McFarlane, D. C. (1992). "A tutorial on loop shaping using H-infinity robust stabilisation." *Transactions of Inst. MC*, 14(3).

8.   Hingwe, P., Wang, J. Y., Tai, M. H., and Tomizuka, M. (2000). "Lateral control of heavy duty vehicles for automated highway system: experimental study on a tractor semi-trailer." *UCB-ITS-PWP-2000-1*.

9.   Hyde, R. A., and Glover, K. (1993). "The application of scheduled H_∞ controllers to a VSTOL aircraft." *IEEE Transactions on Automatic Control*, 38(7).

10.   Le, V. X., and Safonov, M. G. (1992). "Rational matrix GCD's and the design of squaring-down compensators - a state space theory." *IEEE Transactions on Automatic Control*, 36(3).

11.   Mammar, S., and Duc, G. (1992). "Loop shaping H∞ design applied to the robust stabilization of a helicopter." *IEEE*.

12.   McFarland, D., and Glover, K. (1988). "An H_∞ design procedure using robust stabilization of normalized coprime factors." *Proceedings of 27th Conference on Decision and Control 1988*.

13.   McFarland, D., and Glover, K. (1990). *Robust Controller Design Using Normalized Coprime Factor Plant Descriptions*, Springer-Verlag.

14.   Prempain, E., and Postlethwaite, I. (2004). "Static H∞ loop shaping control of a fly-by-wire helicopter." *IEEE Conference on Decision and Control*.

15.   Skogestad, S., and Postlethwaite, I. (1996). *Multivariable Feedback Control: Analysis and Design*, JOHN WILEY & SONS.

16.   Vidyasagar, M., and Kimura, H. (1986). "Robust controllers for uncertain linear multivariable systems." *Aumomatica*, 22.

Chapter 8

Summary and Future Work

8.1 Summary

The results and conclusions from the four major parts of this thesis, namely bus-accident and driver-assistance system surveys, vehicle dynamics modeling, experimental and analytical investigations on bus handling, and AFS controller design, are summarized in this section. The research conducted under this thesis is simplified and far from complete. However, it promotes the study on active yaw-stability enhancement for buses, and can serves as a starting point for the future work.

8.1.1 Traffic Accidents of Buses and Driver-Assistance Systems

While bus accidents constitute only a small portion of the all the traffic accidents, they have significant impact on the safety of the overall traffic system due to the severity of each accident. One of the major causes that lead to bus accidents is loss of yaw stability on the road. Driver-assistance systems, such DBC (differential braking control) and AFS (active front-wheel steering) can greatly improve the safety of the vehicle. Among these active vehicle dynamics control systems, AFS is more suitable for the application on buses, considering the particular physical properties and operating environments of the bus.

8.1.2 Vehicle Dynamics Modeling for Buses

The results from the 2-DOF and 3-DOF models are very similar, when it comes to predict the yaw dynamics for a heavy-duty bus within the linear operating range. The bus would enter the nonlinear operating range when the lateral acceleration is beyond 0.2 g (up to 0.4g for a passenger car), due to the significant lateral load transfer. Within the nonlinear operating range, the roll dynamics of the vehicle have a significant effect on the yaw motions. Therefore, to obtain a reasonable prediction for the yaw dynamics of a bus beyond 0.2 g, a 3-DOF vehicle model with load sensitive tire is required.

During vehicle-dynamics modeling, taking tire-road friction condition into account by multiplying cornering stiffness with friction coefficient is not a proper approach. Tire-road friction does not change cornering stiffness. It is the rate at which the local cornering stiffness changes that tire-road friction does affect.

8.1.3 Handling Characteristics of Buses and the Influence of the Loading Condition

The experimental data from a series of field tests show that the handling characteristics of buses are different from either cars or trucks. A typical heavy-duty bus exhibits consistent understeering characteristic within normal operating range, and will start to show nonlinear yaw characteristics at a relatively low lateral acceleration (less than 0.25g). Due to the large weight and long wheelbase, the heavy-duty bus has a soggy yaw response. For a typical 40-foot transit bus, the bandwidth of the yaw-rate response is about 1.25 Hz.

During daily service, the vehicle weight of a 40-foot bus can change by almost 50%. However, such a significant weight variation does not have an appreciable effect on the yaw dynamics of the bus as long as the vehicle runs within the linear operating range, which is normally the case for transit bus operation. Therefore, it is not very necessary to consider weight as an uncertain parameter when designing a yaw controller based on the linear models.

8.1.4 Controller Designs for Active Front-Wheel Steering System

The disturbance attenuation performance of a PI controller can be characterized by its integral gain k_i. The PI-controller designed by optimizing integral gain under the constraints on sensitivity function and crossover frequency achieved a good compromise between performance and stability without resorting to advanced controller-design technologies. For the specified testing cases, the computer simulation results show that the simple PI controller can achieve similar performance and system robustness to that of the advanced H_∞ loop-shaping controller. The results also suggest that the effectiveness of the AFS system is most appreciable when the vehicle is in limit oversteer. This phenomenon implies a necessity to integrate AFS with other types of active safety systems with an expectation to achieve an optimal performance under all driving conditions.

8.2 Suggestions for Future Work

8.2.1 Vehicle Dynamics Model Upgrade

In order to obtain a more realistic vehicle model for the testing scenarios, such as cornering while braking and split-μ braking, a model for the braking system should be included in the current 3-DOF nonlinear vehicle. Upon adding the braking system, the most critical step is to replace the current pure slip tire model with a model for combined slip, which takes the interactions between the longitudinal and the lateral tire forces into consideration. One of the most frequently cited combined slip tire model is the Magic Tire Formula (Bakker et al. 1989; TNO 2001). A convenient source for the truck/bus tire parameters is ADAMS/Tire user's manual (MSC 2002).

8.2.2 Reference Model Modification

The AFS system is driven by the yaw-rate difference between a reference model and the output of the vehicle. In the current design, the "desired" yaw rate generated by the reference model represents the achievable yaw rate on the dry road. Sometime, this reference yaw rate could become unreasonably high for the vehicle traveling on slippery roads. When the AFS system tries to pursue this high yaw rate, the vehicle's side-slip angle could possibly increase very quickly, leading to the loss of direction. The solution to this problem would be a reference-model modification. According to the published works, three of possible ways to refine the reference yaw rate are introduced as follows:

1. Limit the reference yaw rate with respect to tire-road friction condition (Tseng et al. 1999; Yi et al. 2003). By regulating yaw rate with respect to this constrained reference, the controller can maintain a reasonable limit for the side-slip angle of the vehicle on the low-friction roads. The challenge for this approach is real-time detection of the tire-road friction coefficient, which may be obtained from the tire's longitudinal slip.

2. Use a linear summation of yaw rate and lateral acceleration as the reference signal (Segawa et al. 2002). This approach is also known as D^* control. However, the transfer function from steering angle to lateral acceleration is non-minimum phase, which will create difficulties in analytical controller design.

3. Add side-slip angle to the control loop (van Zanten et al. 1995) and use a combination of yaw rate and side-slip angle as the reference signal. The difficulty lies in this approach is that, for the time being, there exists no economical way to accurately measure the side-slip angle of the vehicle. Therefore, an observer needs to be added to the system to provide an accurate estimation of the vehicle's side-slip angle. Moreover, similar to the D* control case, the transfer function from steering angle to side-slip angle is also non-minimum phase, which will add to difficulties in controller design.

8.2.3 Refinements to the PI Controller

Since there is an integral part in the PI controller, a windup phenomenon (Åström and Hagglund 1995) can occur if the steering actuator stays in saturation for an extended

amount of time. Integrator windup may cause a very slow response for the AFS system under some particular situations, which might ultimately lead to accidents. As a refinement to the current PI controller, adding an anti-windup feature is suggested. The design techniques of anti-windup controllers can be found in various textbooks and articles (Åström and Hagglund 1995). An interesting design that specifically addresses the actuator-saturation problem for an AFS system is called "fading integrator" (Ackermann and Bunte 1996; Guvenc et al. 2004). The fading integrator not only prevents the AFS actuator from saturating, but also gives the AFS system a refined "driver feel".

8.2.4 Two Degree-of-Freedom Controller

The design of the current AFS system relies on a single PI controller to achieve a compromise between the requirements on both performance and stability. A two degree-of-freedom controller enables a designer to independently adjust two closed-loop transfer functions (Horowitz 1963), therefore would allow a greater flexibility in the design of an AFS system. With a two degree-of-freedom structure, a better compromise can be achieved between compensating for uncertainties in the vehicle-dynamics model and obtaining a desirable yaw-rate response. Two degree-of-freedom controllers have been widely used in vehicle-dynamics control (Guvenc et al. 2004; Horiuchi et al. 1996; Yuhara and Tajima 2001).

8.2.5 Survey on AFS implementation

One of the best ways to improve the understanding of a design technique and fully appreciate the controller-design process is to implement the controller. Aside from building and evaluating the controller itself, implementing an AFS system on a bus will involve many practical issues, such as fault detection (Reinelt et al. 2004), CAN (controller area network) design, signal collection and processing, and driver interaction (van Driel and van Arem 2005). Many of these issues are out of the scope of our current knowledge. Therefore, a literature survey on AFS implementation becomes very necessary. In addition, many interesting and valid research topics will be discovered through this survey.

8.2.6 Parameter Identification for the Bus-Driver Model

As a driver-assistance system, the operation of an AFS device will inevitably involve the interactions with the driver's steering input. Thus, a driver model is necessary for evaluating AFS systems in all closed-loop vehicle test cases. The driver model introduced in **6.7.2** or its variations have been widely applied to simulate driver's input in path-following (Allen et al. 1987; Horiuchi and Yuhara 2000; Lin et al. 2004; Wang et al. 2002). The parameters of the driver model are highly vehicle dependant. Due to the limited access to bus testing facilities, driver parameters specific to heavy-duty buses can hardly be found in the literature. The lane-change performance improvement project, which was conducted at PTI in 2006 involved driver-parameter identification.

The preliminary work from the project can be used as a starting point for this bus-driver-parameter study.

8.2.7 Driver-In-Loop Evaluation

The interaction between the automatic control system and the driver is a very significant aspect in the active steering system design. The goal of the active front-wheel steering is to assist the driver in vehicle handling within nonlinear operating range. However, the driver behaviors in this operating range are very difficult to model mathematically. To facilitate the study on human perception of a driver-assistance system and the effects vehicle-parameter variations, a driver-in-loop virtual testing is recommended. TruckSim can be used to implement a driver-in-loop testing environment.

8.2.8 Nonlinear Control Algorithm

The controller introduced in this thesis was design via a linear approach. The nonlinearities were treated as uncertainties. Although the derived linear controller performed well on the nonlinear vehicle, it is still worthwhile trying a nonlinear approach. Since the nonlinearities in vehicle are reserved in the nominal design model during nonlinear controller-design process, a controller applicable to a wider range of operating conditions than the linear controller can possibly be obtained.

References

1.   Ackermann, J., and Bunte, T. (1996). "Automatic car steering control bridges over the driver reaction time."

2.   Allen, R. W., Szostak, H. T., and Rosenthal, T. J. (1987). "Analysis and computer simulation of driver/vehicle interaction." *SAE 871086*.

3.   Åström, K. J., and Hagglund, T. J. (1995). *PID Controllers: Theory Design, and Tuning*, ISA.

4.   Bakker, E., Pacejka, H. B., and L, L. (1989). "A new tire model with an application in vehicle dynamics studies." *SAE 890087*.

5.   Guvenc, B. A., Bunte, T., Odenthal, D., and Guvenc, L. (2004). "Robust two degree-of-freedom vehicle steering controller design." *IEEE Transactions on Control Systems Technology*, 12(4).

6.   Horiuchi, S., and Yuhara, N. (2000). "An analytical approach to the prediction of handling qualities of vehicles with advanced steering control system using multi-input driver model." *Transactions of ASME*, 122.

7.   Horiuchi, S., Yuhara, N., and Takei, A. (1996). "Two degree-of freedom H∞ controller synthesis for active four wheel steering vehicles." *Vehicle System Dynamics*, 25.

8.   Horowitz, I. M. (1963). *Synthesis of Feedback Systems*, Academic Press.

9.   Lin, M., Popov, A. A., and McWilliam, S. (2004). "Stability and performance studies of driver-vehicle systems with electronic chassis control." *Vehicle System Dynamics Supplement*, 41.

10.   MSC. (2002). "Using ADAMS/Tire."

11.   Reinelt, W., Klier, W., Reimann, G., Schuster, W., and Grossheim, R. (2004). "Active front steering (part 2): safety and functionality." *SAE 2004-01-1101*.

12.   Segawa, M., Nishizaki, K., and Nakano, S. "A study of vehicle stability control by steer by wire system." *Proceedings of the International Symposium on Advanced Vehicle Control 2000*, Ann Arbor, MI.

13.   TNO. (2001). "MF-Tyre User Manual v5.2."

14. Tseng, H. E., Madau, D., Ashrafi, B., Brown, T., and Recker, D. (1999). "Technical challenges in the development of vehicle stability control system." *Proceedings of IEEE International Conference on Control Applications*.

15. van Driel, C., and van Arem, B. (2005). "Investigation of user needs for driver assistance: results of an internet questionnaire." *European Journal of Transport and Infrastructure Research*, 5(4).

16. van Zanten, A. T., Erhardt, R., and Pfaff, G. (1995). "VDC The vehicle dynamic control system of Bosch." *SAE 950759*.

17. Wang, B. Y., Abe, M., and Kano, Y. (2002). "Influence of driver's reaction time and gain on driver–vehicle system performance with rear wheel steering control systems: part of a study on vehicle control suitable for the aged driver." *JSAE Review*, 23.

18. Yi, K., Chung, T., Kim, J., and Yi, S. (2003). "An investigation into differential braking strategies for vehicle stability control." *IMechE D04603*.

19. Yuhara, N., and Tajima, J. (2001). "Advanced steering system adaptable to lateral control task and driver's intention." *Vehicle System Dynamics*, 26(2).

Appendix A

Parameters for the Vehicle Models

A.1 Three Degree-of-Freedom Nonlinear Vehicle Model

a	C.G. position from the front axle	4.056 m
b	C.G. position from the rear axle	2.171 m
C_φ	augmented roll damping	139595 N·m·sec/rad
H	C.G. height measured from the roll center	0.5 m
I_{zz}	yaw moment of inertia	136212 kg·m^2
I_{xx}	roll moment of inertia	27242 kg·m^2
I_{xz}	coupled moment of inertia	27242 kg·m^2
K_φ	augmented roll stiffness	621192 N·m/rad
m	vehicle mass	12372 kg
m_s	sprung mass	100410 kg
T_1	front track width	2.184 m
T_2	rear track width	1.968 m

A.2 Two Degree-of-Freedom Linear Model

a	C.G. position from the front axle	4.056 m
b	C.G. position from the rear axle	2.171 m
C_f	Effective cornering stiffness at the front axle	-230150 N/rad
C_r	Effective cornering stiffness at the rear axle	-482090 N/rad
I_{zz}	yaw moment of inertia	136212 kg·m^2
m	vehicle mass	12372 kg

A.3 Two Degree-of-Freedom Nominal Model for Controller Design

a	C.G. position from the front axle	4.056 m
b	C.G. position from the rear axle	2.171 m
C_{f0}	Effective cornering stiffness at the front axle	135000 N/rad
C_{r0}	Effective cornering stiffness at the rear axle	285000 N/rad
I_{zz}	yaw moment of inertia	136212 kg·m^2
m	vehicle mass	123720 kg

A.4 Magic Tire Formula

F_{z0}	30000 N
P_{Cy1}	1.3
P_{Dy1}	-0.67893
P_{Dy2}	0.2145
P_{Ey1}	0.37886
P_{Ey2}	-1.8617
P_{Ky1}	-9.6829
P_{Ky2}	2.3839

Appendix B

Tire Cornering Stiffness

The following text and figures are reproduced from Dr. Thomas Gillespie's «*Fundamentals of Vehicle Dynamics*» (Gillespie 1992).

Under cornering conditions, in which the tire must develop a lateral force, the tire will also experience lateral slip as it rolls. The angle between it direction of heading and its direction of travel is known as slip angle, α. These are illustrated in the following figure.
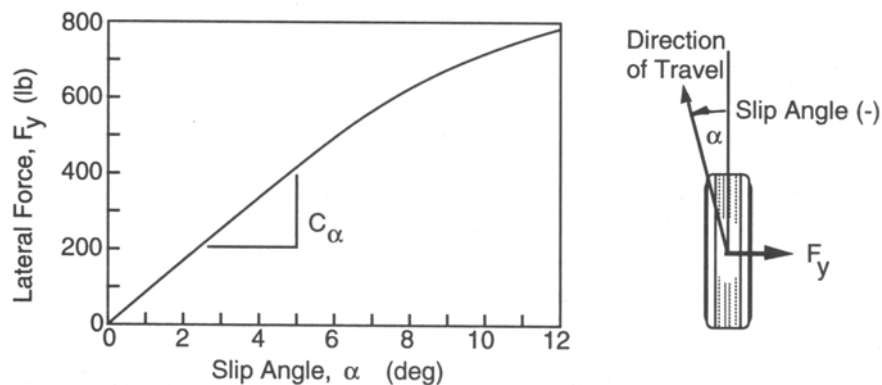
The lateral force, denoted by F_y, is called the "cornering force" when the camber angle is zero. At a given tire load, the cornering force grows with slip angle. At low slip angles ($< 5°$) the relationship is linear, hence $F_y = C \cdot \alpha$.

The proportionality constant, C, is known as the "cornering stiffness", and is defined as the slope of the curve for F_y versus α at $\alpha = 0$. A positive slip angle produces a negative force (to the left) on the tire, implying C must be negative.

The cornering stiffness is dependent on many variables. Tire size and type, number of plies, cord angle, wheel width, and tread are significant variables. For a given tire, the load and the inflation pressure are main variables. Speed does not strongly influence the cornering forces produced by a tire.

Gillespie, T. D. (1992). *Fundamentals of Vehicle Dynamics*, Society of Automotive Engineers, Warren, Pa.

Appendix C

Introduction to the Linear Preview Driver Model

A driver adjusts steering angle to track a path based on the perceived lateral deviation from the desired path at a preview point (Kondo and Ajimine 1968). As illustrated by the following figure, the deviation can be derived as:

$$\Delta = y + L_p\psi - y_0 \approx y - y_0 + L_p[\frac{1}{U}\frac{d}{dt}(y-y_0)]$$

where, L_p is the preview distance, ψ is the yaw angle with respect to the road, and U is vehicle speed.
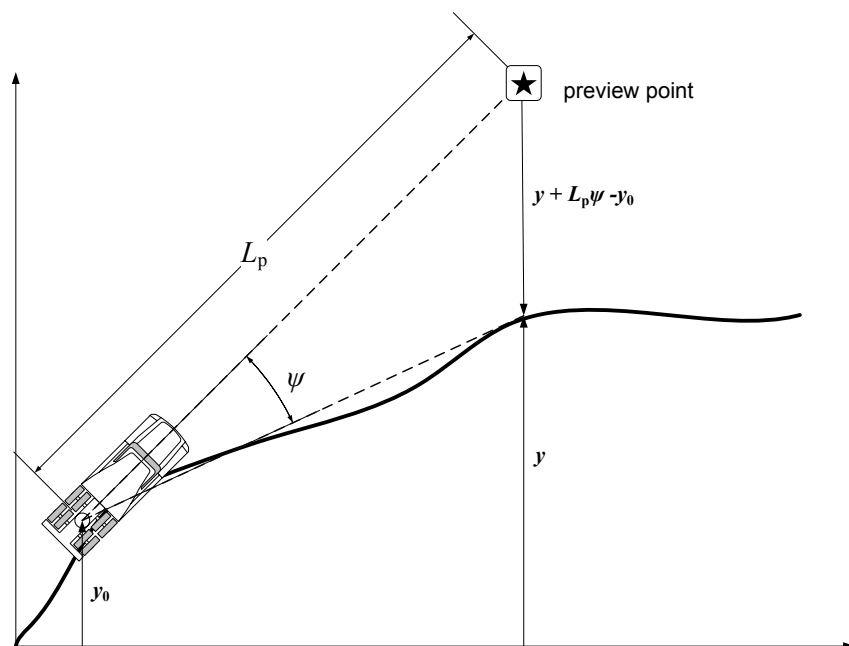
The driver's steering reaction to the lateral deviation can be modeled as a first order dynamic system.

$$T_r \dot{\delta}_d + \delta_d = G_s \Delta$$

where, T_r is the reaction time, δ_d is the driver's steering angle, and G_s is the steering gain.

As a result, the steering input from the driver can be represented by the following transfer function:

$$\frac{\delta_d}{y - y_0} = G_s \frac{1 + \dfrac{L_p}{U} s}{1 + T_r s}$$

1. Kondo, M., and Ajimine, A. (1968). "Driver's sight point and dynamics of the driver-vehicle system related to it." *SAE 680104*.

VITA

Nan Yu

Nan Yu was born in Hang Zhou, China in March 1972. He received his B.S. in Automotive Engineering in July 1995 from TsingHua University, Beijing. After a short period in a foreign trade company, Nan joined automotive division of 3M China Ltd.. From 1997-2000, Nan was in charge of business development in North China for 3M China automotive division.

Nan came to Penn State in January 2001. He received his M.S. in 2002. He is currently a Ph.D. candidate in Mechanical Engineering Department of the same school. Nan Yu has been a graduate research assistant at The Pennsylvania Transportation Institute since January 2001. His research areas of interest focus on vehicle directional and rollover stabilities, and handling performance improvement by active safety systems.